

cy



**DEVELOPMENT AND APPLICATION OF  
CRYOSORPTION PUMPING OF HYDROGEN AT 20°K  
BY MOLECULAR SIEVE ADSORBENT PANELS**

**P. J. Gareis and J. R. Pitlor**

**Engineering Department**

**Linde Division**

**Union Carbide Corporation**

This document has been approved for public release  
its distribution is unlimited.

*See SAC ITR-75/5  
AD 404700  
R 75 July 1975*

**January 1965**

AEDC TECHNICAL LIBRARY



5 0720 00006 8466

**ARNOLD ENGINEERING DEVELOPMENT CENTER  
AIR FORCE SYSTEMS COMMAND  
ARNOLD AIR FORCE STATION, TENNESSEE**

PROPERTY OF U. S. AIR FORCE  
AEDC LIBRARY  
AF 40(600)1000

# ***NOTICES***

When U. S. Government drawings specifications, or other data are used for any purpose other than a definitely related Government procurement operation, the Government thereby incurs no responsibility nor any obligation whatsoever, and the fact that the Government may have formulated, furnished, or in any way supplied the said drawings, specifications, or other data, is not to be regarded by implication or otherwise, or in any manner licensing the holder or any other person or corporation, or conveying any rights or permission to manufacture, use, or sell any patented invention that may in any way be related thereto.

Qualified users may obtain copies of this report from the Defense Documentation Center.

References to named commercial products in this report are not to be considered in any sense as an endorsement of the product by the United States Air Force or the Government.

DEVELOPMENT AND APPLICATION OF  
CRYOSORPTION PUMPING OF HYDROGEN AT 20°K  
BY MOLECULAR SIEVE ADSORBENT PANELS

This document has been approved for public release  
its distribution is unlimited.

Rec 200 TR-75/5  
AD A011 700  
D+4 July 1975

P. J. Gareis and J. R. Pitlor  
Engineering Department  
Linde Division  
Union Carbide Corporation

## FOREWORD

The work reported herein was done by the Engineering Department, Linde Division, Union Carbide Corporation for the Arnold Engineering Development Center (AEDC), Air Force Systems Command, Arnold Air Force Station, Tennessee under Contract AF 40(600)-944, Program Area 850E, Project 7778, Task 777801.

The report has been reviewed and is approved.

Alan J. Shade  
Sqd. Ldr., RCAF  
Technology Division  
DCS/Plans and Technology

Donald D. Carlson  
Colonel, USAF  
DCS/Plans and Technology

## ABSTRACT

An experimental and theoretical investigation of the vacuum pumping of hydrogen by refrigerated panels consisting of Molecular Sieve 5A bonded to metallic substrates was performed in the pressure range of  $10^{-9}$  to  $10^{-6}$  Torr. Initial sticking coefficients approximating unity were obtained with an array utilizing a shield and panel configuration, both refrigerated to 20° K.

An effective, practical, initial activation procedure was developed for utilization with the shielded array wherein desorbed water vapor was cryopumped by the liquid nitrogen cooled elements surrounding the 20° K surfaces.

Successive tests with a particular panel produced a progressive reduction in pumping speed. Methods were developed which resulted in partial recovery of prior pumping speed values; however, further effort is required to define precise conditions of efficient, successive activation procedures capable of maintaining the initial high sticking coefficient values.

A theoretical model is presented which relates observed pumping speed results to diffusion parameters of the cryosorption pumping mechanism.

Criteria are discussed for application of cryogenic arrays, utilizing cryopumping and cryosorption, as practical ultra-high vacuum pumping units.

## CONTENTS

	<u>Page</u>
ABSTRACT . . . . .	iii
NOMENCLATURE . . . . .	xi
1.0 INTRODUCTION . . . . .	1
2.0 EXPERIMENTAL APPARATUS . . . . .	3
2.1 Vacuum Chamber and Array. . . . .	3
2.1.1 77° K Shielded Array and Vacuum Chamber .	3
2.1.2 20° K Shielded Array and Vacuum Chamber .	5
2.2 External Pumping System. . . . .	5
2.3 Gas Metering and Supply System . . . . .	6
2.4 Instrumentation . . . . .	6
2.5 Activation and Instrument Bakeout Systems . . . . .	6
2.6 Refrigeration System . . . . .	7
2.7 Cryosorption Panels . . . . .	7
3.0 EXPERIMENTAL PROCEDURE . . . . .	8
3.1 General Preparation . . . . .	8
3.2 Activation and Instrument Bakeout . . . . .	8
3.2.1 77° K Shielded Array. . . . .	8
3.2.2 20° K Shielded Array. . . . .	9
3.3 Cooldown. . . . .	10
3.4 Leak Rate Calibration . . . . .	11
3.5 Interrupted Flow Technique. . . . .	11
3.6 Instrument Calibration and Pressure Measurement. .	12
4.0 DISCUSSION . . . . .	13
4.1 Experiments With The 77° K Shielded Array. . . . .	14
4.2 Experiments With The 20° K Shielded Array. . . . .	18
4.3 Summary of Experimental Observations. . . . .	22

# **CONTENTS** (Continued)

	<u>Page</u>
5.0 ANALYSIS OF RESULTS . . . . .	24
5.1 Observed Results With Interrupted Flow Technique . . . . .	26
5.2 Model of Cryosorption Pumping . . . . .	28
5.2.1 General Considerations. . . . .	28
5.2.2 Development of Pumping Equation for a Diffusion Controlled Mechanism . . . . .	32
5.2.2.1 Pumping Equation in the Steady- State Region . . . . .	35
5.2.2.2 Pumping Equation for Pumpdown Region . . . . .	38
5.2.3 Deviation from Steady-State Pumping Behavior . . . . .	42
5.3 Summary of Analytical Results . . . . .	44
6.0 APPLICATION OF CRYOSORPTION PUMPING AS AN UHV TECHNIQUE. . . . .	46
7.0 CONCLUSIONS . . . . .	48
REFERENCES . . . . .	49
APPENDIX A Derivation of Pumping Speed Relation for Baffled and Unbaffled Cryosorption Panels . . . . .	51
APPENDIX B Analysis of Activation Time . . . . .	53

## LIST OF TABLES

<u>Table</u>	<u>Title</u>	<u>Page</u>
I	Design and Construction Characteristics of 77° K and 20° K Chevron Assemblies	55
II	Panel No. 1 - Cryosorption Pumping of Hydrogen at 20° K	56
III	Panel No. 2 - Cryosorption Pumping of Hydrogen at 20° K, Activations 1-3	57
IV	Panel No. 2 - Cryosorption Pumping of Hydrogen at 20° K, Activation 4	58
V	Panel No. 3 - Cryosorption Pumping of Hydrogen at 20° K, Runs 3-5	59
VI	Summary of Pumping Speed Results - Panels 1-3	60
VII	Summary of Pertinent Parameters for Cryosorption Pumping of Hydrogen	61

## LIST OF ILLUSTRATIONS

<u>Figure</u>	<u>Title</u>	<u>Page</u>
1	Photograph of Cryosorption Research Apparatus	63
2	Photograph of Liquid Nitrogen Cylindrical Shield and Top Chamber Flange	64
3	Schematic of Vacuum Chamber and 77° K Shielded Array System	65
4	Schematic of Vacuum Chamber and 20° K Shielded Array System	66
5	Photograph of 20° K Shield and Chevron Assembly	67
6	Photograph of 20° K Chevron and Refrigerant Tube Assembly	68
7	Gas Metering and Supply System	69
8	Refrigeration System	70
9	1/8" Thick Molecular Sieve 5A-Aluminum Substrate Adsorbent Panel	71
10	1/64" Thick Molecular Sieve 5A-Stainless Steel Substrate Adsorbent Panel	72
11	Interrupted Flow Technique Curve	73
12	Panel No. 1 - Residual Hydrogen Pressure During Cryosorption Pumping	74
13	Panel No. 1 - Steady-State Hydrogen Pressure as a Function of Hydrogen Leak Rate	75
14	Panel No. 2 - Residual Hydrogen Pressure During Cryosorption Pumping After First Activation	76

**LIST OF ILLUSTRATIONS**  
(Continued)

<u>Figure</u>	<u>Title</u>	<u>Page</u>
15,16	Panel No. 2 - Residual Hydrogen Pressure During Cryo-sorption Pumping After Second Activation	77
17	Panel No. 2 - Residual Hydrogen Pressure During Cryo-sorption Pumping After Third Activation	79
18	Panel No. 2 - Steady-State Hydrogen Pressure as a Function of Hydrogen Leak Rate for Activations 1-3	80
19	Panel No. 2 - Hydrogen Pumping Speed as a Function of Cumulative Activation Time	81
20	Panel No. 2 - Residual Hydrogen Pressure During Cryo-sorption Pumping After Fourth Activation	82
21	Panel No. 2 - Steady-State Hydrogen Pressure as a Function of Hydrogen Leak Rate for Activation 4	83
22	Panel No. 3 - Residual Hydrogen Pressure During Cryo-sorption Pumping - Run No. 3	84
23	Panel No. 3 - Residual Hydrogen Pressure During Cryo-sorption Pumping - Run No. 4	85
24	Panel No. 3 - Residual Hydrogen Pressure During Cryo-sorption Pumping - Run No. 5	86
25	Panel No. 3 - Steady-State Hydrogen Pressure as a Function of Hydrogen Leak Rate - Runs 3-5	87
26	Evaluation of Pumping Speed by the Pumpdown Technique Analysis	88

**LIST OF ILLUSTRATIONS**  
(Continued)

<u>Figure</u>	<u>Title</u>	<u>Page</u>
27	Adsorption of Hydrogen on Molecular Sieve 5A at 20° K	89
28	Pumpdown Characteristics Panel No. 3 (Run No. 3)	90
29	Pumpdown Characteristics Panel No. 3 (Run No. 4)	91
30	Pumpdown Characteristics Panel No. 3 (Run No. 5)	92
31	Pumpdown Characteristics Panel No. 2 (Run No. 2)	93
32	Diffusion Constant as a Function of Surface Layer Concentration	94
33	Concentration Gradient Front as a Function of Surface Layer Concentration	95
34	Cryosorption Pumping Behavior as a Function of Pressure	96
35	Schematic Representation of a Cryogenic Array	97
36	Activation Time Required to Reduce Water Loading to Two Weight Per Cent	98

## NOMENCLATURE

This list contains all symbols utilized in the text. The figure in parentheses next to each symbol refers to the equation where the parameter was first used.

Symbol		Description	Units
Q	(1)	The imposed hydrogen gas inleak	$\frac{\text{Torr-Liters}}{\text{Second}}$ , $\frac{\text{Micron-L}}{\text{Minute}}$
V	(1)	System volume	Liters
P	(1)	Observed pressure	Torr
t	(1)	Time	Second
S	(2)	Pumping Speed	Liters/Second
A	(2)	Panel pumping area	$\text{cm}^2$ , $\text{ft}^2$
$P_{ss}$	(2)	Steady-state pressure observed for a given Q	Torr
$P_o$	(3)	Base system pressure prior to inleak of Q	Torr
$\alpha$	(4)	Sticking coefficient for hydrogen cryosorption pumping	---
$S_t$	(5)	Theoretical pumping speed	Same as S
T	(5)	Absolute temperature	$^{\circ}\text{K}$
M	(5)	Molecular Weight	---

**NOMENCLATURE**  
(Continued)

Symbol		Description	Units
$Q_o$	(6)	Inherent system load of hydrogen	Same as Q
$P_e$	(7)	Equilibrium pressure of an adsorbent mass	Torr
$\nu$	(7)	Henry's Law constant	Liters <sup>-1</sup>
$C_e$	(7)	Equilibrium loading of an adsorbent mass	$\frac{\text{atm-cm}^3}{\text{gram}}$ , $\frac{\text{Torr-liters}}{\text{cm}^3}$
$\Delta t$	(8)	Time of inleakage of Q	Seconds
$\bar{P}$	(9)	Base pressure of a vacuum system	Torr
$E$	(16)	Net pumping speed	Liters/Second
$Q_e$	(18)	Rate of evaporation	Same as Q
$Q_a$	(18)	Rate of adsorption	Same as Q
$Q_d$	(19)	Rate of diffusion	Same as Q
$t'$	(22)	Time from initiation of a gas inleak to attainment of a steady-state pressure	Seconds
$a$	(22)	Thickness of saturated surface layer	cm
$k$	(23a)	Freundlich equilibrium isotherm constant	$\frac{\text{atm-cm}^3}{\text{gram-Torr}^{1/2}}$ , $\frac{\text{Torr-liters}}{\text{cm}^3\text{-Torr}^{1/2}}$
$n$	(23a)	Same as k	---

**NOMENCLATURE**  
(Continued)

Symbol		Description	Units
D	(24)	Diffusion constant	cm <sup>2</sup> /second
dc/dx	(24)	Concentration gradient	Torr-cm/cm <sup>3</sup> -cm
b	(25)	Thickness of concentration gradient front	cm
$\beta$	(34a)	Empirical constant	$\frac{\text{Torr-liter}}{\text{Torr}^{1/2}\text{-Second}^{1/2}}$
m	(36)	Slope of analytical plot of pumpdown region	$\frac{\text{Torr}}{\text{Torr}^{1/2}\text{-Second}^{1/2}}$
D <sub>O</sub>	(40)	Diffusivity constant	cm <sup>2</sup> /second
E <sub>a</sub>	(40)	Activation energy for diffusion	cal./mole
R	(40)	Universal gas constant	cal./mole-°K
$\theta$	(41)	Overall array capture probability	---
g	(42)	Baffle transmission coefficient	---
m	(44)	Mass of adsorbate	gram
W	(44a)	Mass of adsorbent	gram
m <sub>O</sub>	(45)	Initial water loading	gram
K	(46)	Characteristic Henry's Law constant for water adsorption	Torr <sup>-1</sup>

## 1.0 INTRODUCTION

The increasing complexity of space exploration programs has necessitated concurrent advances in associated technologies to effect accurate, reliable, and economical simulation of space environs. Examples of this progress are most noticeable in the area of vacuum production where ultralow pressures, achieved only in small laboratory equipment a decade ago, can now be effected in large environmental facilities. This extension of state-of-the-art capabilities has been due in large part to the increasing role of cryogenic applications in vacuum systems. Of particular import has been the development of practical, low temperature refrigeration units, which have promoted the long recognized mechanism of cryopumping from the status of a laboratory operation to that of an effective ultrahigh vacuum pumping technique for the so-called condensable gases (atmospheric constituents other than hydrogen, helium and neon). Recently, effort <sup>1-7</sup> has been directed toward development of other cryogenic techniques capable of pumping the aforementioned non-condensable species and thus supplementing the cryopumping technique. Particular interest has been expressed in the mechanisms of cryotrapping and cryosorption. Results with the latter approach have been most promising <sup>1,2</sup> and its feasibility as a useful UHV tool has been demonstrated. The present investigation has been concerned with further development of the cryosorption pumping of hydrogen so that its general utility in vacuum applications, for both large and small sized chambers, would be realized.

The ability of certain solids to physically adsorb large quantities of gases at or near their normal boiling point has long been known, and numerous studies of equilibrium <sup>8-10</sup> aspects of this mechanism have been reported. However, very little work has been performed relative to the dynamic pumping characteristics of this phenomenon. This situation is analogous in many respects to the development of vacuum cryopumping and it might be speculated that the practical success of that approach with associated solution of equipment problems has encouraged examination of cryosorption as a vacuum operation. The successful combination of these two cryogenic approaches would effect an independent vacuum pumping technique possessing important advantages over conventional schemes for many applications, particularly where environmental cleanliness is an important factor.

Investigations performed under this contract extension supplement earlier effort <sup>1,2</sup> by Linde personnel relative to the cryosorption pumping of hydrogen at 20° K. Molecular Sieve 5A adsorbent bonded to aluminum and stainless steel substrates was used in all tests since its desirability was demonstrated

in the earlier work. Particular emphasis was placed on development aspects of the pumping process; e.g. allowable thickness of adsorbent, effect of array configuration, development of practical activation procedures, definition of optimum operating techniques, etc. However, correlation between observed results and theoretical implications were given prime consideration in the study, in view of the relative absence of dynamic cryosorption pumping data, so that more overall insight might be obtained.

The interrupted flow technique, used successfully in other investigations of cryopumping and cryosorption phenomena, <sup>1-7</sup> was utilized in the present study. This procedure proved most amenable to analysis of the data and parameters associated with the technique are defined in terms of an overall cryosorption pumping model which correlates well with observed results.

The experimental results obtained in the study, together with previously reported data, allow definition of a practical cryogenic pumping array suitable for general use as an ultrahigh vacuum pumping unit. Criteria for design of this unit are discussed in the report.

## 2.0 EXPERIMENTAL APPARATUS

The experimental apparatus used in the present investigation is identical in most respects to the equipment utilized in previous work<sup>2</sup>. A general description of the unit is given below including a discussion of pertinent modifications made during the current study. A photograph of the unit is pictured in Figure 1.

### 2.1 Vacuum Chamber and Array

Experiments in general were performed with two different pumping array configurations. These systems are described below and for convenience in referencing will be designated as "20° K shielded" and "77° K shielded" configurations.

#### 2.1.1 77°K Shielded Array and Vacuum Chamber

This arrangement was used in the prior effort<sup>2</sup> and for initial tests under the present program.

A vertically oriented, 2-foot diameter by 4-foot long cylindrical chamber constructed of Type 304 stainless steel was used as the basic chamber element. Access to the unit was possible by removal of stainless steel end flanges sealed to the chamber by compression of indium gaskets. All penetrations to the system interior were located in the end flanges and breakable flanged closures utilized copper shear seal gaskets (Granville-Phillips Company design).

The array section is supported from the top flange and consists of two major elements, a 77° K component and a 20° K unit. The liquid nitrogen cooled (77° K) component is a cylindrical copper shield 19 inches in diameter and 32 inches long. A 1/4-inch copper refrigerant tube is brazed to the outside of the cylinder in a helical manner with inlet and outlet penetrations effected through the top flange. The top of the 77° K shield is closed by a plate which is brazed to the refrigeration fill tube for the 20° K section. The bottom of the shield is covered with optically tight aluminum chevron baffles (Clausing factor of 0.26) which are coated with a solution of colloidal graphite in alcohol ("Dag" Dispersion No. 154) to produce a high emissivity. The chevron baffle arrangement is bolted to the cylindrical section and cooled by conduction from that surface. A photograph of the liquid nitrogen cooled cylinder and top flange is presented in Figure 2.

The 20°K section consists of a 17-5/8-inch diameter by 1-inch thick copper plate with a 6-liter volume copper container brazed to the top surface which is used to contain the liquid hydrogen refrigerant. Fill of this container is achieved by transferring liquid through a 1-inch diameter stainless steel tube which extends through the top plate of the 77°K shield and upper chamber flange. Experimental adsorbent panels are bolted to the lower surface of the copper plate.

A pressure probe tube extends through the upper chamber flange, the 77°K top plate, and the 20°K plate. The probe tube does not touch the 20°K surface.

One modification made under the present study was location of thermocouples at pertinent positions in the apparatus. Specifically, temperature of the chevron and adsorbent panel surfaces was measured with two pairs of differential thermocouples made of copper-constantan. This material was selected over gold-cobalt, which has a higher sensitivity but is unstable at temperatures above 100°K. One pair of thermocouples is used to measure the estimated maximum temperature of the 77°K chevron baffle by bonding one junction to the middle of the center chevron facing the ambient temperature chamber wall. The reference junction is bonded directly to a liquid nitrogen cooling coil. A sufficient amount of the thermocouple wire near the junctions was also bonded to respective surfaces to minimize heat leak along the wire so that junction temperature would not be raised more than 0.01°K over that of the surface being measured. The other pair of thermocouples is used to measure the temperature of the adsorbent panel. In this arrangement, the reference junction is bonded to the 20°K refrigeration pot and the other junction is attached to a small cavity located in the side of the metal substrate of the adsorbent panel combination. It would, of course, be most desirable to measure the surface temperature of the adsorbent; however, no suitable technique was developed to effect this configuration. The bonding agent used to seal the thermocouples to the metallic surfaces is an epoxy resin possessing good low temperature strength and negligible vapor pressure at the temperatures of system operation. The thermocouples were introduced to the vacuum chamber interior through a standard electrical feedthrough suitable for UHV service.

No provision was included for bakeout of the chamber walls. The adsorbent panel was, however, activated at elevated temperature by circulation of warm gas as discussed in Paragraph 2.5.

A schematic representation of the described system is presented in Figure 3 including the auxiliary external pumping system discussed in Paragraph 2.2.

### **2.1.2 20°K Shielded Array and Vacuum Chamber**

This system was utilized in the final series of tests conducted under the present effort and reflects modifications aimed at improvement of thermal performance. No major changes were made relative to the external chamber and flange unit. A schematic of this system is given in Figure 4 and the specific alterations are discussed below.

The chevron ring was modified to allow a closer approximation of its surface temperature to 77°K. This modification involved brazing of a continuous, serpentine tube to the inside of each chevron and joining this passage with the existing liquid nitrogen circulation tube located on the cylindrical section of the shield system.

The 20°K cooled panel was completely enclosed with a 20°K shield and chevron arrangement as pictured in Figure 4. The chevron section was mounted on a square frame for ease in fabrication. A 1-1/2-inch diameter tube was brazed to the frame and connected directly to the refrigeration supply container by 1-inch diameter lines. The liquid capacity of the chevron coolant tube is approximately five liters. The complete enclosure of the adsorbent panel by the 20°K surface was achieved by addition of easily removable side shields, cooled by conductance from the chevron section. Installation of adsorbent panels was made by removal of these side shields.

A summary of the pertinent construction and design characteristics of the 20°K and 77°K chevron assemblies is presented in Table I. Photographs of the 20°K baffle and shield modification are presented in Figures 5 and 6.

### **2.2 External Pumping System**

Initial exhaust and roughing of the vacuum chamber was accomplished by a conventional pumping system as depicted in Figures 3 and 4. Appropriate use was made of the mechanical roughing pump and liquid nitrogen trap-oil diffusion pump-forepump combination to achieve pressures in the high vacuum range (approximately  $10^{-5}$  to  $10^{-6}$  Torr) prior to cooldown with liquid hydrogen. All external pumping systems were isolated from the

chamber once cooldown was initiated with liquid hydrogen, and attainment of the ultimate system pressures for the unbaked chamber was achieved solely with the cryopumping-cryosorption pumping combination.

In later experiments with the 20° K shielded array, a liquid nitrogen cooled cryosorption rough pump (Linde SN-14) was used as the initial system exhaust pump.

### **2.3 Gas Metering and Supply System**

Supply of accurately known quantities of hydrogen gas to the chamber was effected by use of an auxiliary gas metering unit. This system is depicted schematically in Figure 7. The principal components of this system include glass storage bulbs, a variable leak valve, McLeod gauge, glass-oil diffusion pump, liquid nitrogen traps, mechanical roughing pump, and suitably located stopcocks and valves per Figure 7.

The experimental method used to deliver a known rate of pure hydrogen gas from this unit to the cryopumping-cryosorption array is described in Paragraph 3.4.

### **2.4 Instrumentation**

Pressure measurement in the high and ultrahigh vacuum regions was performed with a Consolidated Vacuum Corporation Bayard-Alpert ionization gauge (Model GIC-011). Residual gas analysis was effected with a Consolidated Electrodynamics Corporation RGA (Diatron 20-6). A 6-inch Leeds and Northrup strip recorder was utilized for continuous readout of the RGA. Pressures in the low vacuum levels were determined with suitably located thermocouple gauges.

### **2.5 Activation and Instrument Bakeout System**

As mentioned before, the chamber proper was not equipped for bakeout; however, small, external heating mantles were used to bake the ionization gauge and Diatron element. In addition, the adsorbent panel was activated by passage of hot gas, obtained by routing utility air through a Chromalox resistance heating unit, through the 20° K refrigerant pot. Temperature of the instrumentation and hot air was indicated by suitably located thermometers and control was maintained by variable resistance units.

## 2.6 Refrigeration System

Transfer of liquid nitrogen to the 77° K elements was achieved by utilization of a pressurized storage Dewar-insulated line combination. Nitrogen addition was continuous throughout the duration of a test. The two-phase exit stream was vented directly to the atmosphere.

Liquid hydrogen was added in batch fashion as required to the 20° K fill system from a Linde LSH-150 storage Dewar via a vacuum insulated transfer line. Steady-state hydrogen boil-off was monitored by a wet-test meter located in the vent line. Boil-off was routed outside the building through a vent line.

The liquid hydrogen containing lines and pot were precooled with liquid nitrogen prior to a hydrogen fill. Nitrogen was removed by a purge with cold helium gas obtained by heat exchange with cold nitrogen vapor to eliminate any condensation of nitrogen during hydrogen addition. The details of the refrigeration system are outlined schematically in Figure 8.

## 2.7 Cryosorption Panels

The adsorbent panels consisted of pure Linde Molecular Sieve 5A with 20 weight per cent binder bonded directly to aluminum and stainless steel substrates. Details of the bonding technique were reported previously<sup>2</sup>. The adsorbent panel was assembled in the apparatus by bolt attachment to the 20° K refrigerant pot plate.

Two configurations were used in the study:

- a. A 1/8-inch thick layer of adsorbent-binder slurry was applied to an aluminum panel machined on one surface with grooves 1/16-inch wide and spaced 1/16 inch apart. The net adsorbent pumping area of this panel was 1.3 square feet. The panel is pictured in Figure 9.
- b. The surface substrate was composed of a stainless steel screen furnace-brazed to the center of a stainless steel plate. A layer of Molecular Sieve 5A, approximately 1/64-inch thick, was bonded directly to the screen with a resulting net adsorbent area of 0.5 square foot. The reduction in actual pumping area over that of the earlier specimens was necessitated by the 20° K chevron modification which limited actual panel area. Figure 10 illustrates the 1/64-inch panel. For unit area of panel, the screen configuration allows more available adsorbent surface than the cross-milled groove arrangement.

### 3.0 EXPERIMENTAL PROCEDURE

The specific objective in all tests was a determination of panel pumping speed as a function of imposed hydrogen gas loads for different operating conditions such as activation procedure, thermal shielding, adsorbent thickness, and substrate configuration. The study utilized the interrupted flow technique, described in Paragraph 3.5, as the basic approach for realization of these objectives. In general, the sequence of major operations in any given test included panel preparation and installation, initial chamber preparation, activation and instrument bakeout, cooldown, leak rate calibration, gas admission, and instrument calibration. These procedures are discussed in subsequent paragraphs.

#### 3.1 General Preparation

The adsorbent panel of interest was prepared and installed in the cryogenic section of the disassembled chamber. The 77° K cylindrical shield and elements were then lowered into the chamber proper by means of a small hoist arrangement (see Fig. 2) and the top chamber flange closure was secured. The chamber was then moved into position and all external systems were connected to their respective unit penetrations, and instrumentation hookup was effected. Initial exhaust conditions depended on the mode of activation as described below.

#### 3.2 Activation and Instrument Bakeout

Two methods of adsorbent activation were employed in the study for the different array configurations. Their selection was not, however, based on the configuration alone but rather was dictated by other experimental parameters as discussed in Paragraph 4.0. For convenience, their descriptions will be categorized according to the convention used above; i. e., 20° K or 77° K shielded array.

##### 3.2.1 77°K Shielded Array

After closure of the chamber proper and attachment of all systems, the unit was initially pumped with the rough mechanical pump to approximately 0.1 Torr at which point activation was begun by circulation of hot gas through the refrigerant pot. The exit temperature of the hot gas was maintained at approximately 180° C. After about twelve hours at activation conditions, the chamber pressure was sufficiently low to allow cut-in of

the liquid nitrogen trap-diffusion pump system. Activation was continued for total periods of 70-144 hours at temperature. Instrument bakeout was conducted concurrently for the last 24 hours of activation. After activation, the hot elements were cooled to ambient levels prior to cooldown with liquid nitrogen with continuous pumping. Pressures in the  $10^{-5}$  Torr range were generally achieved after this operation.

### 3.2.2 20°K Shielded Array

From experimental results as well as practical considerations, it was decided that the long term activation procedure used with the 77°K shielded array should be replaced with a shorter, but yet effective, technique. From considerations described in Section 4.0 and Appendix B, it was concluded that the effective activation time required to reduce water content to the acceptable limit of less than 5 weight per cent <sup>2</sup> for efficient cryosorption pumping at a panel temperature of approximately 200° C was of the order of minutes if moisture removal were not limited by available pumping speed. As a consequence the following experimental approach was adopted.

Initial exhaust of the chamber was effected by pumpdown with a Linde SN-14 liquid nitrogen cooled cryosorption rough pump. Concurrent with chamber pumpdown, cooldown of the 77°K shield was begun by transfer of liquid nitrogen to the chamber. After a sufficiently low chamber pressure was attained (approximately less than 100 microns), the diffusion pump isolation valve was opened and the system evacuated further with the combination of liquid nitrogen baffled oil-diffusion pump and mechanical rough pump. The cryosorption rough pump isolation valve was closed at this time. Panel temperature was maintained near 50° C during these operations by circulation of utility air through the refrigeration pot. After effective cooling of the liquid nitrogen shield, instrumentation bakeout was begun and conducted for a period of approximately 24-30 hours. After termination of bakeout, panel activation is commenced by circulation of hot gas through the refrigerant pot. Activation was continued until the gas temperature entering the pot was approximately 200° C at which point the air heater was turned off, a period of about 15-20 minutes.

This activation technique wherein desorbed water vapor was essentially cryopumped by the liquid nitrogen cooled shield \* increased available pumping speed for water by a factor of a thousand. The estimated pumping speed of the small oil-diffusion pump including piping conductance limi-

---

\* The vapor pressure of water condensed at 80° K is less than  $10^{-20}$  Torr.

tations was approximately 5 liters per second whereas the estimated value with the liquid nitrogen shield cooled to 77°K was 1150 liters per second. This speed value takes into account the conductance limitations of the chevrons located between the panel and the cold wall (Clausing factor of 0.185). The initial effectiveness of this operation assumes significant practical advantage since the majority of space simulation chambers include liquid nitrogen cooled surfaces to satisfy other operational requirements.

### 3.3 Cooldown

After termination of activation and cooldown of all components to ambient levels in experiments with the 77°K shielded array, further cooldown to cryogenic temperature levels was commenced by transfer of liquid nitrogen. In the tests with the 20°K shielded array, the shield elements were at this temperature level at termination of activation.

In both series of tests the test panel and associated components were precooled to approximately 77°K although the mode of precooling differed in each case. The initial experimental technique utilized direct addition of liquid nitrogen to the refrigerant pot followed by purge with gaseous helium to remove traces of nitrogen. In the latter tests, precool was effected by circulation of cold helium gas, obtained by heat exchange with cold nitrogen vapor, through the refrigerant pot.

Final cooldown of the cryosorption panel to 20°K was achieved by batch addition of liquid hydrogen to the refrigerant pot and 20°K chevrons (in the latter experiments). At the onset of hydrogen addition all external pumping systems were isolated from the chamber by closure of pertinent valving. Cooldown to 20°K was accomplished by slow addition of fluid and the operation generally required 30 minutes. The steady-state boiloff rate was measured by a wet-test meter. It was observed that addition of the polished, low emissivity 20°K chevrons reduced steady-state hydrogen consumption by a factor of about four over corresponding rates obtained with the 77°K shielded array. This result agreed well with the predicted improvement based on design considerations. This reduction in liquid hydrogen consumption allowed continuous operation for periods of approximately 18 hours before refill was required.

### 3.4 Leak Rate Calibration

The setting of accurate gaseous hydrogen admission rates was accomplished with the gas metering and supply system described in Paragraph 2.3 and illustrated in Figure 7. The method consisted of establishing a fixed conductance by an arbitrary setting of the variable leak valve and supplying hydrogen gas from the storage bulbs to the upstream side of the valve at a constant pressure. Prior to admission of this fixed leak rate to the chamber proper, the gas was allowed to enter a known volume of the gas metering system which included an extended range mercury McLeod gauge. The change in pressure in this system with time was determined and the ambient temperature leak rate,  $Q$ , was calculated from the relationship.

$$Q = V \frac{dp}{dt} \quad (1)$$

After a precise determination of  $Q$  was made, the stopcock and chamber valve isolating the calibration system from the chamber were opened to initiate a pumping speed determination test. At the end of each experiment, the aforementioned valve and stopcock were closed and the leak rate was rechecked in the manner described to determine if its value had changed during the course of a test. In the majority of reported pumping speed tests the deviation between observed leak test rate values before and after testing was less than 5 per cent.

The supply of hydrogen to the metering system was accomplished by admission of pure gas (greater than 99.9%) from a Linde storage cylinder through a liquid nitrogen cooled trap to the gas system with subsequent evacuation of the system to less than .001 Torr. This procedure was repeated four times to insure adequate purge of the supply system before final fill of the storage bulbs to 1 atmosphere of hydrogen. This procedure was repeated for each series of tests to minimize any potential contamination problems.

### 3.5 Interrupted Flow Technique

As mentioned previously the experimental objective of determining hydrogen pumping speeds as a function of imposed loads was effected by utilization of the interrupted flow technique.<sup>1-7</sup> Basically, this method involves measurement of system pressure as a function of time for a specific hydrogen admission rate. A typical curve obtained for a test of this nature is illustrated in Figure 11. The significance of the parameters defined by this plot is discussed in detail in Sections 4.0, 5.0; however, it is noted

that the attainment of a constant pressure level,  $P_{SS}$ , after a time,  $t'$ , for a known imposed load,  $Q$ , will define a pumping speed for the panel of interest. The interpretation of these data is, of course, directly related to the program objectives.

In general, the interrupted flow technique will allow definition of three specific regions of interest:

- a. The transient region defined by  $t_i \leq t \leq t'$
- b. The steady-state region where  $dp/dt = 0$
- c. The pumpdown region defined by  $t_t \leq t \leq t_z$

The significance of these areas is discussed in Section 4.0 but their definition is introduced at this time to familiarize the reader with the nomenclature.

### 3.6 Instrument Calibration and Pressure Measurement

The importance of the pressure-time data for a specific hydrogen gas admission rate was discussed in Section 3.5. The realization of these data was achieved by continuous gas analysis of hydrogen with the CEC RGA \* and concurrent readout of this analysis with a strip recorder. As a result, indeterminate errors associated with operator measurement of pressure-time data were eliminated.

The mass spectrometer functioned as a secondary measure of pressure level since calibration with a pressure measuring gauge -- Bayard-Alpert CVC unit -- was required at the termination of a particular run. The ionization gauge was not operated during a leak rate since the filament itself acts as a pump.

---

\* CEC RGA - Residual Gas Analyzer (Mass Spectrometer)

## 4.0 DISCUSSION

Dushman<sup>11</sup> has pointed out that vacuum production may be achieved by utilization of one of two basic mechanisms. Specifically, a reduction in pressure in a closed system may be effected by (1) momentum transferring machines which remove mass from the system and exhaust it to the surroundings, or (2) vacuum can be achieved by capture and retention of molecules with associated energy reduction within the system by physical and/or chemical combination. Examples of the former method include mechanical rough pumps, lobe type blowers, oil diffusion pumps, steam ejector units, etc., whereas techniques such as cryopumping, ion gettering, titanium sublimation, and adsorption phenomena are described under the latter category. It is of interest to note that the pumping speed of units associated with the former division at a given pressure level is time independent (assuming no mechanical failures); however, by nature, pumps of the latter classification possess a finite restriction on constant speed pumping depending on inherent capacity limitations. For example, the pumping speed of a cryopanel, refrigerated at a constant temperature level and operating at a given chamber pressure; i.e., constant gas load, will decrease with time as condensate formation increases and pumping surface temperature is raised. Also, filament life and titanium sublimation deposit capacity will limit constant pumping speed behavior of the getter ion and sputter ion pumps. The adsorbent pump constant speed behavior will be a function of the effective capacity of solid, although, as discussed later, this relationship is not easily related to equilibrium capacity values. Hence the design of vacuum systems employing these pumping techniques requires analysis to allow for capacity-pumping speed ramifications. A primary objective of the present study was definition of this behavior for the cryosorption pumping (physical adsorption at cryogenic temperatures) of hydrogen by Molecular Sieve 5A refrigerated to 20°K.

Kindall<sup>5</sup> has reported that the pressure-time curve for an adsorption pump will always show a small but yet continuous pressure rise for a given gas load, and his results with dynamic pumping of nitrogen by 77°K refrigerated charcoal pellets accentuates this condition. Hemstreet<sup>2</sup> and co-workers have shown that for relatively small, but yet practical hydrogen gas loadings from UHV considerations, no measureable pressure rises are observed for continuous operation of 20°K Molecular Sieve 5A panels. The gas loads used in the former study were typically two to three orders of magnitude higher than those of the latter effort. Consequently, Kindall's conclusion that the concept of pumping speed as applied to conventional pumps (momentum transfer) is not applicable to adsorption pumps is correct since no steady-

state pressure was observed for a given gas loading. Hence pumping speed decreased with time and was actually a function of pressure level. In the latter study, however, such a comparison could be made because pressure-time curves were obtained indicating a practical steady-state pressure level (no measureable deviation from this value was observed with time) and a meaningful pumping speed could be approximated by (see Section 4.1)

$$\frac{S}{A} = \frac{Q}{P_{ss}} \quad (2)$$

It is concluded, therefore, that the practicability of cryosorption pumping as an UHV technique, as well as other pumping techniques of the trapping category, depends on efficient system design to minimize the capacity effects on pumping speed behavior. Efforts were made in the present study to quantify acceptable gas load limits per unit area of adsorbent panels to effect practical pumping speed behavior in addition to gathering more data relative to the magnitude of these speeds. A discussion of the observed experimental results for the different arrays is presented in subsequent sections.

#### 4.1 Experiments With The 77°K Shielded Array

As part of the initial system checkout, it was decided to repeat the last experiment performed under the prior contract effort<sup>2</sup> which involved evaluation of a panel consisting of 1/64-inch thick Molecular Sieve 5A containing five per cent aluminum flakes bonded to a milled groove aluminum plate. The hydrogen pumping speed of the panel was determined as a function of hydrogen leak rate per the procedure described above. Results of the test are summarized in Table II and Figures 12 and 13. For reference this panel is denoted as Panel No. 1.

The calculation of pumping speed used in analysis of these data as well as all subsequent tests was based on the following relation:\*

$$\frac{S}{A} = \left( \frac{Q}{P_{ss} - P_0} \right) = \frac{Q}{\Delta P} \quad (3)$$

---

\* The derivation of this expression is presented in Appendix A. It is pointed out that pumping speeds quoted in this report are for warm gas (300°K), unbaffled configurations. Corrections for a baffled array are also discussed in the cited appendix.

where	Q	=	Imposed hydrogen gas load
	$\Delta p$	=	The difference between the observed steady-state pressure, $P_{SS}$ , and the base system pressure prior to gas inleakage, $P_O$ .
	S	=	Hydrogen pumping speed of the panel
	A	=	Adsorbent panel area

The results with this panel indicated a pumping speed (unbaffled) for 300° K hydrogen gas of 1640 liters/sec-sq. ft. of adsorbent surface (the actual panel area including substrate pegs amounted to 1.75 sq. ft., 75 per cent of which was occupied by adsorbent surface). This value corresponds to a sticking coefficient of 0.04 where the sticking coefficient,  $\alpha$ , is defined as the ratio of the actual pumping speed to the theoretical value predicted by kinetic theory.

$$\alpha = \frac{S}{S_t} \quad (4)$$

$$S_t = (3.38 \times 10^3) \left( \frac{T}{M} \right)^{1/2} \frac{\text{LITERS}}{\text{SEC-SQ. FT.}} \quad (5)$$

where	T	=	Absolute temperature of the impinging gas in °K
	M	=	Molecular weight of the gas

The value of 0.04 for the sticking coefficient did not compare well with the previously reported figure<sup>2</sup> of 0.16 for this panel. The discrepancy was traced, however, to hydrocarbon contamination of the panel during the initial exhaust period. The contamination was confirmed by chromatographic analysis of the bed and was traced to improper cooling of the diffusion pump resulting in oil degradation. The significance of this operational error is that it emphasizes the need for proper shielding of the cryosorption panel during all phases of preparation and testing if efficient pumping is to be effected. This difficulty was corrected and no recurrences were encountered in subsequent tests.

In order to determine the pumping characteristics of thicker adsorbent panels, particularly with respect to larger gas loadings, a specimen was prepared

{Panel No. 2) consisting of 1/8-inch thick Molecular Sieve 5A bonded to a cross milled groove aluminum plate (see Figure 9). Since the mass of adsorbent associated with this panel was so much larger than that of previous samples, it appeared that longer activation periods would be required to effectively remove adsorbed water. As a consequence, tests with this panel were preceded by activation at 180°C for periods of 70-144 hours.

After an activation period of 144 hours, an evaluation of the hydrogen pumping speed was made as a function of imposed gas loads. The results of this test indicated a hydrogen pumping speed of approximately 5100 liters/sec-ft<sup>2</sup>. The range of imposed gas loads for this test approximately doubled earlier studies<sup>2</sup> and in all cases a steady-state pressure was observed. Two subsequent experiments were performed with this panel preceded by activation periods of approximately 113 and 70 hours respectively. \* In all leak rate tests for each experiment a steady-state pressure was observed; however, the magnitude of the pumping speed value for the three experiments decreased progressively from 5100 liters/sec-sq. ft. to 1220 liters/sec-sq. ft. These results are summarized in Table III and Figures 14-18 inclusive

This anomalous behavior was not reported in previous work with hydrogen cryosorption pumping although a closer examination of experimental conditions indicated that the earlier work did not pursue the effect of identical test conditions past the second activation for a given panel. Furthermore, the activation times were much shorter than those employed in the present series of tests. It was initially believed that the reduction in pumping speed was a further reflection of a hydrocarbon contamination problem as experienced with Panel No. 1; however, chromatographic analysis of the adsorbent after the last test indicated no detectable hydrocarbons present. Since the activation times employed in these tests were, as stated, much longer than those used in former experiments, it was decided to analyze this point further. A plot of observed pumping speed as a function of cumulative activation time at 180°C is presented in Figure 19. The empirical linear relationship between pumping speed reduction and cumulative activation time is not only observed for the panel of interest but the consistent extrapolation to the panel evaluated in prior studies<sup>2</sup> seemed to imply more than a coincidental relationship. The results were qualitatively related to recent observations of the equilibrium capacities of Molecular Sieves for nitrogen as a function of activation history.<sup>12</sup> Specifically there was experimental evidence that long term activation at elevated temperatures in the presence of water vapor promoted an undesirable cation rearrangement in the adsorbent with resultant reduction in equilibrium capacity. The results of that effort indicated the phenomenon

---

\* The panel and chamber were not exposed to the atmosphere between tests.

was reversible in that re-exposure to atmospheric conditions; i. e., moisture loading, followed by a relatively short activation period produced expected capacity values.

As a consequence, the panel was removed from the chamber and exposed to atmospheric conditions until it had adsorbed an equilibrium loading (approximately 20 weight per cent) of water. The panel was then re-assembled and activated for 40 hours at 200°C. A subsequent evaluation of hydrogen pumping speed produced a value of 2230 liters/sec-sq. ft. which approximately doubled that obtained in the last test prior to water conditioning. Results of this experiment are summarized in Table IV and Figures 20, 21.

These experiments tended to indicate that long term activation of Molecular Sieve 5A panels was undesirable and that water conditioning could, at least partially, restore prior pumping speed behavior. It was decided, however, that a more positive approach to the problem would involve definition of shorter, more efficient activation conditions with fresh panels which would be more compatible with practical vacuum chamber operation and which would hopefully eliminate the observed speed reductions apparently associated with long term activation periods.

In addition to the aforementioned pumping speed reduction, pertinent observations were made relative to the thermal performance of the 77°K shielded array. Specifically, temperature level of the liquid nitrogen cooled chevrons and adsorbent panels as indicated by the thermocouple modification was determined to be larger than expected. The results indicated that portions of the liquid nitrogen cooled chevron surface were at temperatures as high as 170 - 180°K and that the cryosorption panel surface temperature approximated 24°K. This situation would tend to indicate that observed sticking coefficients obtained under these conditions are conservative and that more efficient refrigeration of panels and chevrons might produce correspondingly higher values. Dawson<sup>13</sup> reports that the gas temperature of a molecule approaching a cryogenic surface has a pronounced effect on the sticking coefficient for cryopumping. While it is recognized that the mechanisms of cryopumping and cryosorption differ, it nevertheless seems reasonable that both processes are similar in this respect. In view of these considerations as well as the former results relative to activation conditions, the experimental apparatus and procedure were modified. A discussion of these procedure modifications and experimental results is presented in the next section.

#### 4.2 Experiments With The 20°K Shielded Array

The apparent deleterious effect of long term activation observed above as well as the impracticability of these extended operations in normal chamber operation indicated a more efficient mode of adsorbent preparation was required. In addition, there had been some speculation<sup>14</sup> that a reaction may occur between the alkaline adsorbent and aluminum substrate in the presence of water which might have a harmful effect on capacity and/or pumping speed parameters. Since the observed results relative to pumping speed reduction occurred with a panel possessing an aluminum substrate, it was not possible to eliminate this parameter from consideration as a potential source of pumping speed reduction. As a result, it was decided that tests would be performed with a 1/64-inch thick Molecular Sieve 5A adsorbent bonded to a stainless steel substrate (Panel No. 3 -- see Figure 10). In addition, modifications (described in 2.1.2) were made to the apparatus to correct its thermal performance deficiencies. Finally, an analysis of the required activation time for efficient water removal from the adsorbent was performed. The details of that study are discussed in Appendix B. It was concluded that the necessity for long activation periods was determined to a large extent by the available pumping speed in the system. It was proposed, therefore, to avoid this limitation by cryopumping desorbed water vapor with the liquid nitrogen shield during activation as well as with the conventional oil diffusion pump. This auxiliary pumping system increased available pumping speed for water vapor by about three orders of magnitude and indicated that operation in this manner could reduce activation time to the order of minutes. Utilization of a liquid nitrogen cooled surface to hasten activation time seemed reasonable from practical considerations if effective, since most chamber designs include this capability to satisfy other operational requirements.

Further operational deviations from prior tests involved use of the apparent benefit derived from air exposure; i. e., moisture loading of the sieve between tests as well as rough pumping of the system by a Linde Model SN-14 cryosorption rough pump to safeguard against any possible oil contamination during initial chamber exhaust. The exact sequence of operation employed for each of the remaining tests is outlined below.

Prior to each pumping speed experiment, the following operations were performed:

- a. The chamber was exposed to the atmosphere by opening appropriate valving for a period of approximately 40 hours.

- b. The chamber was isolated from the atmosphere and liquid nitrogen flow initiated to cool the 77°K shield. Flow was continued for the duration of the experiment. Concurrently, the external cryosorption pump was opened to the system for initial chamber pumpdown.
- c. When chamber pressure was below 100 microns, the diffusion pump isolation valve was opened and the system evacuated further with the combination of liquid nitrogen baffled oil diffusion pump and mechanical rough pump. The rough cryosorption pump isolation valve was closed at this time.
- d. Panel temperature was maintained near 50° C during these previously described operations (steps b and c) by circulation of utility air through a temperature controlled electrical heater into the liquid hydrogen pot.
- e. After effective cooling of the liquid nitrogen shield has been attained (approximately 20 hours from initiation of flow), the instrumentation bakeout is begun. Bakeout is conducted for approximately 30 hours.
- f. Immediately after termination of bakeout the activation of the panel is initiated by temperature regulation of the hot gas flowing into the liquid hydrogen pot. Activation is continued until the gas temperature entering the pot is about 200° C, at which point the power to the air heater is turned off and the panel allowed to cool to ambient temperature levels. The time required to heat the air from 50° C to 200° C varied between 15 to 20 minutes for each of the five runs.
- g. After activation, the panel is precooled to approximately 77°K by circulation of cold helium gas into the liquid hydrogen refrigerant pot. The cold gas is obtained by heat exchange with liquid nitrogen.
- h. The pot is filled with liquid hydrogen. The isolation valve to the external diffusion pumping system is closed at initiation of cooldown with liquid hydrogen.

Five consecutive pumping speed experiments were performed with the 1/64-inch thick Molecular Sieve 5A-stainless substrate panel utilizing the procedure outlined above. This panel has an adsorbent-binder area of 0.5 sq. ft. as compared with previous panels whose pumping area approximated 1.3 sq. ft. As a result of system modification, gas approaching the panel approximates 20°K quite closely. Details and results of the tests are summarized below.

### Run Number One

Four leak rate additions varying from 3.7 micron-liters per minute to 95 micron-liters per minute were performed. In each case the change in hydrogen pressure as indicated by the mass spectrometer was unusually small and could not be quantified with the usual degree of accuracy. However, calculation of pumping speed based on the maximum observable pressure during the last run indicated a value of 30,000 - 40,000 liters/sec-sq. ft. corresponding to a sticking coefficient of approximately 0.73 - 0.96.

After instrument calibration, an attempt was made to measure a pumping speed with an extremely large leak rate of 630 micron-liters per minute ( $2.1 \times 10^{-2}$  Torr-l/sec-ft<sup>2</sup>). A steady pressure rise was observed; however, an evaluation of the pumping speed in the initial region of rise indicated a value of about 10,000 liters/sec-sq. ft.

### Run Number Two

Operational problems were encountered during this test with the liquid hydrogen addition; however, a run was performed at a leak rate of 208 micron-liters per minute with a calculated pumping speed of approximately 30,000 liters/sec-sq. ft. (unbaffled, 300° K gas) corresponding to a sticking coefficient of 0.73. An interesting observation occurred during this test in that during the leak rate admission the liquid hydrogen pot required refilling as evidenced by an instantaneous, large pressure rise. Liquid addition produced an immediate decrease in pressure to the previous pressure level. It appeared that the observed high pumping speed is quite sensitive to gas and/or panel temperature.

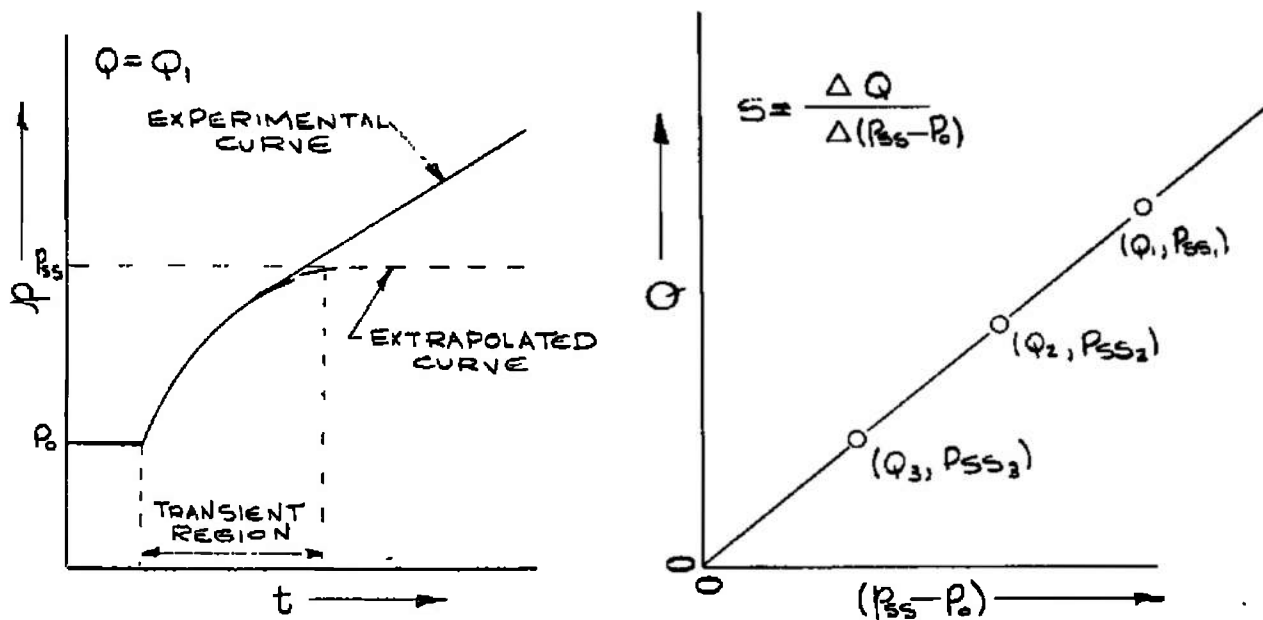
### Run Number Three

Results of this test are summarized in Table V and Figures 22 and 25. It is observed that steady-state pressures were obtained for hydrogen leak rates of 73 and 33.5 micron-liters per minute; however, a continuous pressure rise was observed with the largest loading of 127 micron-liters per minute. The pumping speed value of 9600 liters/sec-sq. ft. as defined by analysis of Figure 25 needs explanation therefore, since the plot does contain a steady-state pressure value for the latter loading.

As discussed in 4.0, excessive gas loadings applied to adsorption pumped systems produce a continuous pressure rise. Hence pumping speed decreases with time and is a function of pressure level. A plot of leak rate versus

pressure for this behavior therefore loses some meaning relative to pumping speed. The investigator may however choose to derive qualitative information about the phenomenon by comparing pressures as a function of leak rate after the loading has been applied for an arbitrarily selected time interval.

Hemstreet<sup>2</sup> utilized this approach to analyze the hydrogen pumping speed dependence of an adsorbent previously contaminated with nitrogen frozen on the surface. In the present study however, an alternate approach has been adopted for qualitative analysis of experiments wherein steady-state pressures were not observed. Specifically, the experimental pressure-time data were extrapolated through the initial transient region (see Section 3.5 and figures below) to an apparent steady-state pressure value that would have been obtained if the loading had not been excessive. It is believed that this approach yields pumping speed values consistent with data obtained for lesser loadings, wherein actual steady-state pressures are experimentally observed, and hence is indicative of the available panel pumping performance. It is observed that results pictured in Figure 25 for this test (Number Three) and for Number Five described below indicate good agreement between actual steady-state values and extrapolated data.



#### Run Number Four

Results of this experiment are listed in Table V and pictured graphically in Figures 23 and 25. Steady-state pressures were obtained for both leak rates and a pumping speed of 8700 liters/sec-sq. ft. was observed. It was intended that additional leak rates would be evaluated during this test; however, after the second run, the chamber was accidentally loaded with a considerable quantity of hydrogen (approximately 1200 torr-liters) producing a rapid pressure rise to about .5 Torr causing burnout of the mass spectrometer filament. This development did not allow calibration of the mass spectrometer against the ionization gauge and reported results are based on an average instrument sensitivity from prior tests.

#### Run Number Five

Experimental results for this panel are summarized in Table V and illustrated in Figures 24 and 25. An average pumping speed of 1310 liters/sec-sq. ft. was obtained. It is of interest to note that steady-state pressures were not obtained for leak rates of 42.9 and 25.2 micron-liters/minute whereas in the last test this panel exhibited constant pumping speed behavior for an inleak of 47.5 micron-liters per minute.

The results obtained with this panel compared to those of Panel No. 2 are summarized in Section 4.3. For convenience, these data are listed in Table VI.

#### **4.3 Summary of Experimental Observations**

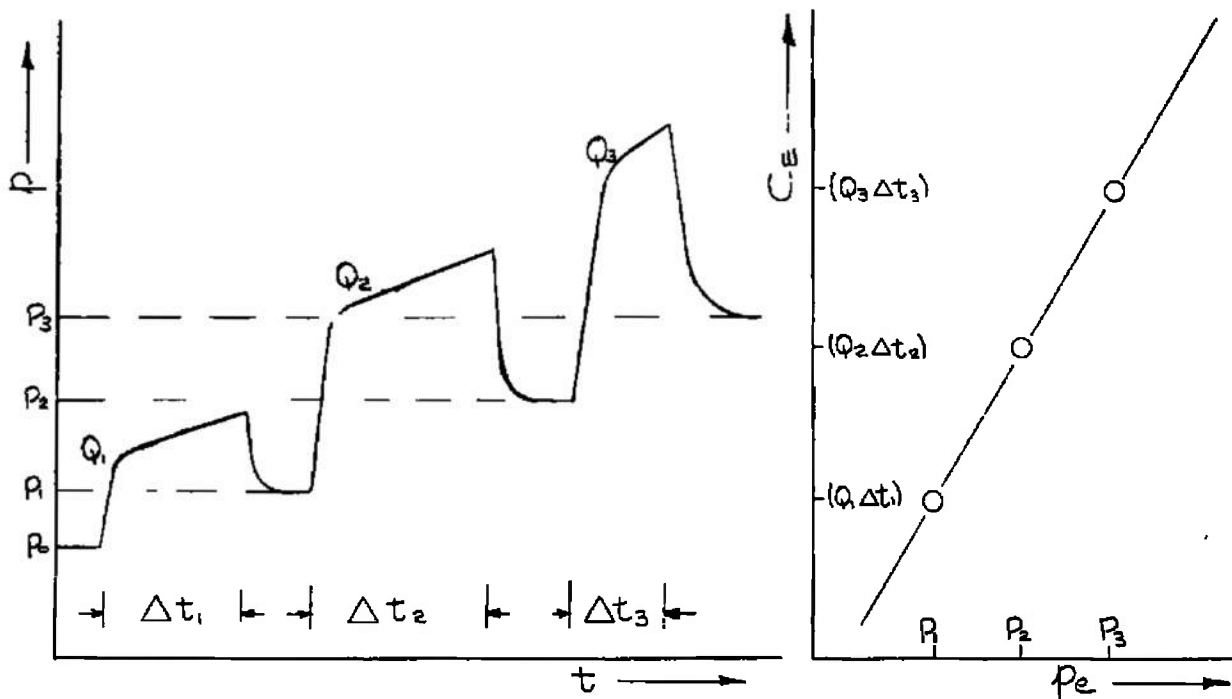
The following general observations relative to experimental results obtained in this study are summarized below for consideration. An analysis of these data is offered in Section 5.0.

- a. A reduction in pumping speed to a level of approximately 1200 liters/sec-sq. ft. occurred with both panels after successive testing. This reduction in pumping speed for Panel No. 2 occurred after a cumulative activation time of approximately 340 hours whereas a similar result was observed for Panel No. 3 after about 1-1/2 hours. On the assumption that reduction of speed in both cases proceeds via the same mechanism, it is concluded that activation time, per se, is not the unique cause for the observed phenomenon.
- b. Effective water loading of Panel No. 2, after exhibiting a low pumping speed, produced some recovery in pumping speed behavior.

- c. Initial sticking coefficients approximating maximum theoretical values (unity) were obtained in the modified apparatus. It is believed that these results are directly related to the lower gas temperatures approaching the panel and/or lower panel temperatures.
- d. The reduction in pumping speed observed with Panel No. 3 as well as Panel No. 2 tends to eliminate the previously mentioned aluminum-adsorbent incompatibility as the source of the effect.
- e. Initial high pumping speed values were obtained after relatively mild activation conditions indicating that these techniques are promising from practical application considerations. Further definition of consecutive activation conditions; e.g. temperature variation is required, however, to maintain initial high pumping speeds.
- f. For relatively low values of sticking coefficient, deviations from a steady-state pumping behavior were observed for mild gas loadings. Similar results were reported by Hemstreet<sup>2</sup> for panels which were contaminated with pre-adsorbed nitrogen and water vapor; however, in those instances a continuous pressure rise was observed for all gas loads. The present observations differed from those results in that the behavior appeared to be a function of load rate only. For example, consider the sequence of runs illustrated in Figure 24. The first test at the highest leak rate exhibited a constant pressure rise whereas the subsequent two experiments at lower loadings produced a steady-state pressure. The fourth run at a higher gas influx again produced a constant pressure rise. These results tend to eliminate external panel contamination as a contributing factor to the observed behavior.

## 5.0 ANALYSIS OF RESULTS

Prior to formal analysis of the experimental data, a discussion of particular experimental parameters is in order. Other investigators<sup>4,5,6</sup> who have used the interrupted flow technique for examination of cryosorption pumping have observed that the final system pressure after termination of a gas influx rate is always larger than the value prior to the admission of gas. Furthermore, the change in base pressure value has been related to the amount of gas adsorbed during the test by a linear function (Henry's Law) such that these data define an equilibrium isotherm as illustrated below.



Thus, the base pressure value observed in these tests reflects an apparent equilibrium pressure for a uniformly loaded adsorbent bed. Results of the present study (see Figures 15 and 16) as well as earlier effort<sup>2</sup> under this contract have always produced data exhibiting no change in observed base pressure before and after a given leak rate for a single test. Since the equilibrium pressure for any adsorbent must increase with adsorbate loading, it is concluded that the observed base pressure does not reflect a true equilibrium pressure for an adsorbent mass but rather is indicative of a steady-state value defined by:

$$P_0 = \frac{Q_0}{S} \quad (6)$$

- where  $P_o$  = The observed system base pressure for hydrogen  
(see Figure 11).
- $Q_o$  = An inherent system load of hydrogen.
- $S$  = Adsorbent panel pumping speed for hydrogen.

This consideration resulted in the definition of an experimental pumping speed given in equation (3) and discussed in Appendix A.

As mentioned above, the equilibrium pressure of an adsorbent mass for low coverages generally increases linearly with loading such that

$$P_e = \gamma C_e \quad (7)$$

$$P_e = \gamma (Q \Delta t) \quad (8)$$

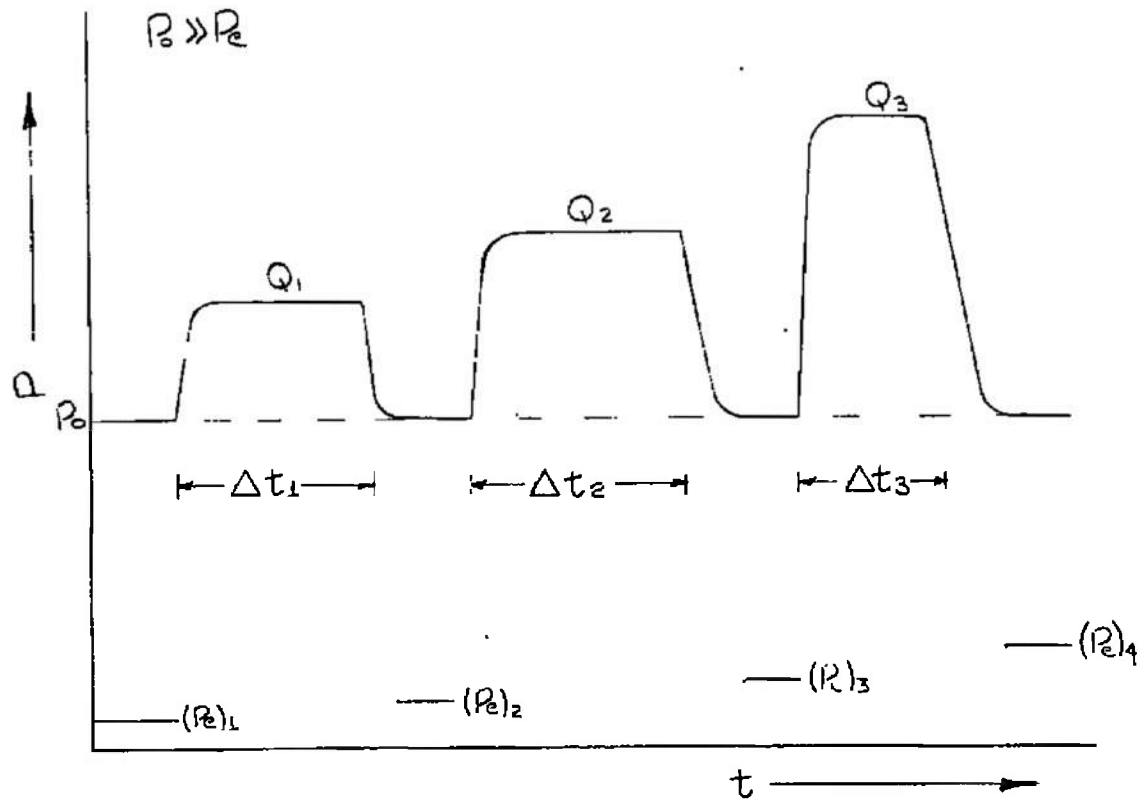
- where  $\gamma$  = Henry's Law constant
- $\Delta t$  = Time of inleakage of rate,  $Q$
- $C_e$  = Equilibrium loading

Since all systems will exhibit some inherent system load as a result of outgassing, permeation, virtual leaks, etc., the base pressure,  $\bar{P}$ , in a cryosorption pumping system will be generally given by

$$\bar{P} = P_o + P_e = \left[ \frac{Q_o}{S} + \gamma (Q \Delta t) \right] \quad (9)$$

If adsorbate loadings are small (applicable in present investigation) relative to system loads,  $\bar{P}$  approaches  $P_o$  and conversely, if imposed leaks are relatively large,  $\bar{P}$  will be defined by  $P_e$ . Since  $Q_o$  for any given system can be reasonably assumed to be constant, it is seen that in the former case, i. e., small imposed loadings, a reproducible base pressure may be achieved.

For example



It is, therefore, concluded that the results of the present investigation do not contradict previously reported data relative to this effect but rather that the selected conditions of testing render the pressure rise due to adsorbent loading negligible. This situation is not arbitrary since practical utilization of cryosorption panels for UHV applications would require proper load to adsorbent mass sizing to approximate the condition of a negligible pressure rise as discussed earlier in Section 4.0. As a consequence, subsequent development of data analysis assumes base pressure, as observed, does not reflect a true equilibrium adsorption pressure but rather a steady-state pumping pressure for a very small imposed load.

### 5.1 Observed Results With Interrupted Flow Technique

The experimental measurement of the speed of a vacuum pump may be effected by utilization of one of two conventional methods. For reference purposes

these techniques are designated as the steady-state and pumpdown methods. A description of each is perhaps best illustrated by consideration of the differential equation which defines the speed of a vacuum pump.

$$V \frac{dp}{dt} = Q - S(p - p_o - p_e) \quad (10)$$

where  $dp/dt$  = Rate of change of pressure in a system of volume  $V$ .

$Q$  = Rate of gas admission to the system from the surroundings.

$S$  = Speed of the pump assumed independent of pressure.

$p_e$  = Component of total pressure due to evaporation of molecules from the pump (adsorbent).

$p_o$  = Component of total pressure due to inherent system outgassing, leakage, etc. (virtual leaks).

From equation (9) it is seen that

$$V \frac{dp}{dt} = Q - S(p - \bar{p}) \quad (10a)$$

The determination of pumping speed by the steady-state technique assumes  $dp/dt = 0$  and hence

$$S = \frac{Q}{(p_{ss} - \bar{p})} \quad (11)$$

where  $p_{ss}$  is the observed steady-state pressure. Equation 11 is identical to that used in the present study wherein  $\bar{p}$  is replaced by  $p_o$  for reasons discussed above.

The determination of pumping speed by the pumpdown technique assumes that  $Q = 0$  which from Figure 11 is satisfied when  $t \geq t_t$  (termination of leak rate) and hence  $p \leq p_{ss}$ .

$$\therefore S = - \frac{2.303V}{(t - t_t)} \log_{10} \left[ \frac{(p - \bar{p})}{(p_{ss} - \bar{p})} \right] \quad (12)$$

Thus the pumping speed can be evaluated from experimental data by a plot of

$$\text{LOG}_{10} \left[ \frac{(P - \bar{P})}{(P_{ss} - \bar{P})} \right] \text{ VS } (t - t_t)$$

which should be linear with slope =  $-\left[\frac{S}{2.303V}\right]$

Since the above treatments assume the pumping speed to be constant for the pressure ranges investigated, an analysis of the interrupted flow technique plot, at least for a conventional pump, should allow evaluation of  $S$  by both methods. It has been shown<sup>5,6</sup> that the pumpdown technique analysis for a cryosorption pump does not yield a linear plot for the described function; rather an expression possessing three exponential terms is required. It is of interest to note, however, that a plot of this type for the observed data of the study yielded an initial, instantaneous linear portion whose slope indicated a pumping speed typically three orders of magnitude less than that observed by the steady-state technique prior to gas termination. This result is illustrated in Figure 26. If this pump had obeyed equation (12) and possessed the speed determined by the steady-state method, the change in pressure would have been defined by the dotted curve. This marked deviation between pumping behavior of the cryosorption pump and conventional units has led to a further examination of the cryosorption pumping model.

## 5.2 Model of Cryosorption Pumping

### 5.2.1 General Considerations

The discussion of the previous section as well as the observed experimental results relative to time reductions in pumping speed require further analysis of the pumping model for cryosorption.

In the prior study<sup>2</sup>, data analysis generally assumed that the imposed gas loadings were sufficiently small and diffusion rate through the adsorbent bed was rapid enough that uniform bed loading was attained during all phases of gas inleakage. Under these conditions, therefore, the definition of an instantaneous evaporation pressure,  $P_e$ , from the surface approximated that of an equilibrium adsorption pressure for the mass of adsorbent present. It was pointed out that this convention assumed one could meaningfully discuss an equilibrium pressure during a dynamic pumping process. Since surface coverage during these tests was purposely controlled at low levels, the resulting value of  $P_e$  was assumed quite small and, since typically  $P \gg P_0$

equation (10) was rewritten such that

$$V \frac{dP}{dt} = Q - SP \quad (13)$$

and for a unit area of cryosorption panel, combination of (13) with (4) yields

$$V \frac{dP}{dt} = Q - \alpha S_t P \quad (14)$$

and in the steady-state region

$$\alpha = \frac{Q}{S_t P} \quad (15)$$

In view of the results obtained in the present study, i.e., discrepancy in speed values when comparing experimental results by the two analytical techniques for a given test, a revision of previous assumption was made.

It is suggested that the following conditions apply:

- a. Although adsorbate loadings are small, it is assumed that diffusion of adsorbate throughout the bed is rate limiting and that uniform loading of the entire adsorbent mass is not achieved during continuous gas in-leakage. Rather, it is proposed that a small surface layer of the panel effectively exhibits uniform loading and that the concentration in the inner portion of the bed does not change significantly from that prior to inleakage. Under these conditions, a steady-state will be established with an associated  $P_e$  for the saturated surface volume which is not necessarily negligible.
- b. Since loadings are small, the Langmuir<sup>9</sup> theory would predict a sticking coefficient approximating unity and it is assumed this result applies for the experimental conditions employed.
- c. Although the sticking coefficient is assumed to approximate unity, the competing effect of a relatively large evaporation pressure during gas in-leakage makes it desirable to define a new parameter,  $E$ , such that

$$E = S \left( 1 - \frac{P_e}{P - P_e} \right) \quad (16)$$

where  $P_e$  is the equilibrium pressure associated with the saturated surface layer. Physically  $E$ , the net evacuation rate, quantifies the volumetric

rate of removal of molecules from the system (rate of adsorption minus the rate of evaporation), whereas  $S$  is the rate of adsorption. Since  $\alpha$  is assumed equal to unity, from equation (4),  $S = S_t$ . Hence, if  $P_e \ll (P - P_0)$ ,  $E$  approaches  $S_t$  (the theoretical speed); if however  $P_e \simeq (P - P_0)$ ,  $E$  approaches zero.

Substitution of (16) into (10) yields

$$V \frac{dP}{dt} = Q - E(P - P_0) \quad (17)$$

hence under steady-state conditions ( $dp/dt = 0$ )\*,

$$E = \frac{Q}{(P_{ss} - P_0)} \quad (17a)$$

Since the proposed model assumes a unity sticking coefficient ( $S = S_t$ ), from equation (16) it is observed that for

$$\frac{E}{S_t} \simeq 0$$

which is approximated when net speeds of about 1200 liters per second-sq. ft. are obtained

$$\frac{P_e}{(P - P_0)} \simeq 1 \quad \text{OR} \quad (P - P_0) \simeq P_e$$

This development predicts that the pressure observed during gas inleakage for a panel exhibiting a low net speed value is essentially defined by evaporation of mass from a uniformly loaded surface volume.

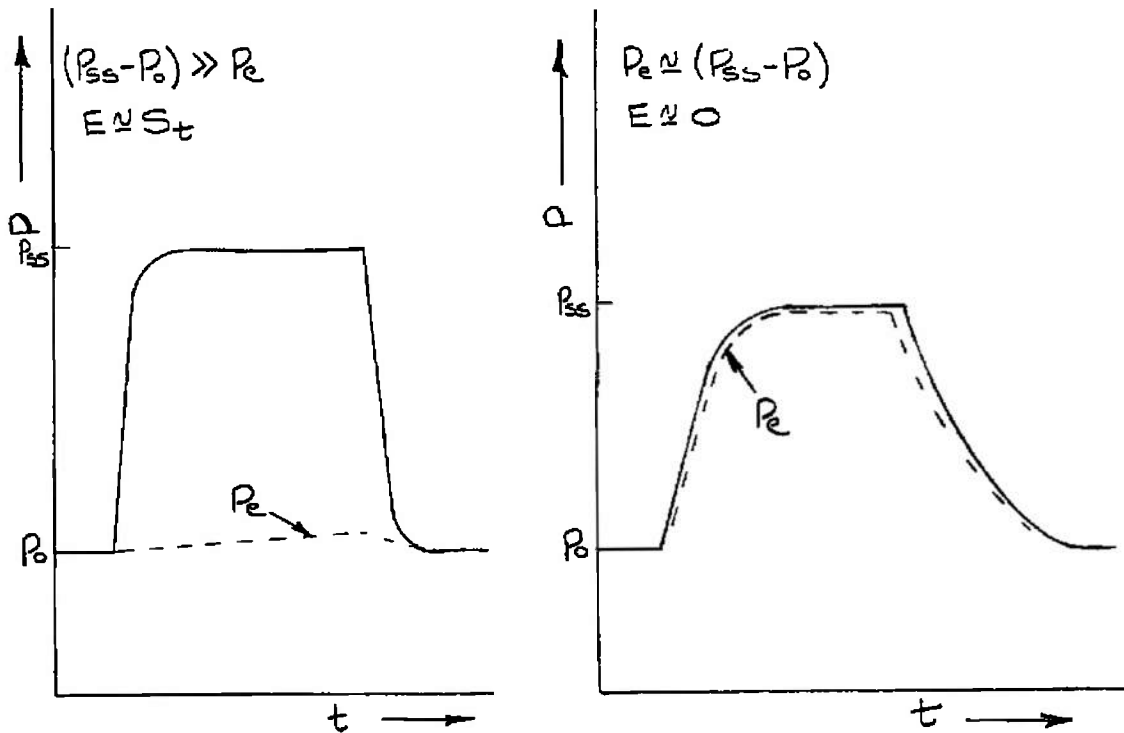
A second limitation on these conditions is defined by

$$\frac{E}{S_t} \simeq 1 \quad \text{OR} \quad E = S_t$$

---

\* Earlier, in equation (3),  $S$  was defined by the same relation expressed in (17a). This notation was selected for convenience to avoid misunderstanding until the concept of a net evacuation rate,  $E$ , could be logically introduced. However, all reported speed values were calculated from the relation expressed in (17a) and hence reflect net speed values.

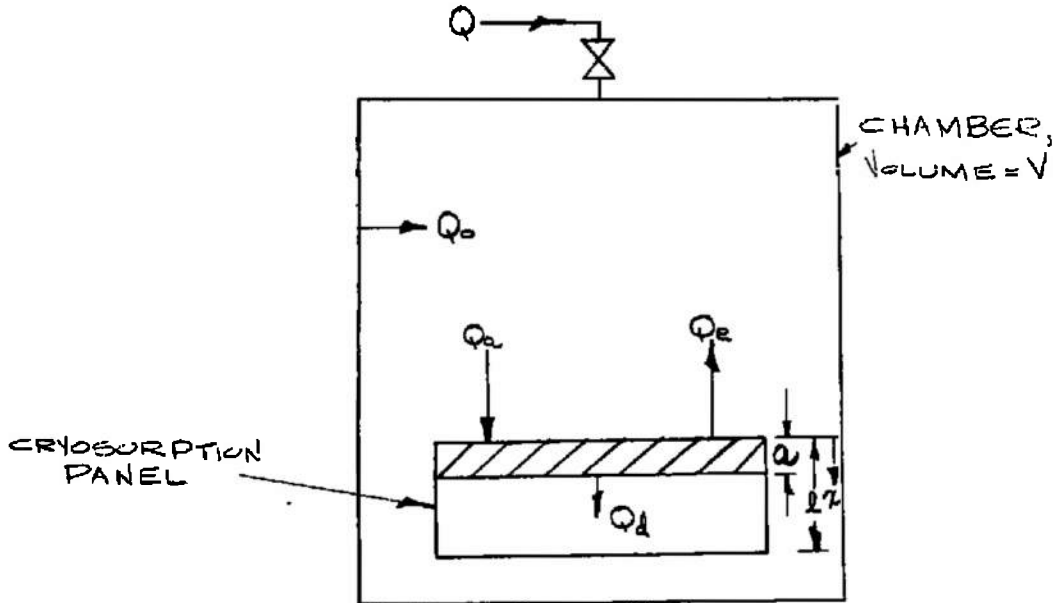
In this situation, the observed pressure is defined by the maximum rate of mass transfer to the pumping panel, i. e.,  $P_e \approx 0$ . These limiting cases are illustrated below.



If this model were accurate, one might reasonably expect that observed pumping speed reduction was related, at least in part, to factors influencing the diffusion step in the overall pumping mechanism. As a consequence, a cryosorption pumping model based on the assumptions outlined above was developed.

### 5.2.2 Development of Pumping Equation for a Diffusion Controlled Mechanism

Consider the system pictured below:



- $Q$  = Controlled inleak rate\*
- $Q_o$  = Inherent system load (leakage, outgassing, permeation, etc.)
- $Q_a$  = Surface adsorption rate
- $Q_e$  = Surface evaporation rate
- $Q_d$  = Rate of diffusion of adsorbate from saturated surface into bulk of adsorbent bed (diffusion assumed unidirectional in x direction).
- $a$  = Thickness of the saturated surface layer.
- $l$  = Adsorbent bed thickness

\* All parameters denoted by  $Q$  have units of  $\frac{\text{pressure-volume}}{\text{time}}$ .

From the model assumption of  $\alpha = 1$ , an overall system mass balance may be written whereby

$$\left[ \begin{array}{c} \text{Rate of} \\ \text{Accumulation in} \\ \text{Chamber Volume} \end{array} \right] = \left[ \begin{array}{c} \text{Rate of} \\ \text{Inleak} \end{array} \right] + \left[ \begin{array}{c} \text{Rate of} \\ \text{Inherent} \\ \text{Load} \end{array} \right] + \left[ \begin{array}{c} \text{Rate of} \\ \text{Evapo-} \\ \text{ration} \end{array} \right] - \left[ \begin{array}{c} \text{Rate of} \\ \text{Adsorp-} \\ \text{tion} \end{array} \right]$$

or 
$$V \frac{dP}{dt} = Q + Q_o + Q_e - Q_a \quad (18)$$

An analysis of the mass balance associated with the cryosorption panel indicates that

$$Q_a = Q_e + Q_d \quad (19)$$

Thus

$$\boxed{V \frac{dP}{dt} = Q + Q_o - Q_d} \quad (20)$$

This relation is the basic pumping equation for the proposed cryosorption pumping mechanism. Its form, however, is not amenable to analysis relative to interrupted flow technique parameters. Further treatment is best effected by individual consideration of  $Q_d$  during the steady-state ( $dp/dt = 0$ ) and pumpdown ( $Q = 0$ ) regions as discussed in the subsequent Sections (5.2.2.1 - 2).

From the above considerations, it is observed that

$$Q_a = Q + Q_o + Q_e \text{ for the steady-state region}$$

and

$$Q_a = Q_o + Q_e - V dp/dt \text{ for the pumpdown region.}$$

In general, however, since  $\alpha = 1$

$$Q_a = S_t P \quad (21)$$

and

$$Q_e = S_t P_e \quad (21a)$$

where  $P_e$  is the equilibrium adsorption pressure for the saturated volume defined by unit area and bed thickness,  $a$ . When low net pumping speeds are observed, the model assumptions indicate that (see Section 5.2.1),

$$P_e \simeq P$$

Hence, the value of " $a$ " can be estimated by the following procedure. Since  $P \simeq P_e$ , reference to the equilibrium adsorption isotherm for the hydrogen-Molecular Sieve 5A system at 20°K, shown as Figure 27, will yield a corresponding equilibrium capacity value,  $C_e^*$ . It is pointed out that the units of  $C_e$  are

$$\frac{(\text{pressure} - \text{volume of adsorbate})}{\text{volume of adsorbent}}$$

Thus,

$$a = \frac{Q t'}{C_e A} \quad (22)$$

where  $t'$  = time from initiation of a gas inleak,  $Q$ , to attainment of a steady-state pressure.

---

\* Note that the isotherm lists data corrected for the thermomolecular effect (see reference 11 for a discussion of this phenomenon) whereas pressures measured in the experiments were at ambient levels. Hence, in order to use the isotherm data correctly, observed pressures had to be corrected in the following manner.

$$P_e \text{ (from isotherm)} = (P \text{ observed}) \left[ \sqrt{\frac{20^\circ\text{K}}{300^\circ\text{K}}} \right]$$

Rearrangement of equation (22) yields

$$C_e = \frac{Qt'}{aA} \quad (23)$$

From the experimental data of the isotherm, it is observed that

$$C_e = kp^n \text{ (Freundlich}^8 \text{ relation)} \quad (23a)$$

The values of  $k$  and  $n$  evaluated from Figure 27 are:

$$k = 2.85 \times 10^4 \frac{\text{atm} - \text{cm}^3}{\text{gram} - \text{Torr}^n} \quad p < 6 \times 10^{-7} \text{ Torr}^{**}$$

$$k = 5.39 \times 10^2 \frac{\text{atm} - \text{cm}^3}{\text{gram} - \text{Torr}^n} \quad 6 \times 10^{-7} < p < 1 \times 10^{-4} \text{ Torr}$$

$$n = 0.5 \quad p < 6 \times 10^{-7} \text{ Torr}$$

$$n = 0.15 \quad 6 \times 10^{-7} < p < 1 \times 10^{-4} \text{ Torr}$$

#### 5.2.2.1 Pumping Equation in the Steady-State Region

In the steady-state region,  $dp/dt = 0$ , and the concentration in the saturated surface layer is constant. Under these conditions, one can apply Fick's first law of unidirectional flow<sup>15</sup> in a solid to the proposed cryosorption pumping model. At constant temperature, this relation is expressed by

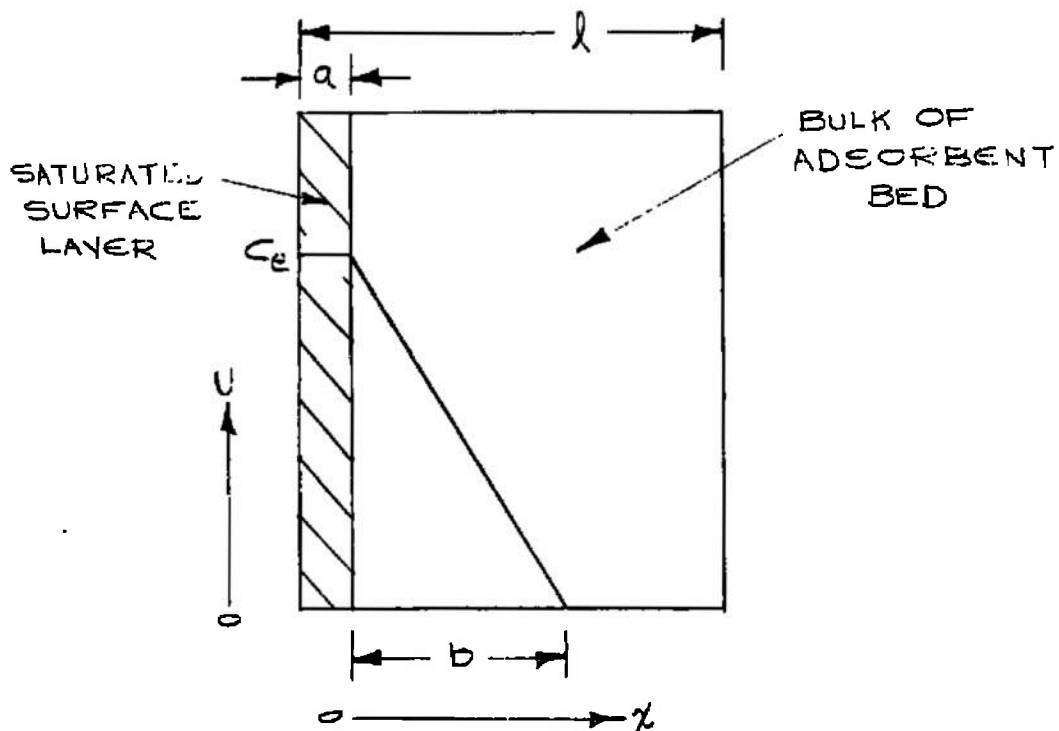
$$Q_d = -DA \frac{dc}{dz} \quad (24)$$

---

\*\* Pressures corrected for thermomolecular effect.

- where  $Q_D$  = Rate of mass transfer through the adsorbent bed by a diffusional mechanism in the x direction under the influence of a constant concentration gradient.
- $D$  = Characteristic diffusion constant, assumed independent of concentration.  $D$  is a function of the particular gas-solid system and temperature only. Note that  $D$  has units of area/time.
- $A$  = Area of adsorbent panel normal to flow
- $\frac{dc}{dx}$  = Concentration gradient

Application of this relation to the system of interest is seen by reference to the figure below.



- a = Thickness of the saturated surface layer
- b = Thickness of the concentration gradient front
- l = Adsorbent bed thickness
- $C_E$  = Concentration of the saturated surface layer under steady-state conditions

Equation (24) can be integrated for the boundary conditions that

$$C = C_E \text{ at } x = 0 \text{ for all } t$$

$$C = 0 \text{ at } x = b \text{ for all } t$$

$$Q_d \int_0^b dx = -DA \int_{C_E}^0 dC$$

Integrating

$$\boxed{Q_d = DA \frac{C_E}{b}} \quad (25)$$

Equation (25), therefore, expresses the functional dependence of the cryo-sorption pumping rate in the steady-state region. From (20), it is observed that in the steady-state region

$$Q_d = Q + Q_o \quad (26)$$

Since  $Q_o$  is generally small relative to  $Q$ , equation (25) may be rewritten as:

$$D = \frac{Qb}{AC_E} \quad (27)$$

A dimensional check\* of this relation indicates that  $D$  has units of  $\text{cm}^2/\text{sec}$ . which agree with reported<sup>15</sup> units. The value of  $Q_D$  could be estimated, therefore, if independent evaluation of  $D$  and  $b$  could be effected. In the subsequent section, a method is developed for calculation of  $D$  from analysis of the pumpdown portion of the interrupted flow technique curve. On the assumption that an accurate value of  $D$  can be obtained from that method,  $b$  could be estimated by rearrangement of (27)

$$b = \frac{DAC_e}{Q} \quad (28)$$

#### 5.2.2.2 Pumping Equation for Pumpdown Region

During the pumpdown region on an interrupted flow technique plot  $dp/dt \neq 0$  and hence, the concentration in the saturated surface layer is not constant. As a consequence, the former relationship (see Section 5.2.2.1) utilized to analyze the steady-state situation is no longer applicable. This region can, however, be expressed by Fick's second law which takes the form:

$$\frac{dC}{dt} = DA \frac{d^2 C}{dz^2} \quad (29)$$

where  $D$  is again assumed independent of concentration.

Dushman<sup>11</sup> reports a solution of this equation for the rate at which gas diffuses into a solid such that

$$Q_d = C_0 A \left( \frac{D}{\pi} \right)^{1/2} \left( \frac{1}{t} \right)^{1/2} \quad (30)$$

where  $C_0$  = the concentration at the surface.

It is seen that for the proposed model,  $C_0 = C_e$  and  $C_e$  is defined by equation (23a) as a function of pressure. If the observed steady-state pumping speed is small relative to  $S_t$ , then from considerations discussed in Section 5.2.1,  $C_e$  is directly related to the observed pressure by

$$C_e = kp^n$$

\*

$$\left[ \frac{\text{CM}^2}{\text{SEC}} \right] = \frac{\left[ \frac{\text{ATM-CM}^3}{\text{SEC}} \right] [\text{CM}]}{[\text{CM}^2] \left[ \frac{\text{ATM-CM}^3}{\text{CM}^3} \right]} \quad (31)$$

Hence,

$$Q_d = \left[ kA \left( \frac{D}{\pi} \right)^{1/2} \right] P^m t^{-1/2} \quad (32)$$

During pumpdown, since  $Q = 0$ , equation (20) is written as:

$$V \frac{dP}{dt} = Q_0 - \left[ kA \left( \frac{D}{\pi} \right)^{1/2} \right] P^m t^{-1/2} \quad (33)$$

Initially, the contribution to pressure change by  $Q_0$  is small because of the relatively low value of  $Q_0$ . Therefore, equation (33) can be simplified to

$$V \frac{dP}{dt} = - \left[ kA \left( \frac{D}{\pi} \right)^{1/2} \right] P^m t^{-1/2} \quad (34)$$

Let

$$\beta = kA \left( \frac{D}{\pi} \right)^{1/2} \quad (34a)$$

For the range of pressures of experimental tests,  $n = 0.5$  (see Section 5.2.2).

$$\begin{aligned} V \int_{P_{ss}}^P P^{-1/2} dP &= -\beta \int_0^t t^{-1/2} dt \\ (P_{ss}^{1/2} - P^{1/2}) &= \left( \frac{\beta}{V} \right) t^{1/2} \end{aligned} \quad (35)$$

Hence of plot of  $[(P_{ss})^{1/2} - (P)^{1/2}]$  versus  $t^{1/2}$  should be linear with slope,  $m$ , for reasonable values of time, i. e., before the contribution of  $Q_0$  to pressure change becomes significant,

$$m = \frac{\beta}{V} \quad (36)$$

From relations (34), (34a), and (35),

$$D = \pi \left[ \frac{mV}{kA} \right]^2 \quad (37)$$

Consistent units for this expression are

$$D, \quad \text{cm}^2/\text{sec.}$$

$$m, * \quad \frac{\text{Torr}}{(\text{Torr}^{1/2}) (\text{Sec.}^{1/2})}$$

$$V, \quad \text{liters (chamber volume = 360 liters)}$$

$$k, \quad \frac{\text{Torr} - \text{liters}}{\text{cm}^3 - \text{Torr}^{1/2}}$$

$$A, \quad \text{cm}^2$$

$$\text{Hence,} \quad D = (5.0 \times 10^{-10}) \text{ m}^2 \text{ (Panel 2)} \quad (38)$$

$$D = (3.2 \times 10^{-9}) \text{ m}^2 \text{ (Panel 3)} \quad (39)$$

Figures 28, 29, 30, and 31 are plots of equation (35) for various experimental tests. The diffusion constants calculated from these plots are summarized in Table VII together with the corresponding values of  $b$  obtained from equation (28). This table also lists values of other pertinent experimental parameters.

The data of Table VII indicate  $D$  and hence  $b$  are functions of concentration. Thus, the model assumption of a constant  $D$  is incorrect. This result is not surprising, since Barrer<sup>15</sup> reports that very frequently this situation occurs and he cites the diffusion of water in zeolites as a typical example. Mathematical treatment and evaluation of this phenomenon is, however, quite complex. The simple model discussed in this report was meant to reflect a first approximation to definition of the pumping speed-diffusion rate relationship for cryosorption pumping. More rigorous treatment is required to develop an accurate model.

A qualitative analysis of the results indicates, however, a direct relationship between pumping speed and the observed diffusion constant. Figures 32 and 33 are plots of  $D$  and  $b$  as a function of concentration (expressed as equilibrium pressure for the saturated surface layer). It is observed that for a given concentration, the diffusion constant for Panel 3 exhibiting a speed of 8000 to 9100 liters/sec.-sq. ft. is approximately ten times larger

---

\* Dimensions of  $m$  are

$$\frac{(\text{pressure})^{1-n}}{\text{sec.}^{1/2}} = \frac{(\text{pressure})}{(\text{pressure})^n (\text{sec.})^{1/2}}$$

than the corresponding value for this panel when it possessed a net speed of 1200 to 1600 liters/sec.-sq. ft. In addition, the results for Panel 2 when it possessed a speed of 2500 to 3300 liters/sec.-sq. ft. correlate well insofar as diffusion constant value is concerned. It is interesting to note that in Figure 33, the calculated value of  $b$  for Panel 2 at a given concentration is less than the corresponding value of Panel 3 for both cases. The interpretation of this effect is discussed in Section 5.3 and is believed related to the relative adsorbent mass of Panels 2 and 3. An attempt to verify the accuracy of reported values for the "D" and "b" parameters is difficult since no published data for hydrogen diffusion in solids at cryogenic temperature levels were found which approximated the proposed model.

Extensive data have been published for diffusion in metals, glasses, plastics, and rubbers at ambient and above temperature levels. (See, for example, references 11 and 15 for a summary of these investigations.) In general, it may be concluded from investigation of this work that the temperature dependence of the diffusion constant is given by an equation of the form

$$D = D_0 \exp\left(\frac{-E_a}{RT}\right) \quad (40)$$

where	$D_0$	=	Characteristic constant of the gas-solid system
	$E_a$	=	Activation energy
	$R$	=	Universal gas constant
	$T$	=	Absolute temperature

The activation energy is usually found to be a constant over reasonably small temperature ranges; however, Barrer<sup>15</sup> reports that he, as well as numerous other investigators, has reported that  $E_a$  is a function of temperature over extended temperature ranges.

Tiselius<sup>16</sup> reports a value of  $2.7 \times 10^{-7}$  cm<sup>2</sup>/sec. for the diffusion of water in zeolite (heulandite) at 20°C and an activation energy of 5400 cal./mole for the range of 20 to 75°C. Barrer reports a value of about  $1 \times 10^{-6}$  cm<sup>2</sup>/sec. for the diffusion of hydrogen in silica at about 20°C with an activation energy of about 4000 cal./mole. If it is assumed that hydrogen diffusion in Molecular Sieve at 20°C approximates  $10^{-6}$  to  $10^{-7}$

cm<sup>2</sup>/sec., then an activation energy of 500 to 1000 cal./mole would be predicted from the observed values of 10<sup>-18</sup> to 10<sup>-19</sup> cm<sup>2</sup>/sec. at 20° K. Since E<sub>a</sub> for the hydrogen-silica system has been reported to decrease with absolute temperature, these results are not unreasonable. It is appreciated that more precise determination of D by alternate techniques is necessary to establish the accuracy of these values.

The calculated values of "b" however, which has been defined physically as the thickness of concentration gradient front, appear unrealistically small. This parameter is evaluated from equation (28) and is dependent on the calculation of "D", the diffusion constant. From equation (37) it is observed that

$$D \propto \frac{1}{A^2}$$

In the analysis, the selected area term corresponded to the geometrical panel area. Further consideration of the model ramifications indicate this assumption is inaccurate. Synthetic zeolites such as Molecular Sieve 5A are characterized by a three dimensional network consisting of relatively large cavities wherein the bulk of the adsorbate is contained. These cavities are interconnected by relatively small channels through which the adsorbate must pass before entering the cavities and it is believed that the integrated area of these pores normal to gas inleakage flow more closely approximates the model description of area. Since this area is considerably smaller than the assumed area values, actual values of "D" and "b" should be much larger than those tabulated in this report. Further refinement in this respect is required to verify the reasonableness of the proposed model.

### 5.2.3 Deviation From Steady-State Pumping Behavior

Equation (26) predicts that for Q<sub>0</sub> small relative to Q, in the steady-state region

$$Q_D = Q$$

From (25)

$$\frac{Q_D}{A} = D \left( \frac{C_e}{b} \right)$$

Figures 32 and 33 give the empirical pressure dependence of "D" and "b" and the pressure dependence of  $C_e$  can be obtained from the isotherm; hence the pressure dependence of  $Q_D$  can be approximated.  $Q$ , of course, is independent of pressure and a plot of  $Q$  versus pressure for a pump of constant pumping speed is linear. Figure 34 is a plot of  $Q$  and  $Q_D$  versus pressure for adsorbent panels exhibiting different pumping speeds. As the loading per unit panel area increases, the plot of  $Q_D$  versus pressure deviates from linearity and for a given pressure,  $Q > Q_D$ . From equation (20), for  $Q \gg Q_0$ , it is observed that a pressure rise is predicted ( $dp/dt > 0$ ) if  $Q > Q_D$ .

Figure 34 predicts a deviation from attainment of a steady-state pressure value for a panel whose speed at low gas loadings is 8000 - 9100 liters/sec. - sq. ft. (Panel No. 3) if the imposed gas loading exceeds  $(20 \times 10^{-7})$  Torr-liters/sec. - square centimeter. Since this panel has an area of 464 square centimeters, this load corresponds to a  $Q$  of 56 micron-liters per minute. Analysis of Figure 22, which depicts actual pressure-time data for this panel when a speed of 8000 - 9100 liters/sec. - sq. ft. was observed, indicates a pressure rise for  $Q$  of 127 micron-liters per minute in agreement with the data of Figure 34. No rise was detected however for  $Q$  of 73 micron-liters per minute. Since the plot of Figure 34 is based on empirical data, its accuracy may not detect differences between 56 and 73 micron-liters per minute. Better agreement was obtained when comparing predicted pressure behavior for this panel when a speed of 1200 - 1600 liters/sec. - sq. ft. was observed. Figure 34 predicts this deviation if  $Q$  exceeds 17 micron-liters per minute. Experimental results with this panel (Figure 24) agree well with this prediction.

The data of Figure 34 predict attainment of steady-state pressures for Panel No. 2 ( $A = 1180$  square centimeters) if  $Q$  is less than 85 micron-liters per minute. Figures 14 to 17 summarize pressure-time data for this panel. Steady-state pressures were obtained in all runs for leak rates as large as 80.5 micron-liters per minute.

A closer analysis of the pressure dependence of  $Q_D$  indicates that the  $C_e$  term strongly influences the function and its tendency toward non-linearity as gas loading per unit area is increased. This effect is a direct consequence of the decrease in value of the Freundlich isotherm constants (see Section 5.2.2) as pressure is increased. This observation is most significant in the sense that a direct correlation is implied between equilibrium isotherm data and dynamic pumping speed behavior. Specifically, it would appear that an adsorbent whose equilibrium isotherm for a given adsorbate approaches

Henry's Law ( $n = 1$ ) for the vacuum region is more desirable as a constant speed pump than an adsorbent which reflects a Freundlich isotherm, even though the latter solid may exhibit larger equilibrium loadings per unit mass for the same pressure region.

### 5.3 Summary of Analytical Results

The analytical approach developed in this report represents a first approximation attempt to consideration of dynamic cryosorption pumping as a mechanism in which adsorbent bed diffusion of adsorbate is rate limiting. The discussion has indicated areas where model refinement is necessary. There is, however, qualitative evidence that the observed net pumping speeds are directly related to diffusion parameters and, hence, factors which adversely affect these variables might be expected to produce corresponding reductions in net pumping speeds.

Time did not permit further experimental examination of the observed pumping speed reduction in terms of the diffusion rate limitation. It may be concluded from the rate expression that reduction can be caused by decrease in  $D$ , increase in  $b$ , or a combination of these two circumstances. A decrease in  $D$  could be conceivably effected by a reduction in available pore size opening caused by undesirable cation rearrangement. This possibility was discussed earlier in Section 4.1. Perhaps a more likely possibility involves consideration of experimental techniques which may cause an increase in  $b$  or, more accurately, a decrease in the concentration gradient front.

Hemstreet<sup>2</sup> reported a decrease in  $\alpha$  (sticking coefficient) when Molecular Sieve 5A panels were preloaded at 20° K with quantities of hydrogen. Since  $\alpha$  is proportional to the observed net pumping speed,  $E$ , a loading of this type, in effect, produces results similar to reduction in pumping speeds observed for successive tests. The pertinent effect of a preloaded panel in terms of the proposed model is that the concentration gradient for the diffusion mechanism would be decreased. An apparent result of this effect would be a quantitative increase in the observed value of  $b$ . These considerations imply that the conditioning, i. e., activation of panels, utilized in these tests may not have effectively removed all hydrogen adsorbed at lower temperatures and that a cumulative increase in hydrogen concentration resulted. The feasibility of this postulate may be questioned when consideration is given to the temperature levels, e. g., 200° C, of activation. There is, however, the possibility that two competing mechanisms function to minimize hydrogen desorption, e. g.,

- a. The temperature dependence of  $E_a$ , described in Section 5.2.2.2, would produce a hysteresis effect in the sense that the rate of diffusion of

hydrogen from a panel at higher temperatures would not be as large as predicted by the rate of diffusion during adsorption at 20° K.

- b. At higher temperatures, hydrogen present within the adsorbent matrix may be chemisorbed hence decreasing the probability of desorption.

If cumulative retention of hydrogen within the adsorbent bed resulting in a decrease in concentration gradient were the unique cause of pumping speed reduction, it would appear that the effect should be less pronounced as the mass of adsorbent is increased. Panel No. 2 had a mass approximately 20 times that of Panel No. 3\*. The experimental results indicate that the rate of speed reduction for Panel No. 3 with successive tests was considerably more pronounced than that for Panel No. 2. Furthermore, the calculated dependence of  $b$  on pressure for Panel No. 2 did not correlate to values for Panel No. 3 when considering the effect of net pumping speed (see Figure 33). If these considerations are correct, then more precise definition of activation conditions is required to minimize hydrogen concentration in the bed prior to cooldown and also to minimize any adverse cation rearrangements resulting from long high temperature activation periods.

A practical solution to this problem might involve use of mild activation periods (see Section 3.2.2) together with relatively large masses of adsorbent. The latter effect could be enhanced by utilization of the parallel plate configuration described in the former work<sup>2</sup>. Further optimization of these parameters is, however, required.

---

* Relative areas	-	1180 cm <sup>2</sup> for Panel No. 2, 464 cm <sup>2</sup> for Panel No. 3
Relative thickness	-	1/8 inch for Panel No. 2, 1/64 inch for Panel No. 3

## 6.0 APPLICATION OF CRYOSORPTION PUMPING AS AN UHV TECHNIQUE

Westbrock<sup>17</sup> and John<sup>18</sup> have discussed the practicability of cryosorption pumping as an ultrahigh vacuum technique. Specifically, arrays utilizing the mechanisms of cryopumping and cryosorption have been proposed as independent ultrahigh vacuum pumps. A schematic representation of such a design is pictured in Figure 35. Basically, the elements represented conform to the array utilized in the latter experiments of the present study (20°K shielded array). The specific function of these elements may be summarized as follows:

Liquid Nitrogen Shield	-	Cryopump high boiling species, i. e. , $H_2O$ , $CO_2$
Liquid Nitrogen Chevrons	-	Intercept radiant heat load to minimize helium consumption. Also function as a cryopump for $H_2O$ , $CO_2$ , etc.
Gaseous Helium Chevrons	-	Cryopump $O_2$ and $N_2$ to prevent loading of cryosorption panel. Thermal radiation shield for liquid helium cooled cryosorption panel (if applicable).
Gaseous (Liquid) Helium Cryosorption Panel	-	Cryosorption pumping of non-condensable gases

Since the cryogenic array is an example of an ultrahigh vacuum pump achieving pressure reduction by a retention of mass within the system (see Section 4.0), the capacity factor must be considered in an efficient system design. The initial consequence of this effect is the proper reduction of chamber pressure by an efficient roughing process.\* Initial chamber pressure can be effected by use of conventional mechanical pumps, or the combination of cryosorption rough pumps together with a cryogenic array may be utilized as described by Westbrock<sup>17</sup> to effect an all-cryogenic vacuum pumping process.

---

\* From this standpoint, the cryogenic array is similar to an oil-diffusion pump which cannot operate above a certain forepressure.

The obvious advantages of cryogenic-UHV pumping include relatively high pumping speeds together with an ultraclean environment. The ability to predict a practical loading limit on a cryosorption panel, thus maintaining a steady-state pumping speed for a given imposed gas influx, together with efficient activation conditions to maintain the initial near theoretical pumping speed values, should render this mode of vacuum pumping most attractive for practical use.

## 7.0 CONCLUSIONS

Consideration of the experimental results has led to the following conclusions:

1. The mechanism of dynamic cryosorption pumping involves adsorbent bed diffusion as the rate-limiting step.
2. When optimum conditions relative to diffusivity exist, near theoretical hydrogen pumping speeds result (i. e., sticking coefficients close to unity).
3. Effective adsorbent activation can be initially achieved with relatively mild conditions. Successive activations require further, precise definition to duplicate initial high pumping speed results.
4. The steady-state pumping performance of a cryosorption panel as a function of pressure will depend on the nature of the equilibrium adsorption isotherm, i. e., Henry's Law, Freudlich, Langmuir, etc.
5. It appears desirable that practical utilization of cryosorption pumping involve relatively mild activation periods together with large adsorbent masses per unit projected area.

## REFERENCES

1. S. A. Stern, J. T. Mullhaupt, F. S. DiPaolo, and L. Marasco, "The Cryosorption Pumping of Hydrogen and Helium at 20° K," AEDC-TDR-62-200, Interim Report, October (1962).
2. R. A. Hemstreet et al., *ibid.*, Final Report, AEDC-TDR-64-100, May (1964).
3. R. A. Hemstreet, D. J. Webster, W. J. Wirth, and J. R. Hamilton, "Research Study of the Cryotrapping of Helium and Hydrogen by Solid Oxygen and Nitrogen at 20° K," AEDC-TDR-62-199, October (1962).
4. A. E. Lennert, "Experimental Studies on Vacuum Cryosorption Pumping," AEDC-TDR-45, March (1962).
5. S. M. Kindall and E. S. J. Wang, "Vacuum Pumping by Cryosorption," Trans. Ninth Nat. Vac. Symp. (1962).
6. S. M. Kindall, "Study of Adsorption Rate in Vacuum Cryosorption," AEDC-TDR-62-80, June (1962).
7. S. M. Kindall, "Treatment of Vacuum Cryosorption," Trans. Tenth Nat. Vac. Symp. (1963).
8. H. Freundlich, *Kapillarchemie*, 1, Leipzig (1930).
9. Langmuir, J. Am. Chem. Soc., 40, 1361 (1918).
10. S. Brunauer, P. H. Emmett, and E. Teller, J. Am. Chem. Soc., 60, 309 (1938).
11. S. Dushman, Scientific Foundations of Vacuum Technique, Second Edition, J. M. Lafferty, Editor, John Wiley and Sons, New York (1962), Page 120.
12. Unpublished studies of the Research Department, Linde Division, Union Carbide Corporation.

## REFERENCES

(Continued)

13. J. P. Dawson, J. D. Haygood, and J. A. Collins, Jr., ARO, Inc., Cryogenic Engineering Conference, August (1963).
14. R. A. Hemstreet, S. A. Stern, et al., Contract AF 40(600)-944, Monthly Progress Report No. 23, March (1963).
15. R. M. Barrer, Diffusion In and Through Solids, Cambridge Press (1951).
16. A. Z. Tiselius, Z. Phys. Chem., 169A, 425 (1935).
17. A. J. Westbrook, Linde Division, Union Carbide Corporation, Presentation to the Northwest Regional Meeting, Institute of Environmental Sciences, November (1963).
18. J. E. A. John and W. F. Hardgrove, Goddard Space Flight Center, "Creation of Space Vacuum Utilizing Cryogenic Techniques," Annual Symp. Inst. Envir. Sci., March (1964).
19. C. W. Oatley, "The Flow of Gases Through Composite Systems at Very Low Pressures," Brit. J. Appl. Phys., 5, 358 (1954).

## APPENDIX A

### Derivation of Pumping Speed Relation For Baffled and Unbaffled Cryosorption Panels

The pumping speed equation used to determine net experimental values is given by equation (3) as

$$\frac{S}{A} = \frac{Q}{(P_s - P_0)}$$

This relation is based on the following considerations. Prior to inleak of a known gaseous hydrogen load to the system a constant base pressure was observed such that for a panel of unit area

$$P_0 = \frac{Q_0}{S}$$

Rearranging

$$Q_0 = P_0 S$$

For conditions of an interrupted flow experiment, the resulting pressure will therefore be defined as

$$P = \frac{Q + Q_0}{S} = \frac{P_0 S + Q}{S}$$

hence

$$S = \frac{Q}{(P - P_0)}$$

This derivation assumes  $S$  to be independent of pressure which is valid for the majority of pressures used in the investigation.

Values of  $S$ , or more correctly  $E$ , are reported in terms of a warm gas (approximately 300° K), unbaffled pumping speed. Calculation of the net available pumping speed for hydrogen for the baffled arrangement used in this test may be obtained in the following manner.

$$E = \theta S_t \quad (41)$$

**APPENDIX A**  
**(Continued)**

where  $\Theta$ , a dimensionless constant, is obtained from utilization of the Oatley<sup>19</sup> relation

$$\frac{1}{\Theta} = \frac{1}{g_1} + \frac{1}{g_2} + \frac{1}{\alpha} - 2 \quad (42)$$

$g_1, g_2$  = Conductances of the two chevron  
baffles

## APPENDIX B

## Analysis of Activation Time

For a system where the removal of gas from the adsorbent is limited by the rate evacuation of the system pump and not by desorption from the panel, the evacuation rate is given by

$$Q = PS \quad (43)$$

In an activation process for the removal of water,  $Q$  represents the throughput and under steady-state conditions

$$Q = - \left( \frac{RT}{M} \right) \left( \frac{dm}{dt} \right) \quad (44)$$

where  $M$  = Molecular weight

$dm/dt$  = Rate of mass removal per unit time

$$\therefore PS = - \left( \frac{RT}{M} \right) \left( \frac{dm}{dt} \right)$$

From the isotherms for adsorption of water on Molecular Sieve 5A

$$P = f \left( \frac{m}{W} \right) \quad (44a)$$

where  $W$  = mass of adsorbent

Hence,

$$\left( \frac{RT}{M} \right) \left( \frac{dm}{dt} \right) = - f \left( \frac{m}{W} \right) S$$

or

$$t = - \frac{RT}{MS} \int_{m_0}^m \frac{dm}{f \left( \frac{m}{W} \right)} \quad (45)$$

## APPENDIX B

(Continued)

$m_0$  = initial water loading

For regions of relatively low adsorbate coverage, Henry's Law applies and

$$P = \frac{m}{KW} \quad (46)$$

where  $K$  = characteristic constant

Integration of (43) under these condition gives

$$t = \frac{RTKW}{SM} \ln \frac{m_0}{m} \quad (47)$$

or

$$t = \frac{2.303 RTKW}{SM} \log_{10} \frac{m_0}{m} \quad (48)$$

From reported data<sup>2</sup>, the initial water content should be reduced to less than 5 weight per cent for efficient cryosorption pumping, preferably 2 per cent. Figure 36 is a plot of the time required to reduce water loading to approximately this level as a function of temperature based on isotherm data for the water-Molecular Sieve 5A system. This plot predicts that if large pumping speeds for desorbed water vapor are available (e.g., liquid nitrogen cooled surfaces), then the required activation time for the panels utilized in the study is of the order of minutes at 200° C.

TABLE I

**Design and Construction Characteristics  
of 77°K and 20°K Chevron Assemblies**

<u>Detail</u>	<u>77° K Chevron</u>	<u>20° K Chevron</u>
Material of Construction	Aluminum	E. T. P. Copper
Clausing Factor	0.260	0.185
Estimated Maximum Temperature Rise	<1.0° K	<0.1° K

TABLE II

Cryosorption Pumping of Hydrogen  
by Panel No. 1 at 20°K

<u>Hydrogen Leak Rate</u>		$(P_{ss} - P_o),$ <u>Torr x <math>10^8</math></u>	<u>E/A,</u> <u>Liters/Sec. -Ft<sup>2</sup></u>
<u>Micron-L</u> <u>Minute</u>	<u>Torr-L*</u> <u>Sec. -Ft<sup>2</sup> x <math>10^4</math></u>		
3.64	0.47	2.5	1880
10.9	1.39	8.7	1600
14.3	1.83	12.7	1440

---

\* The actual adsorbent pumping area for this panel is 1.3 ft<sup>2</sup> considering cross-milled grooves.

TABLE III

Cryosorption Pumping of Hydrogen by  
Panel No. 2 at 20°K, Activations 1-3

<u>Hydrogen Leak Rate</u>		$(P_{ss} - P_0),$ <u>Torr x 10<sup>8</sup></u>	<u>E/A,</u> <u>Liters/Sec.-Ft<sup>2</sup></u>
<u>Micron-L</u>	<u>Torr-L</u>		
<u>Minute</u>	<u>Sec.-Ft<sup>2</sup> x 10<sup>4</sup></u>		
<u>First Activation</u>			
14.9	1.91	3.8	5030
27.9	3.57	6.7	5330
43.7	5.59	10.6	5260
50.3	6.44	12.9	5000
72.1	9.23	19.1	4830
<u>Second Activation</u>			
5.7	0.73	3.0	2430
21.8	2.79	9.6	2900
33.1	4.24	14.6	2900
46.6	5.96	18.3	3260
60.2	7.70	28.1	2740
68.8	8.80	34.0	2590
80.5	10.3	40.5	2540
<u>Third Activation</u>			
5.6	0.77	6.7	1150
20.5	2.62	20.7	1270
48.2	6.16	49.5	1250

TABLE IV

Cryosorption Pumping of Hydrogen  
by Panel No. 2 at 20°K, Activation 4

<u>Hydrogen Leak Rate</u>		<u>(P<sub>ss</sub> - P<sub>o</sub>), Torr x 10<sup>8</sup></u>	<u>E/A, Liters/Sec.-Ft<sup>2</sup></u>
<u>Micron-L Minute</u>	<u>Torr-L Sec.-Ft<sup>2</sup> x 10<sup>4</sup></u>		
8.5	1.09	4.9	2220
23.5	3.08	13.9	2220
32.3	4.14	18.3	2260

TABLE V

Cryosorption Pumping of Hydrogen by  
Panel No. 3 at 20°K, Runs 3-5

Hydrogen Leak Rate		$(P_{ss} - P_o),$ <u>Torr x 10<sup>8</sup></u>	$E/A,$ <u>Liters/Sec. - Ft<sup>2</sup></u>
<u>Micron-L</u>	<u>Torr-L<sup>a</sup></u>		
<u>Minute</u>	<u>Sec. - Ft<sup>2</sup> x 10<sup>4</sup></u>		
<u>Run No. 3</u>			
127	42.1	45.0 <sup>b</sup>	9,400
73	24.2	25.9	9,300
33.5	11.1	11.0	10,100
<u>Run No. 4</u>			
47.5	15.7	17.9	8,800
26.7	8.9	10.5	8,500
<u>Run No. 5</u>			
42.9	14.2	114 <sup>b</sup>	1,250
9.2	3.1	19.6	1,560
15.3	5.1	41.6	1,210
25.2	8.4	69 <sup>b</sup>	1,220

a. Actual adsorbent pumping area for this panel is 0.5 ft<sup>2</sup>.

b. A steady-state pressure was not obtained. Value of  $(P_{SS} - P_O)$  is taken from extrapolation of linear portion back to initiation of gas inleak (see Section 4.2).

TABLE VI

Summary of Pumping Speed Results  
Panels 1, 2, and 3

<u>Test Number</u>	<u>Cumulative Activation Time<sup>a</sup>, Hours</u>	<u>E/A, Liters/Sec. -Ft<sup>2</sup></u>	<u>Remarks</u>
<u>Panel No. 1</u>			
1	96	1,640	Panel contaminated with oil
<u>Panel No. 2</u>			
1	185	5,100	Panel kept in chamber without air exposure between runs
2	255	2,620	
3	340	1,220	
4	380	2,230	Panel loaded with 20% water prior to test
<u>Panel No. 3</u>			
1	0.3	30,000 -40,000	Panel exposed to atmosphere after each test
2	0.6	30,000 -40,000	Panel exposed to atmosphere after each test
3	0.9	9,600	Panel exposed to atmosphere after each test
4	1.2	8,700	Panel exposed to atmosphere after each test
5	1.5	1,310	Panel exposed to atmosphere after each test

a. Activation conducted by circulation of hot gas (200° C) through the liquid hydrogen refrigeration pot.

TABLE VII

Summary of Pertinent Parameters for  
Cryosorption Pumping of Hydrogen

$\frac{Q}{\mu-1}$ Min.	$\frac{\text{Torr-L}}{\text{Sec.}-\text{Ft}^2}$	$t',$ Sec. $\times 10^{-3}$	$P_{ss},$ Torr $\times 10^8$	$CE$ $\frac{\text{Torr-L}}{\text{Cm}^3}$	$a,$ Cm $\times 10^5$	$\frac{D,2}{\text{Cm}^2}$ Sec. $\times 10^{18}$	$E$ $\frac{L}{S-\text{Ft}^2}$	$\frac{L}{S-\text{Cm}^2}$	$m,$ $\frac{\text{Torr}}{\text{Torr}^{1/2}-\text{Sec.}^{1/2}}$	$b,$ Cm $\times 10^{11}$	$P_o,$ Torr $\times 10^8$
<u>Run No. 3, 1/64" M.S. 5A-SS, A = (464 cm<sup>2</sup>) (0.5 ft<sup>2</sup>)</u>											
73	$2.42 \times 10^{-3}$	0.60	27	20.4	7.7	2.32	9300	9.7	$2.7 \times 10^{-5}$	1.8	1.1
<u>Run No. 4, Same Panel as Run No. 3</u>											
26.7	$0.89 \times 10^{-3}$	0.48	11.6	14.5	3.2	0.82	8000	8.6	$1.6 \times 10^{-5}$	1.2	1.1
47.5	$1.57 \times 10^{-3}$	0.90	19.2	17.9	8.6	1.55	8500	9.5	$2.2 \times 10^{-5}$	1.6	1.1
<u>Run No. 5, Same Panel as Run No. 3</u>											
9.2	$0.31 \times 10^{-3}$	1.02	26	20.4	1.7	0.19	1560	1.7	$7.7 \times 10^{-6}$	1.1	6.4
15.3	$0.51 \times 10^{-3}$	1.44	48	26.4	3.0	0.63	1210	1.3	$1.4 \times 10^{-5}$	3.0	6.4
<u>Run No. 2, 1/8" M.S. 5A - Aluminum Panel, A = (1180 cm<sup>2</sup>) (1.27 ft<sup>2</sup>)</u>											
21.8	$0.29 \times 10^{-3}$	0.66	12.8	14.5	1.4	0.07	2900	3.1	$1.2 \times 10^{-5}$	0.3	2.9
33.1	$0.43 \times 10^{-3}$	0.72	17.5	17.0	2.2	0.18	2900	3.1	$1.9 \times 10^{-5}$	0.6	2.9
46.6	$0.61 \times 10^{-3}$	0.90	22.0	18.7	3.5	0.39	3260	3.5	$2.8 \times 10^{-5}$	1.0	2.3
60.2	$0.71 \times 10^{-3}$	1.20	31.9	22.2	5.1	0.42	2740	2.9	$2.9 \times 10^{-5}$	1.0	2.4
80.5	$1.05 \times 10^{-3}$	1.80	45.0	25.5	8.8	0.84	2540	2.7	$4.1 \times 10^{-5}$	1.7	2.4

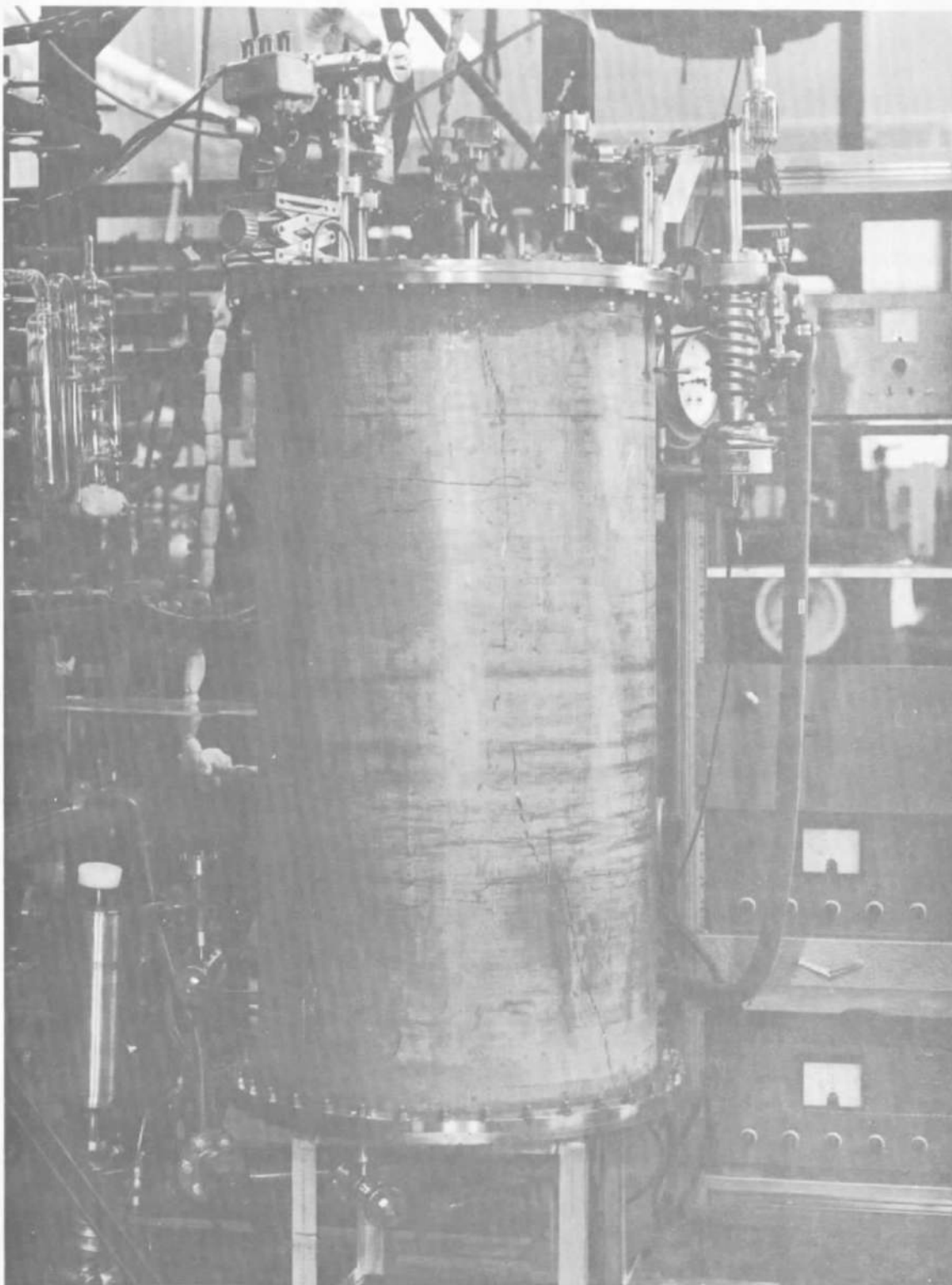


Fig. 1 Photograph of Cryosorption Research Apparatus



Fig. 2 Photograph of Liquid Nitrogen Cylindrical Shield and Top Chamber Flange

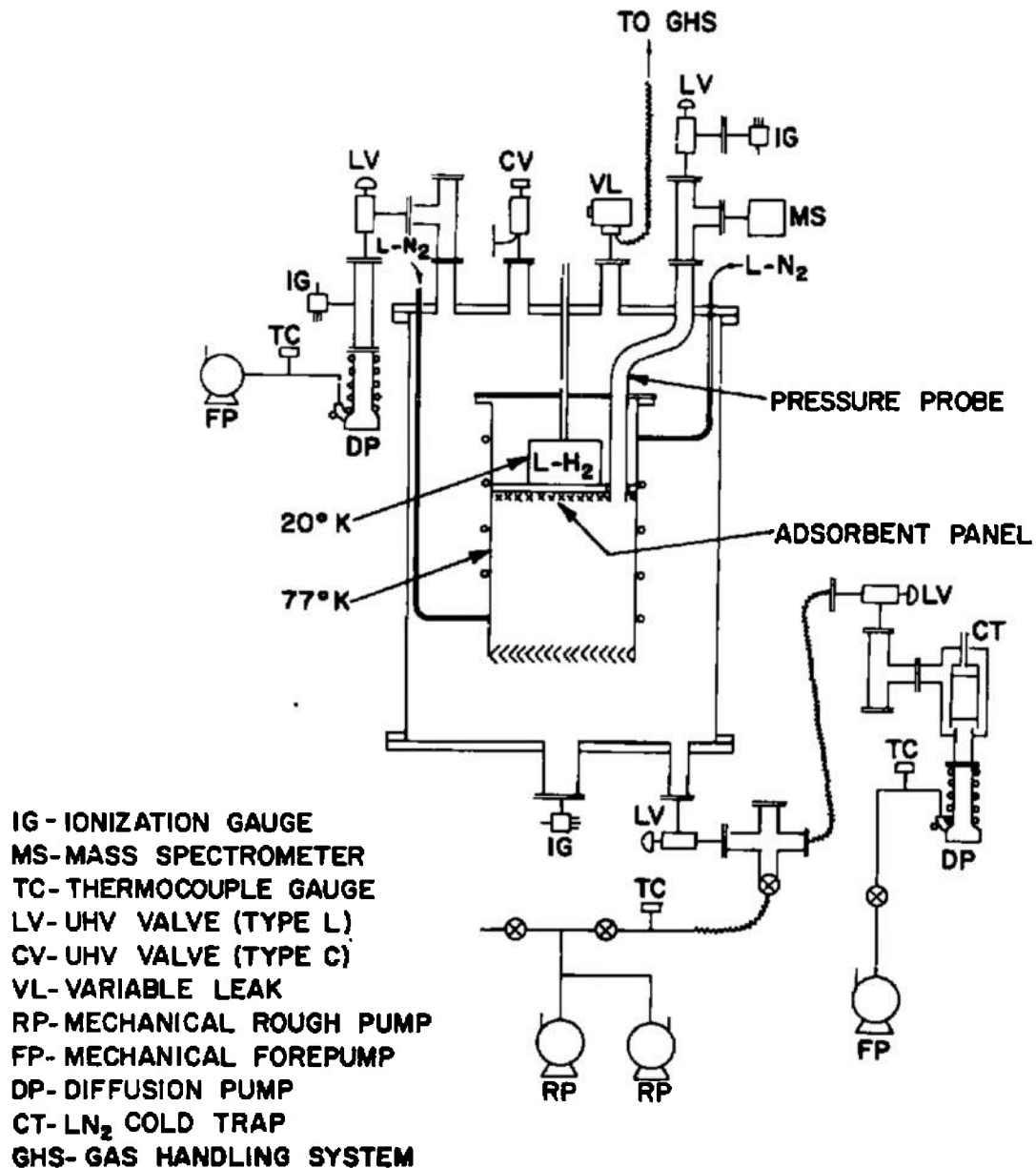


DIAGRAM OF APPARATUS FOR TESTING CRYOSORPTION PANELS. NOT TO SCALE

Fig. 3 Schematic of Vacuum Chamber and 77°K Shielded Array System

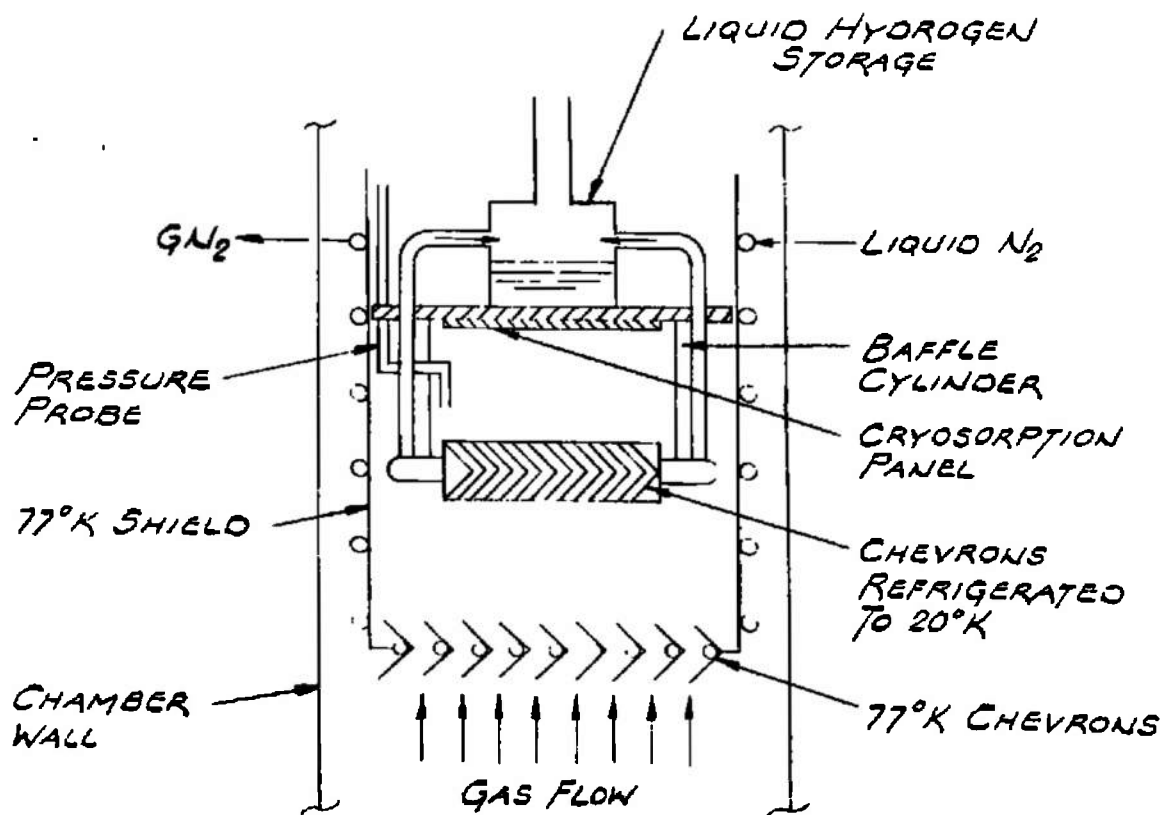


Fig. 4 Schematic of Vacuum Chamber and 20°K Shielded Array System

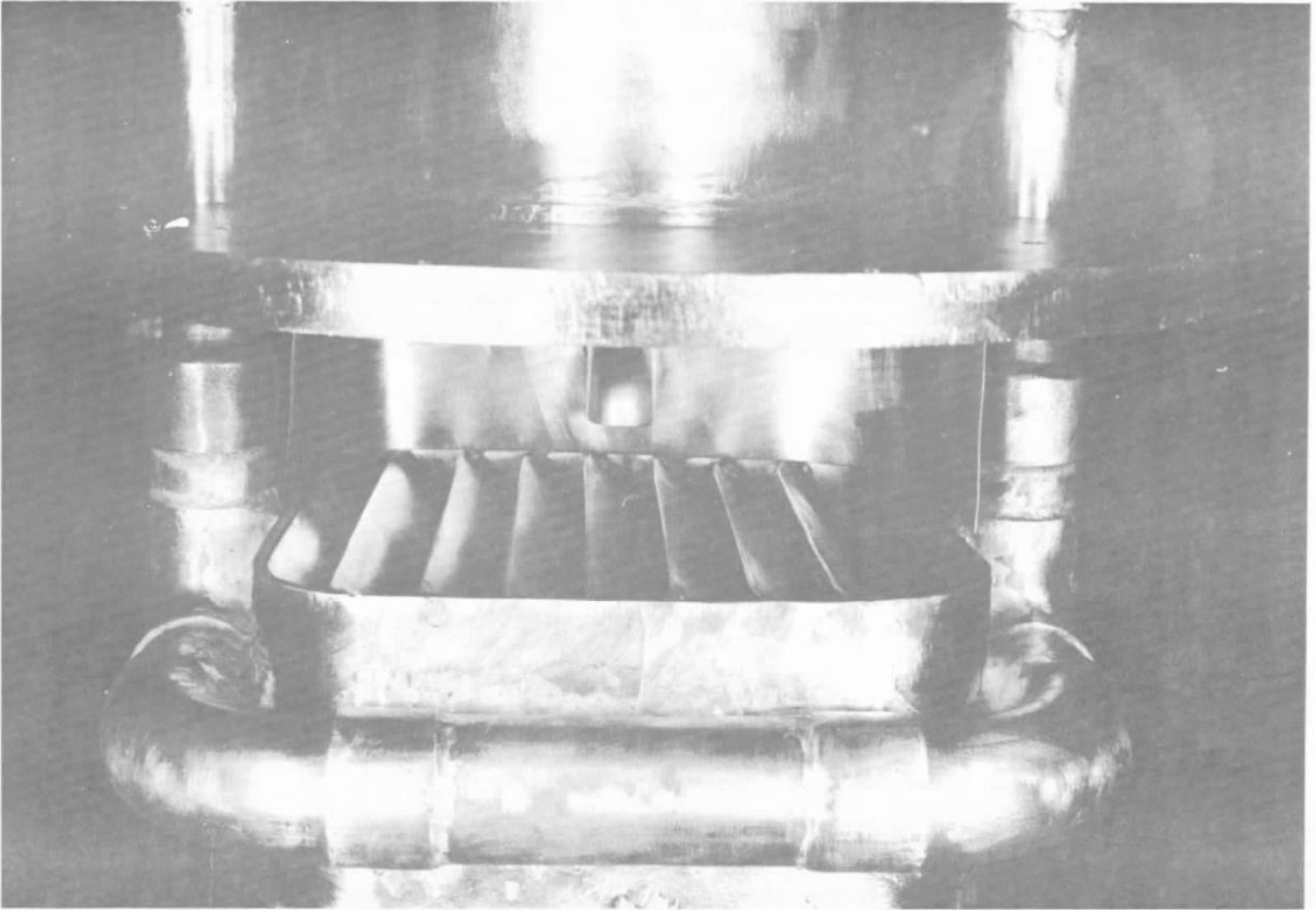


Fig. 5 Photograph of 20°K Shield and Chevron Assembly

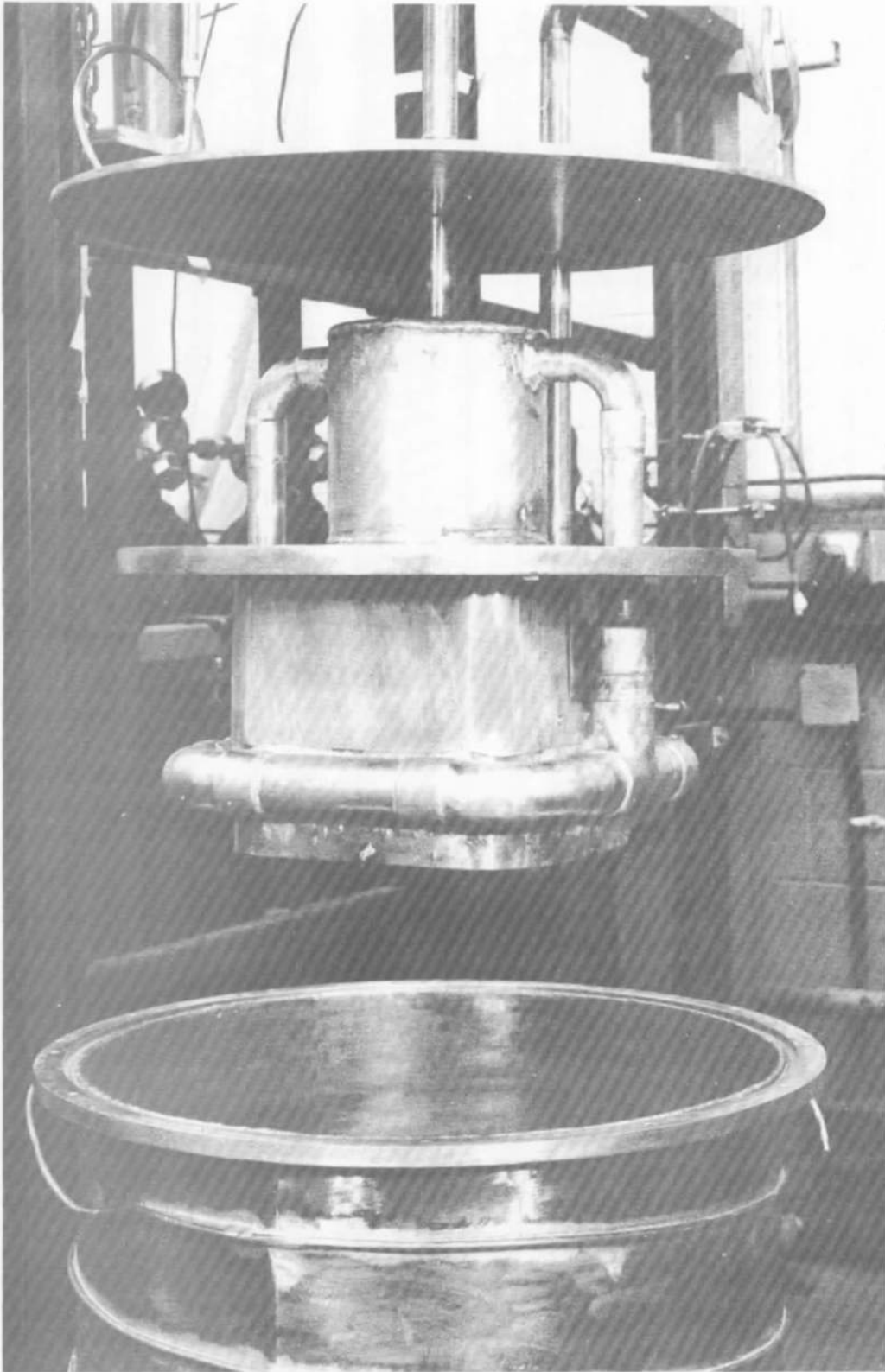


Fig. 6 Photograph of 20°K Chevron and Refrigerant Tube Assembly

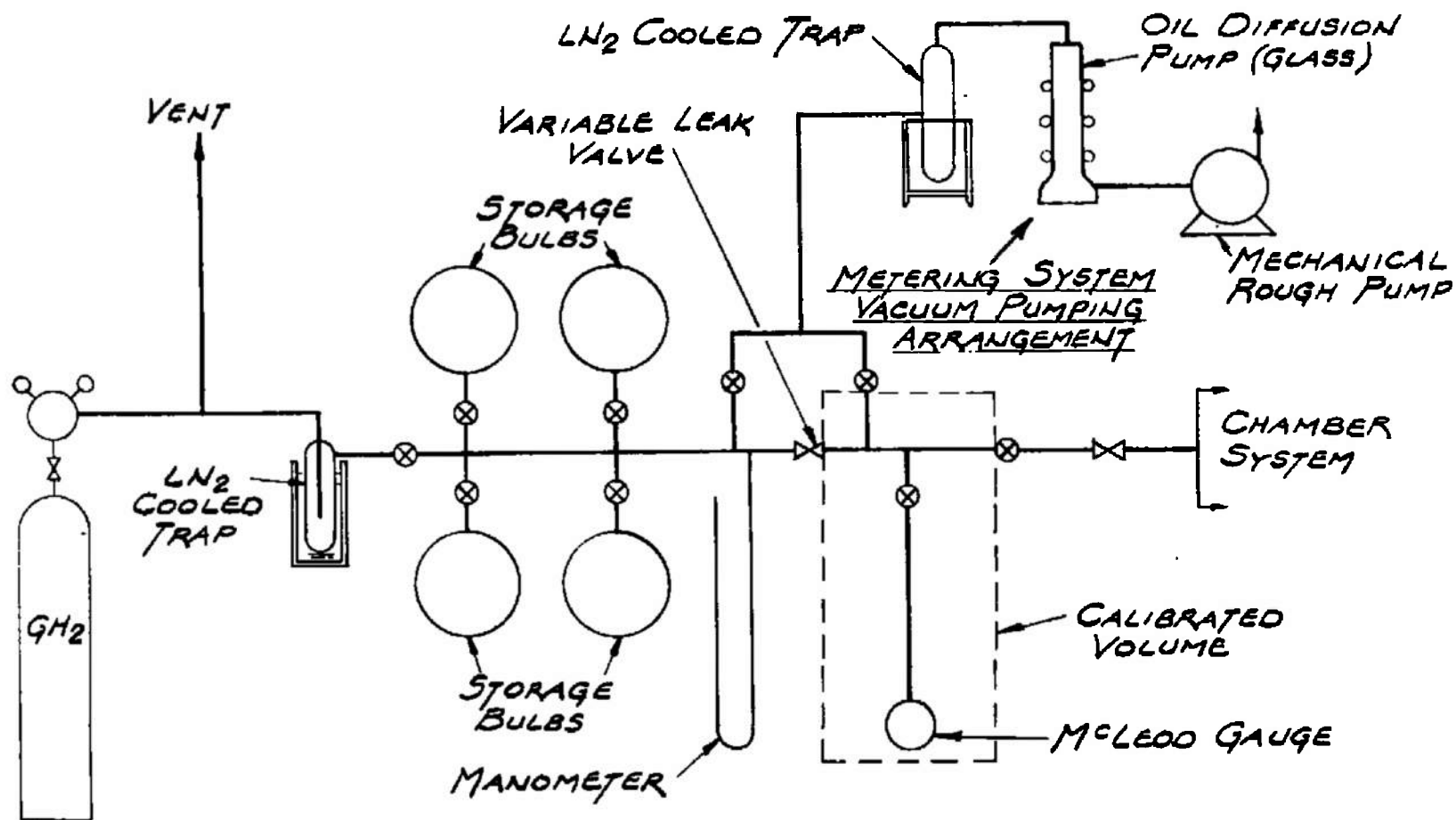


Fig. 7 Gas Metering and Supply System

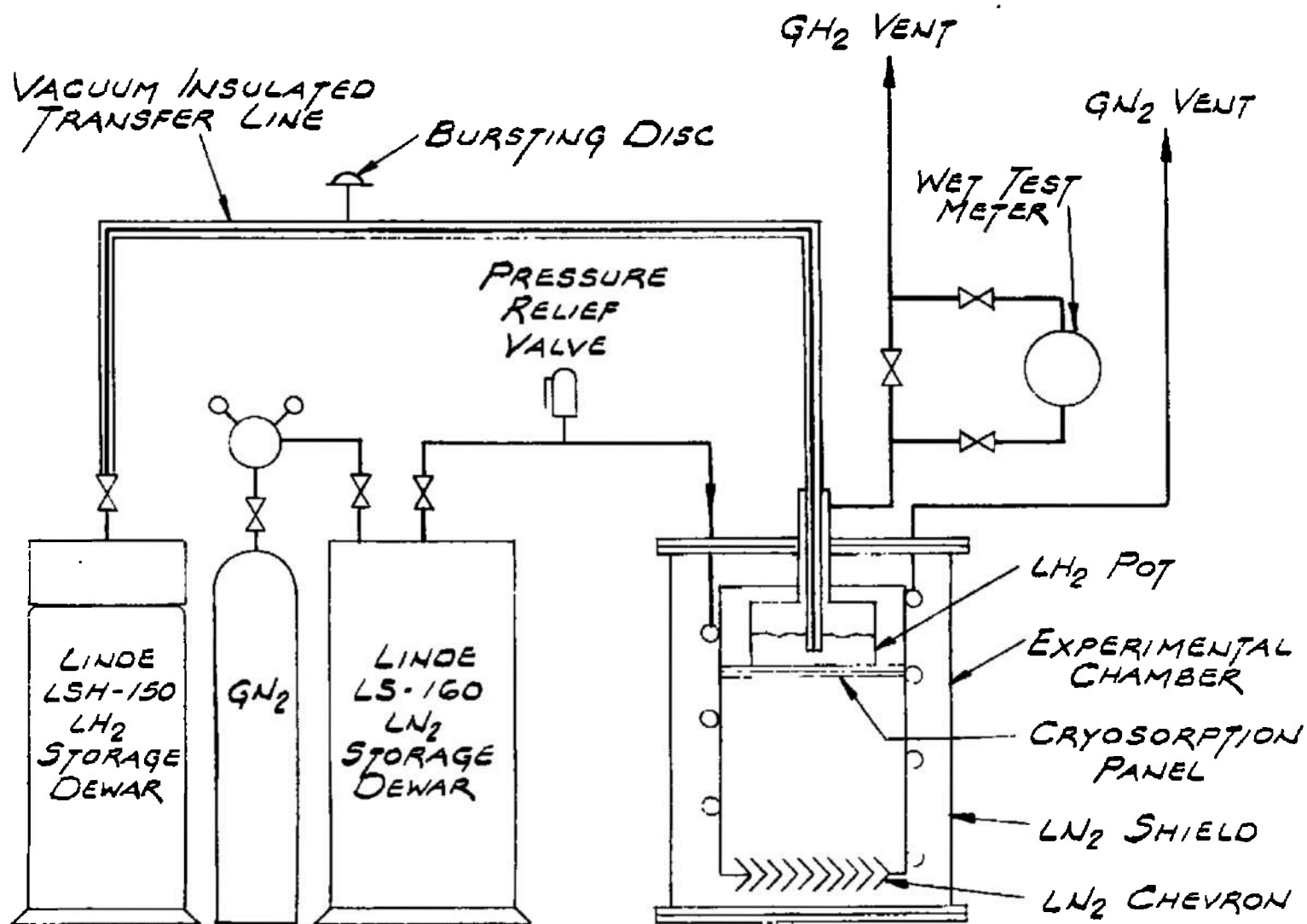


Fig. 8 Refrigeration System

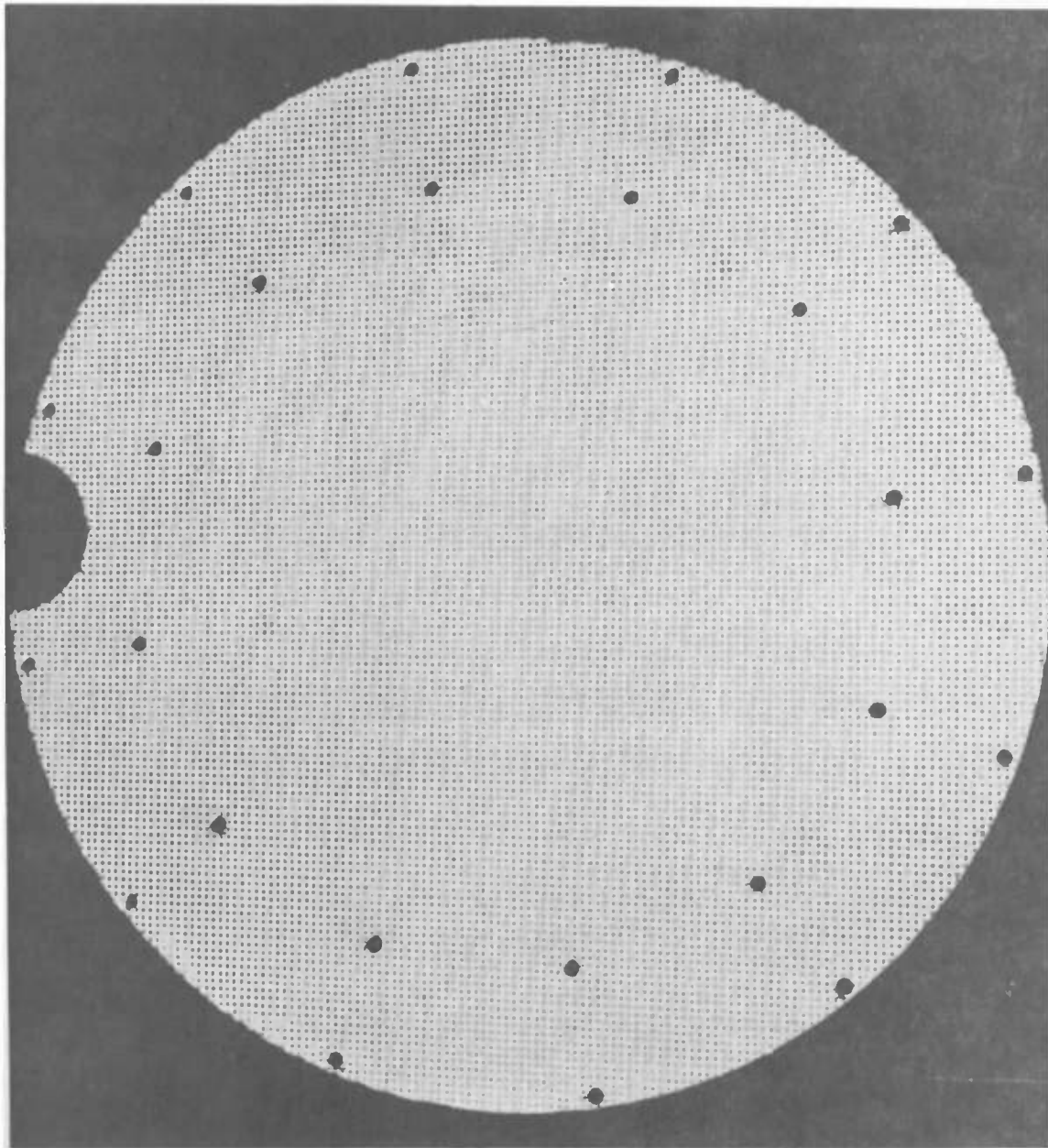


Fig. 9 1/8" Thick Molecular Sieve 5A-Aluminum Substrate Adsorbent Panel

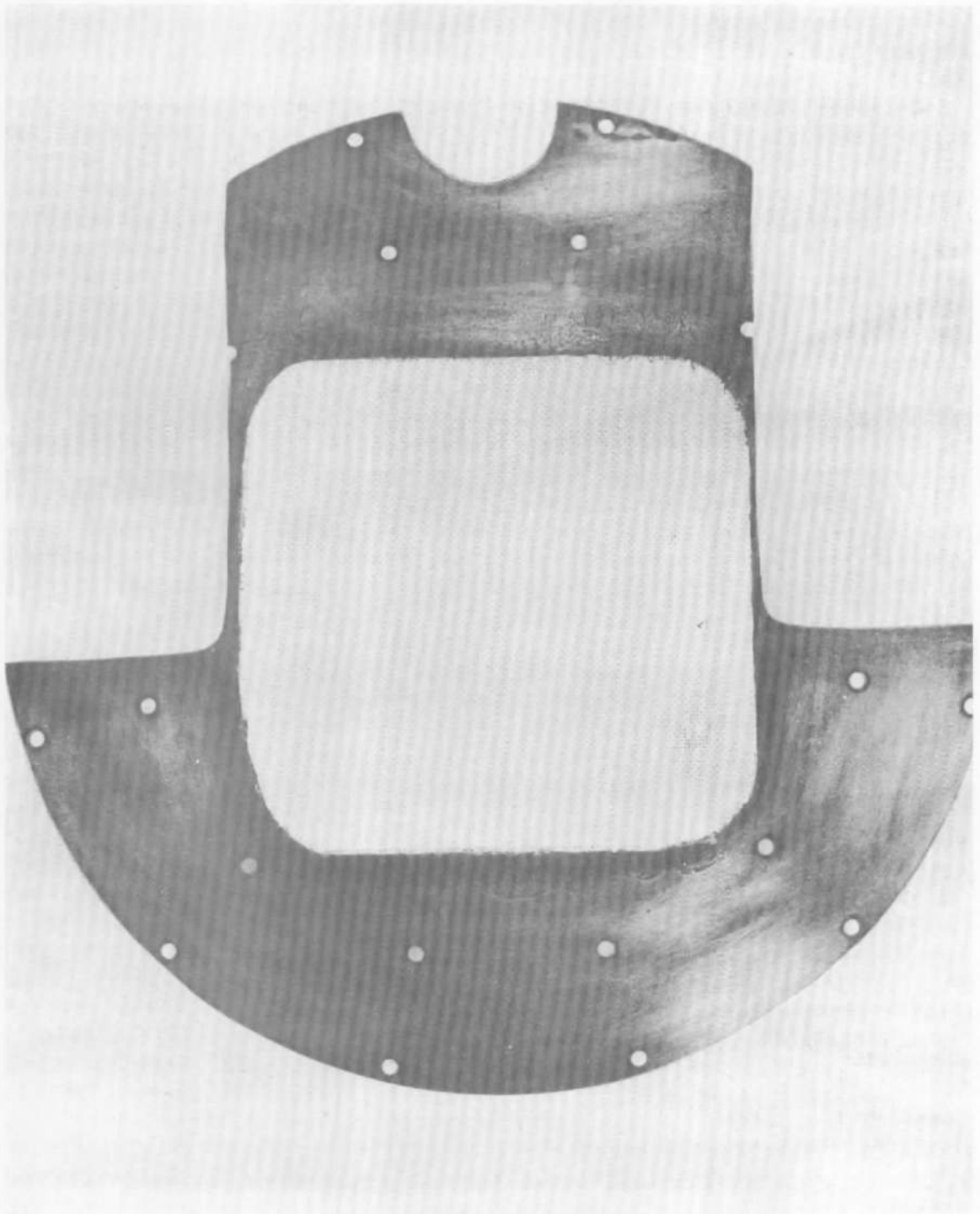


Fig. 10 1/64" Thick Molecular Sieve 5A-Stainless Steel Substrate Adsorbent Panel

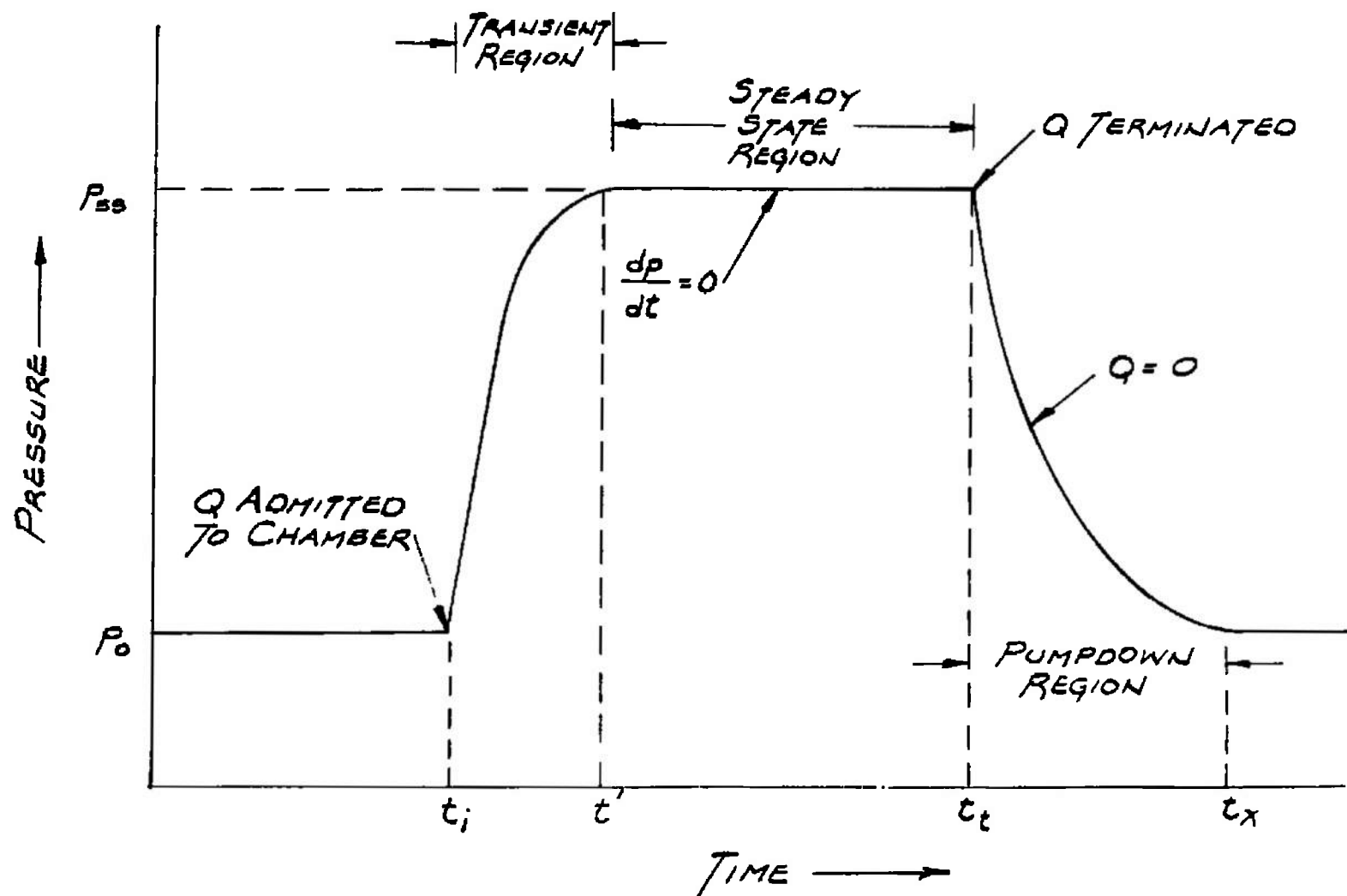


Fig. 11 Interrupted Flow Technique Curve

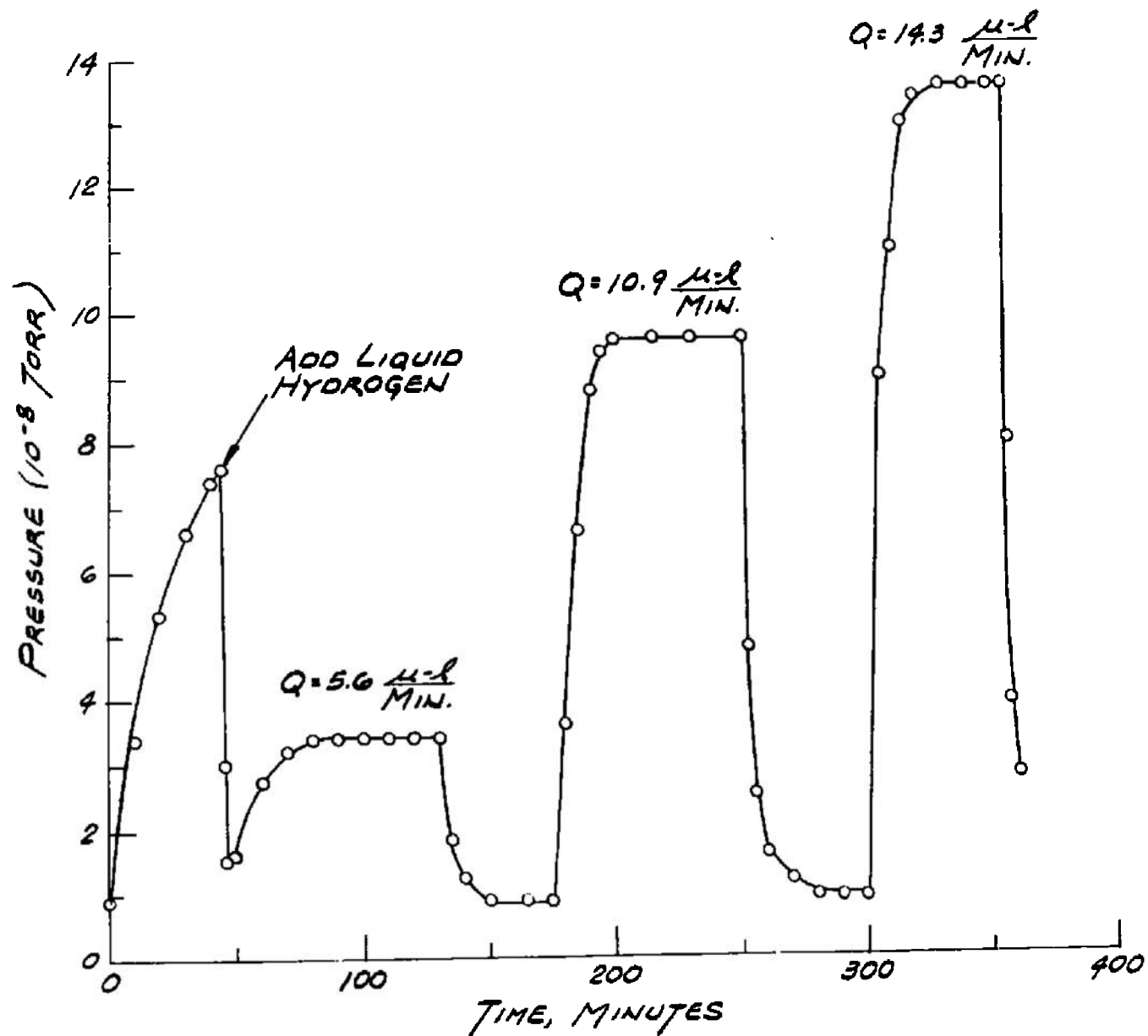


Fig. 12 Panel No. 1 - Residual Hydrogen Pressure During Cryosorption Pumping

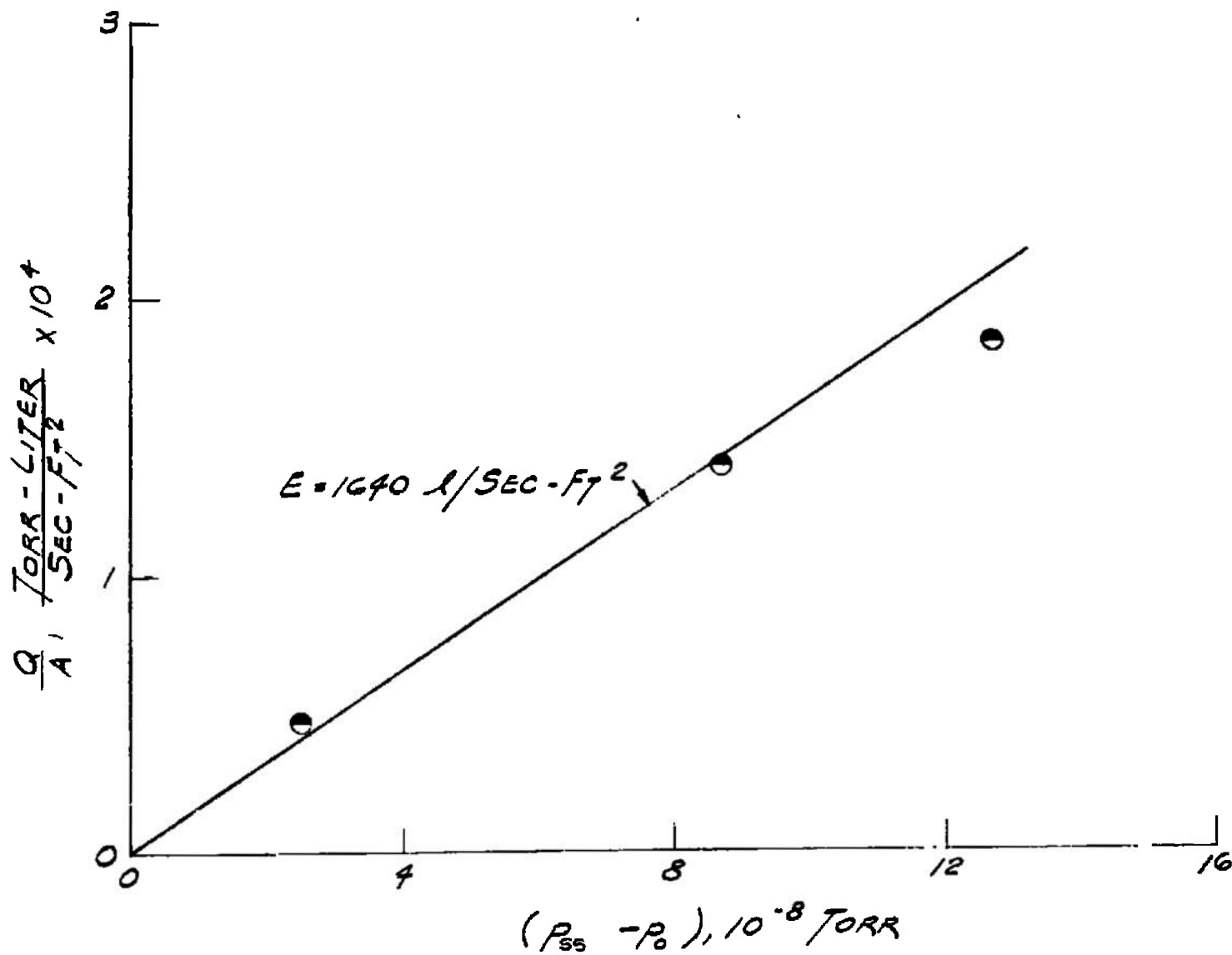


Fig. 13 Panel No. 1 - Steady-State Hydrogen Pressure as a Function of Hydrogen Leak Rate

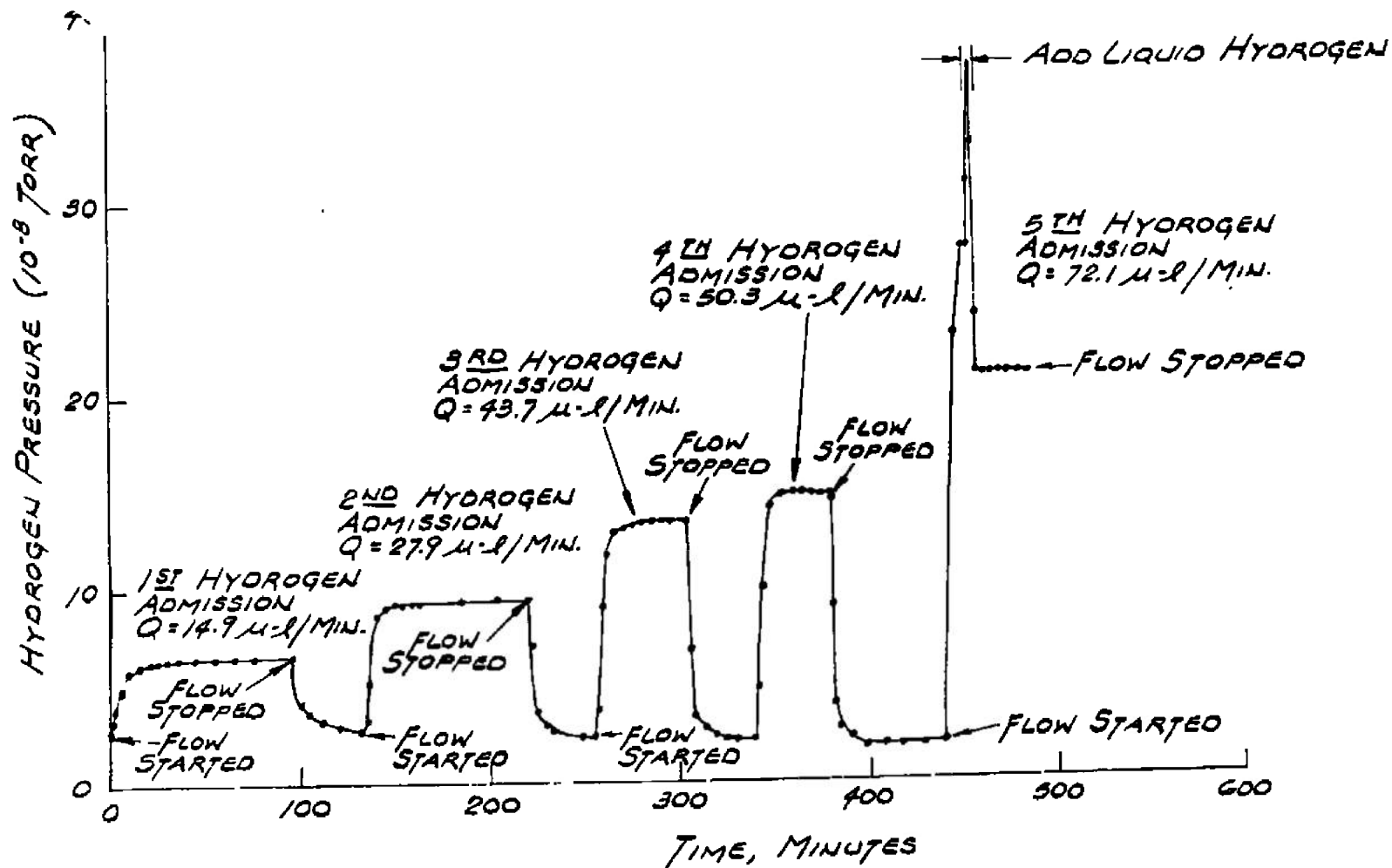


Fig. 14 Panel No. 2 – Residual Hydrogen Pressure During Cryosorption Pumping After First Activation

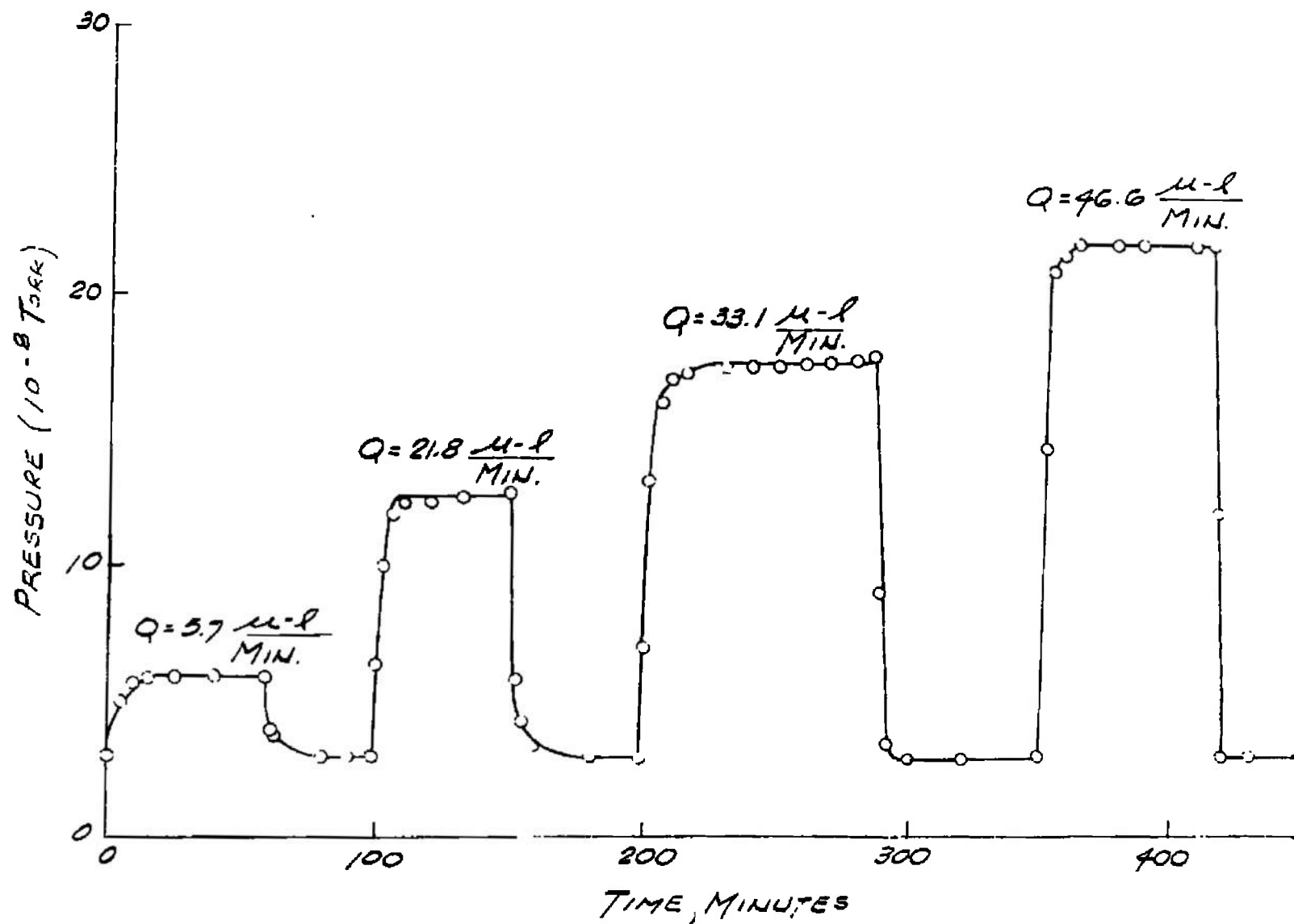


Fig. 15 Panel No. 2 - Residual Hydrogen Pressure During Cryosorption Pumping After Second Activation

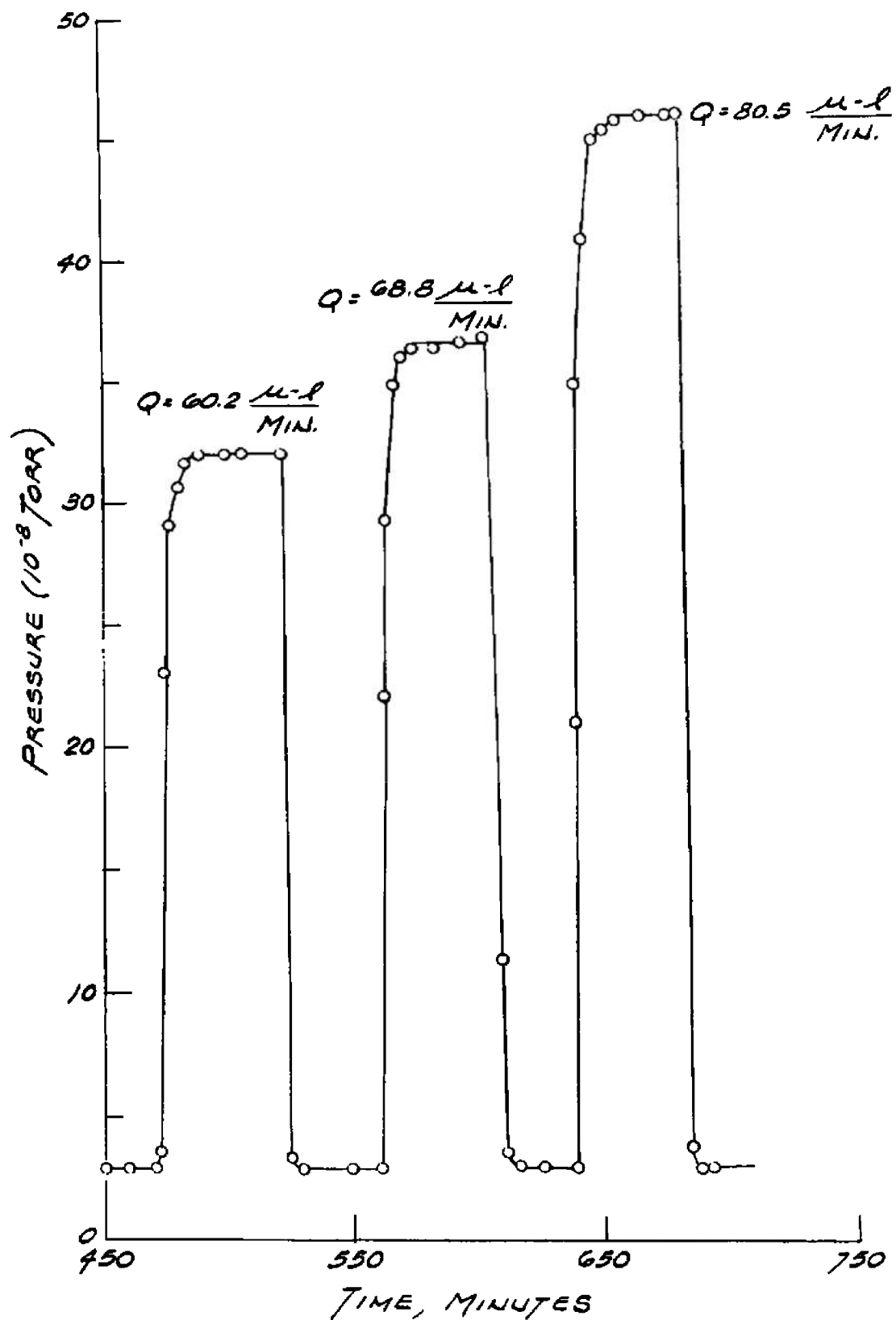


Fig. 16 Panel No. 2 - Residual Hydrogen Pressure During Cryosorption Pumping After Second Activation

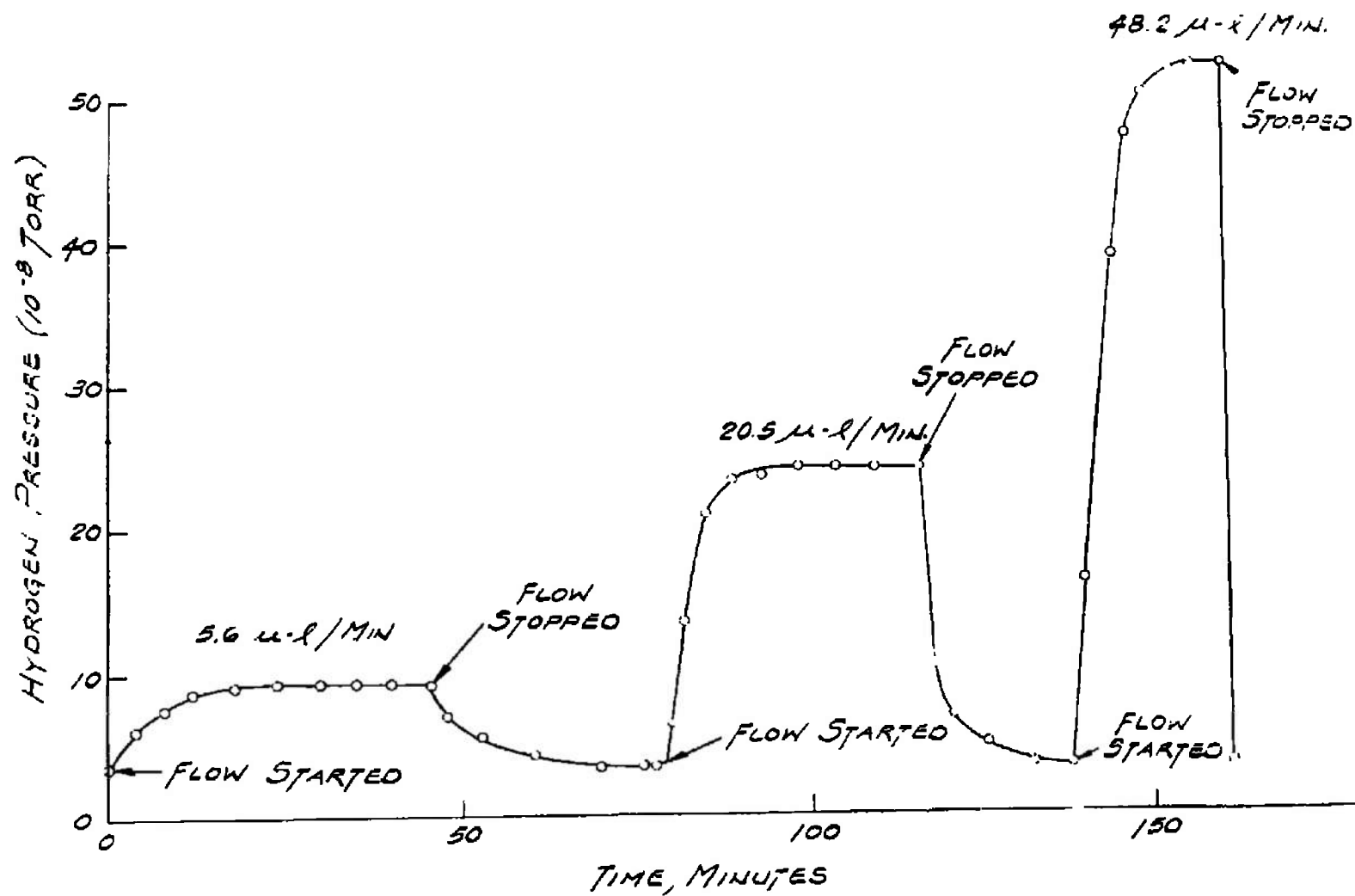


Fig. 17 Panel No. 2 - Residual Hydrogen Pressure During Cryosorption Pumping After Third Activation

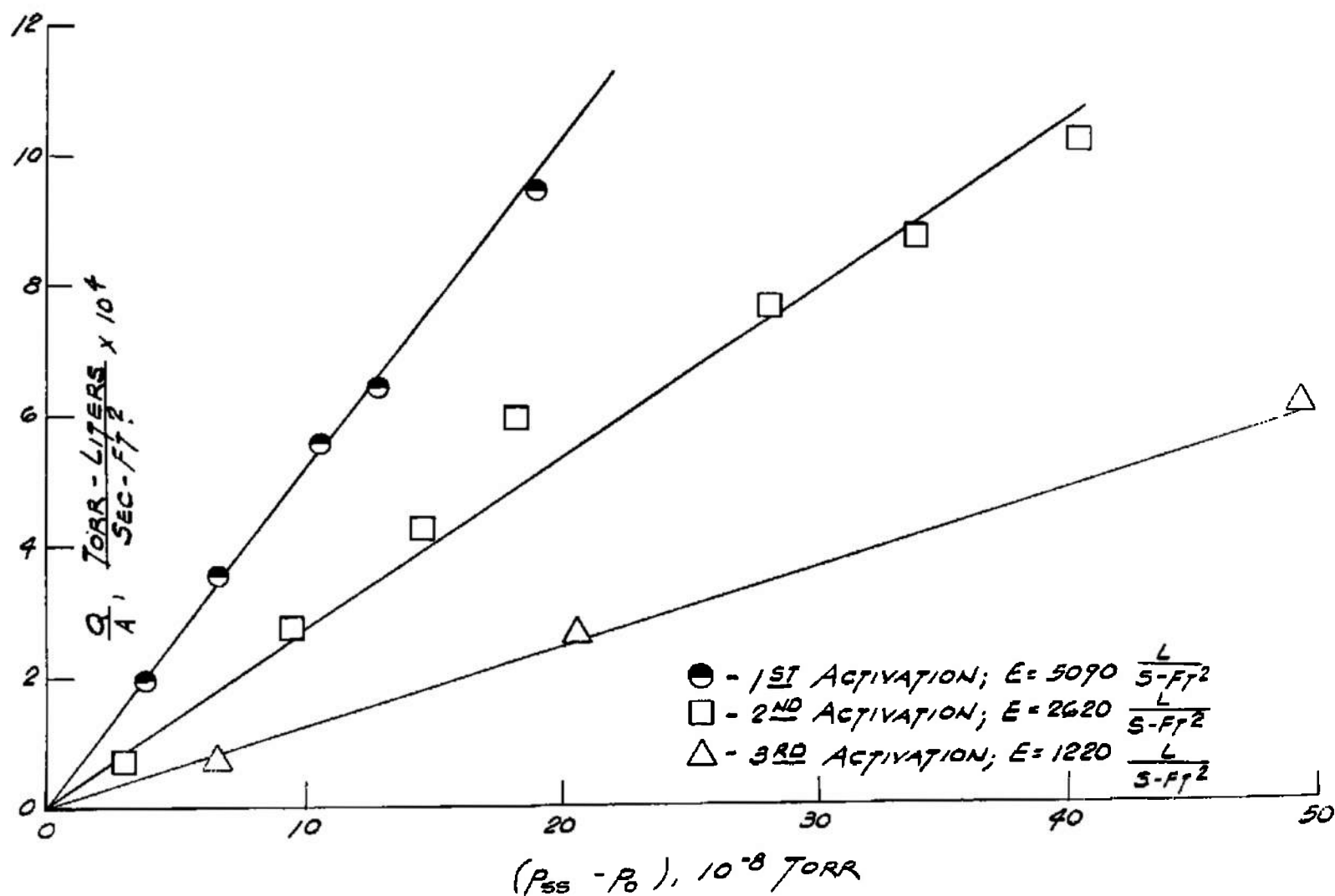


Fig. 18 Panel No. 2 - Steady-State Hydrogen Pressure as a Function of Hydrogen Leak Rate for Activations 1-3

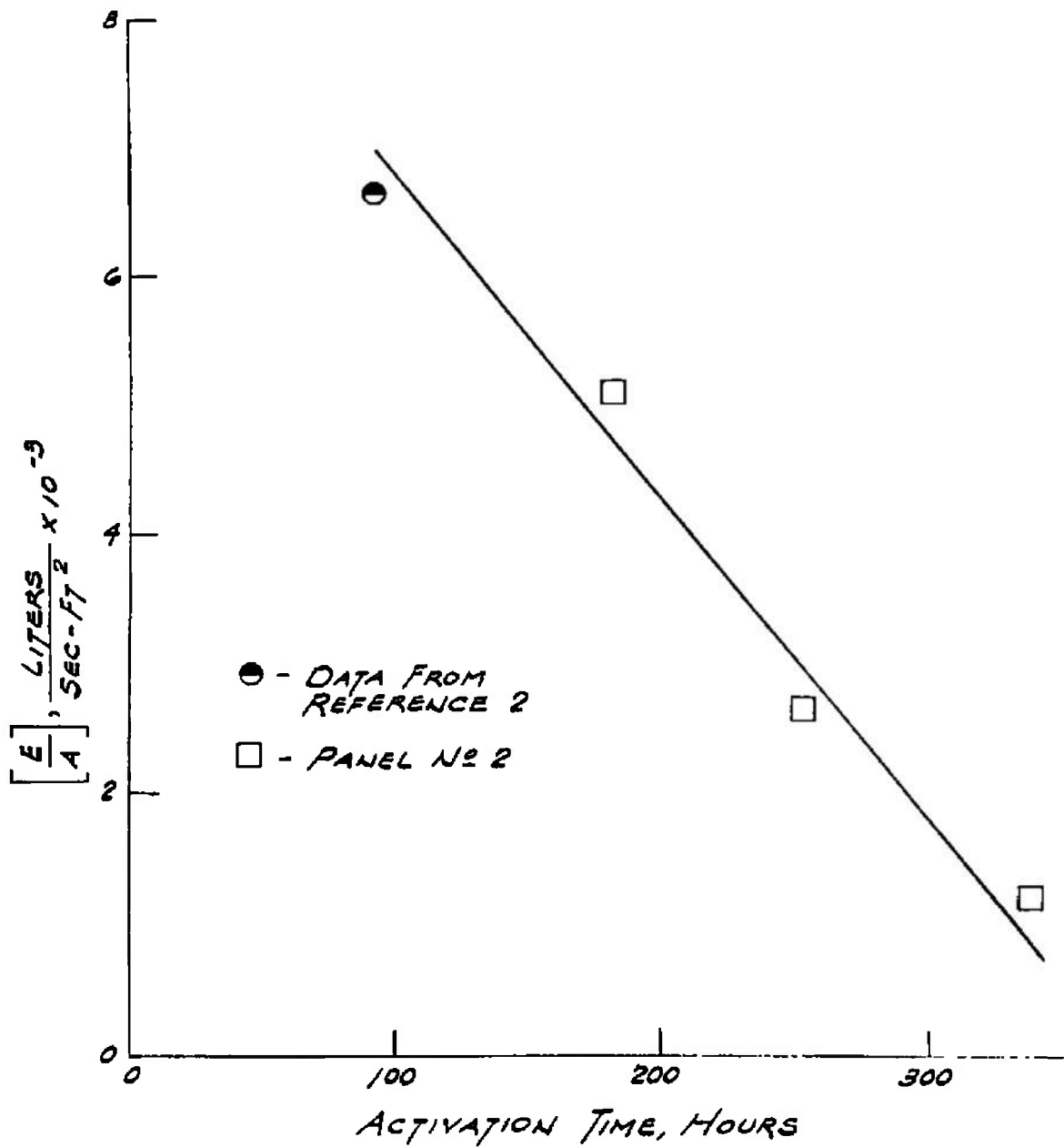


Fig. 19 Panel No. 2 - Hydrogen Pumping Speed as a Function of Cumulative Activation Time

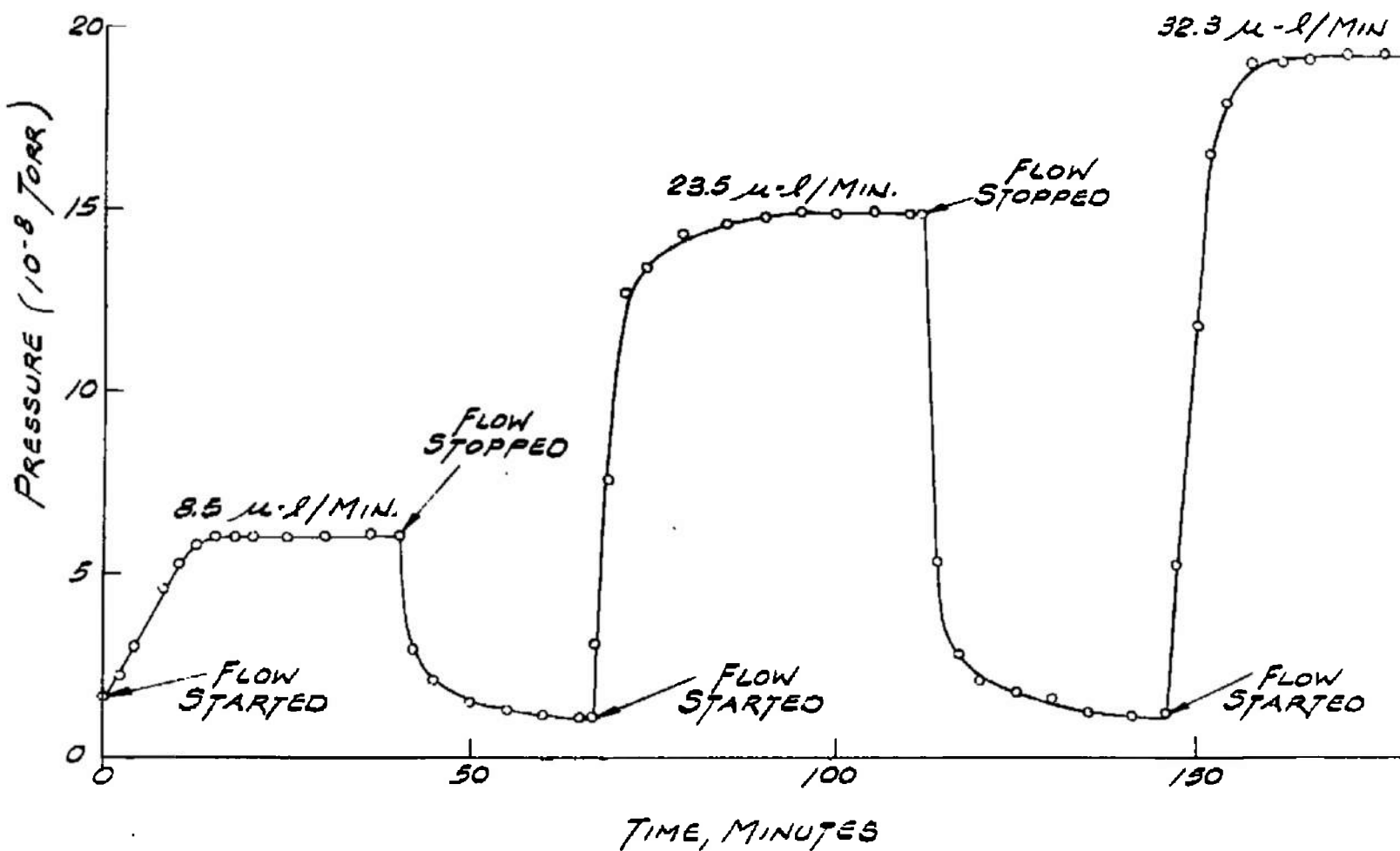


Fig. 20 Panel No. 2 - Residual Hydrogen Pressure During Cryosorption Pumping After Fourth Activation

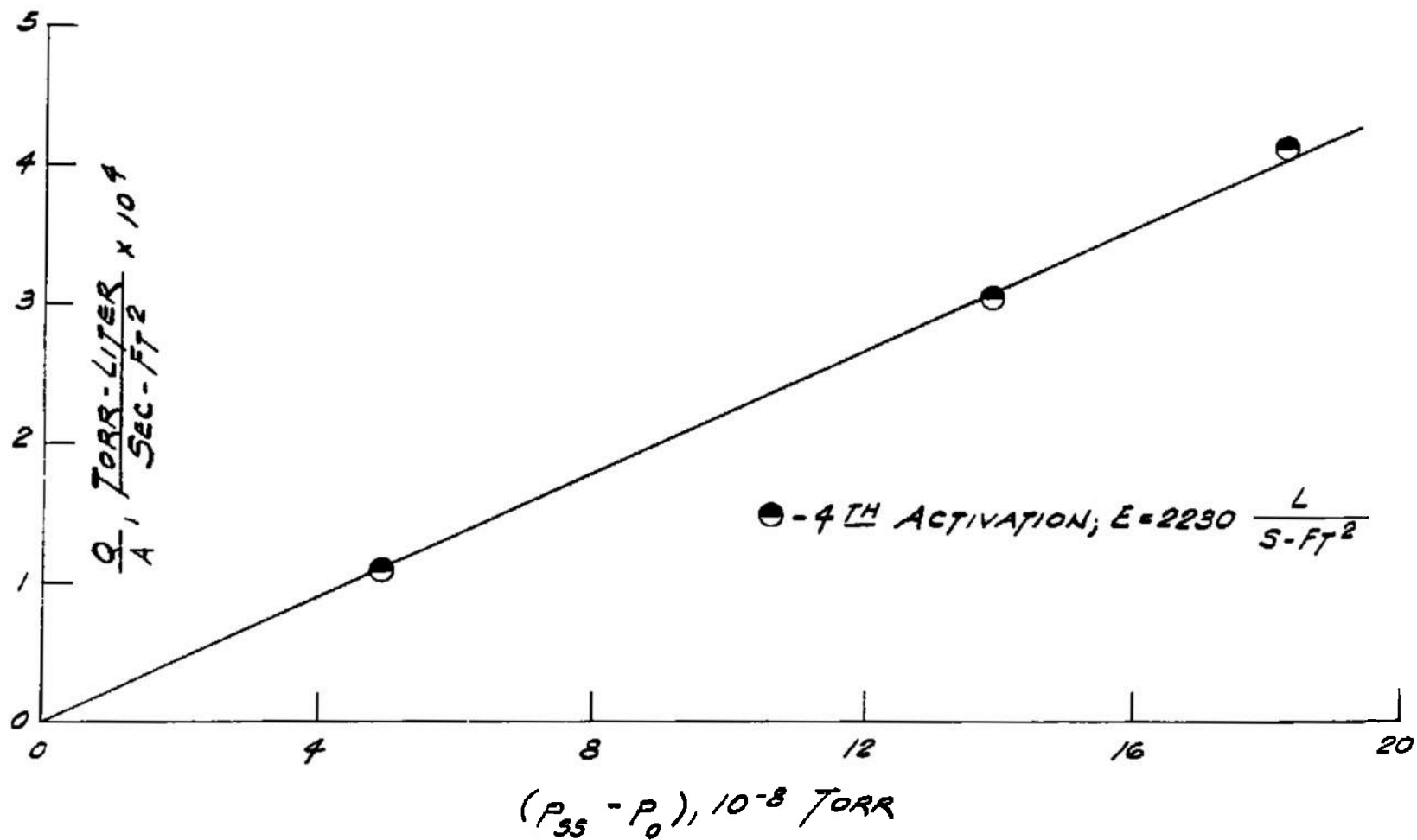


Fig. 21 Panel No. 2 - Steady-State Hydrogen Pressure as a Function of Hydrogen Leak Rate for Activation 4

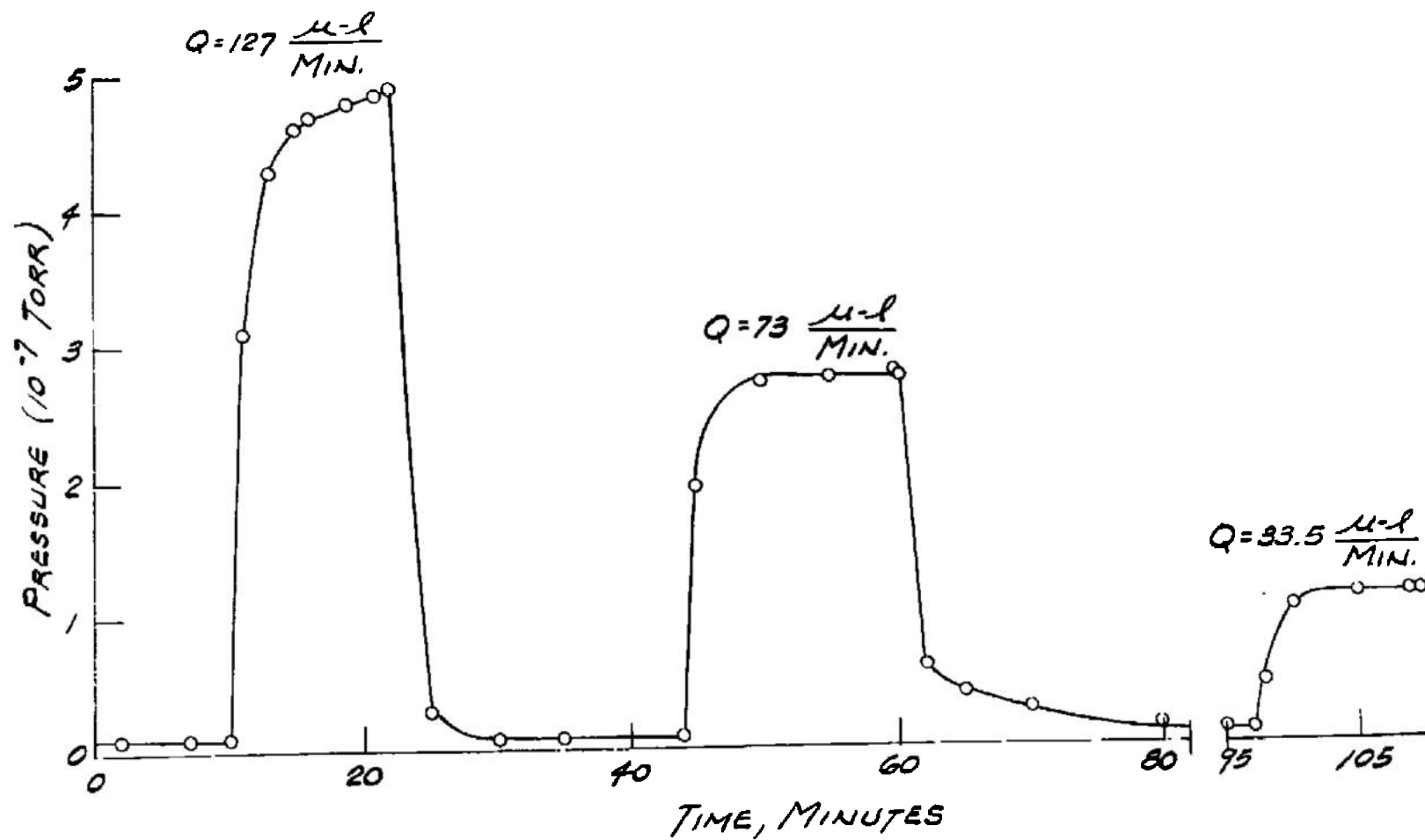


Fig. 22 Panel No. 3 - Residual Hydrogen Pressure During Cryosorption Pumping - Run No. 3

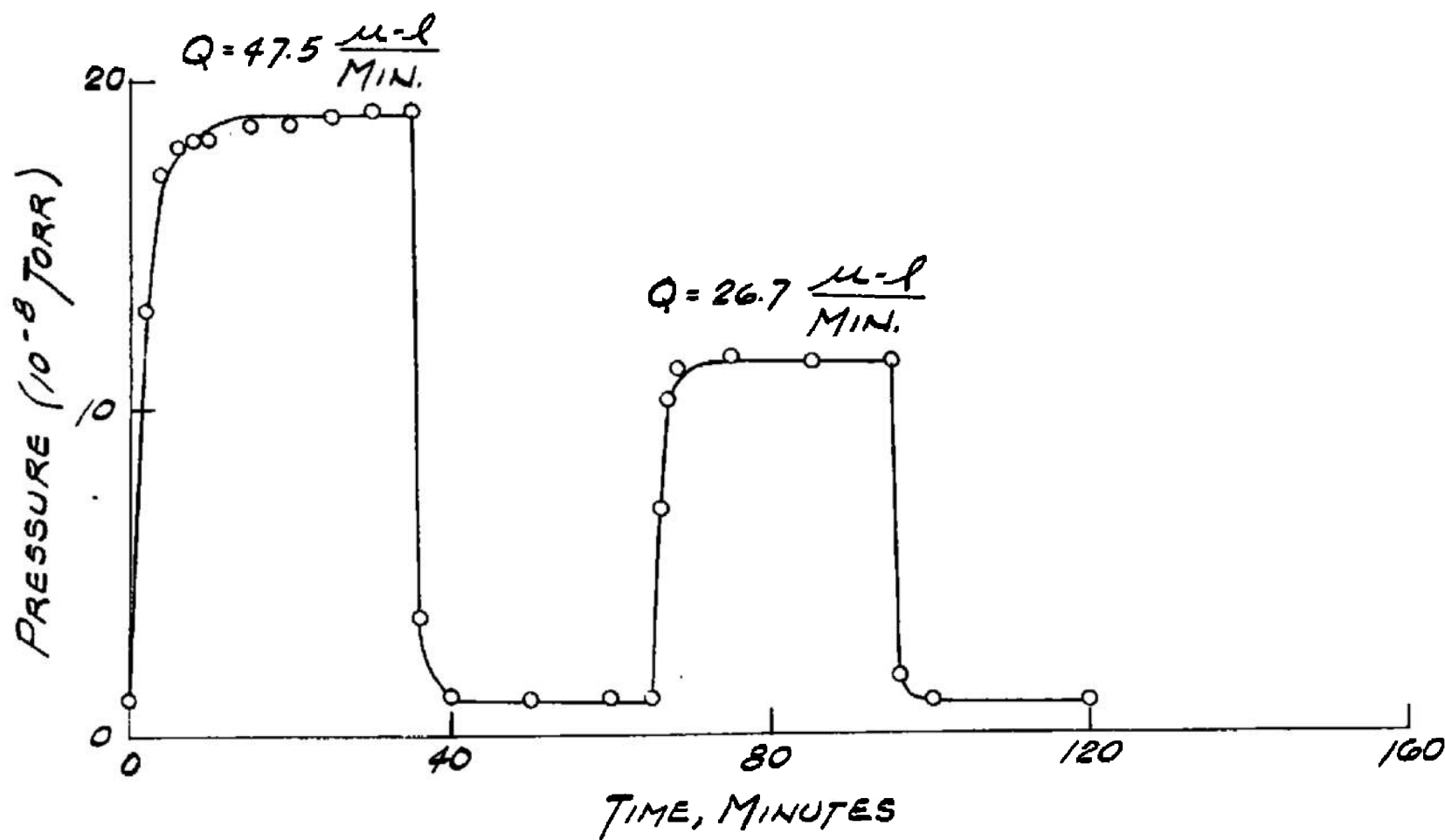


Fig. 23 Panel No. 3 – Residual Hydrogen Pressure During Cryosorption Pumping – Run No. 4

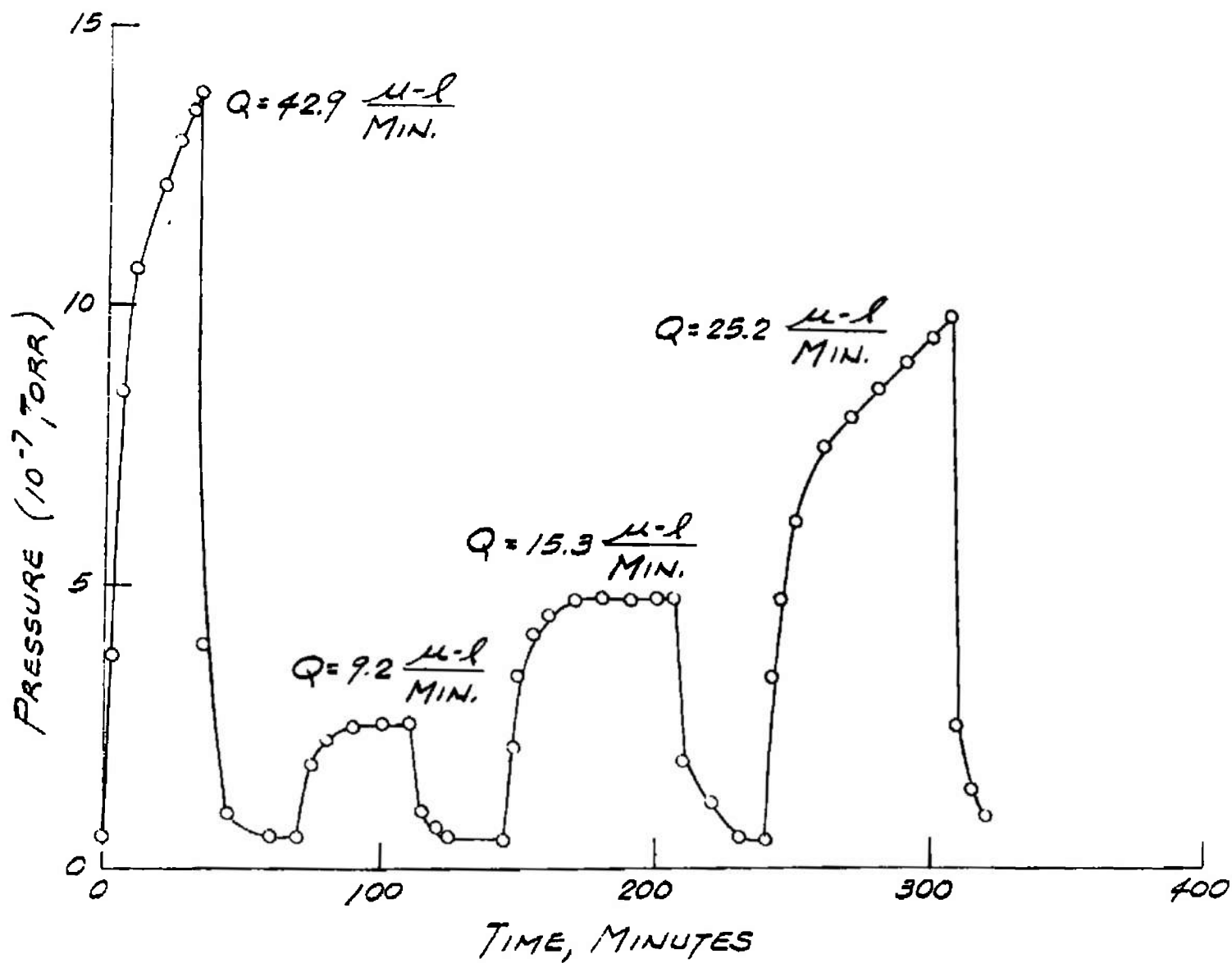


Fig. 24 Panel No. 3 - Residual Hydrogen Pressure During Cryosorption Pumping - Run No. 5

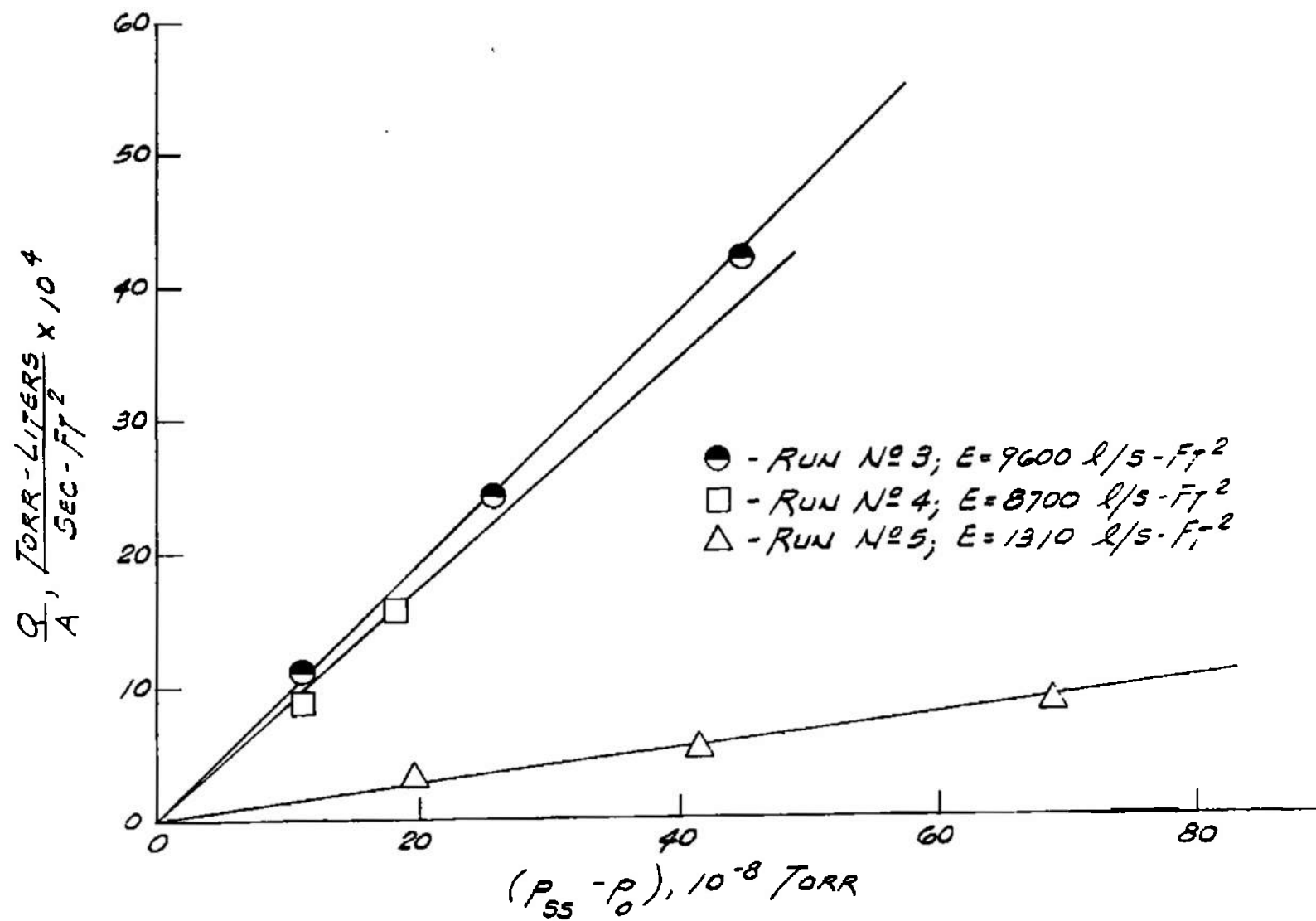


Fig. 25 Panel No. 3 - Steady-State Hydrogen Pressure as a Function of Hydrogen Leak Rate - Runs 3-5

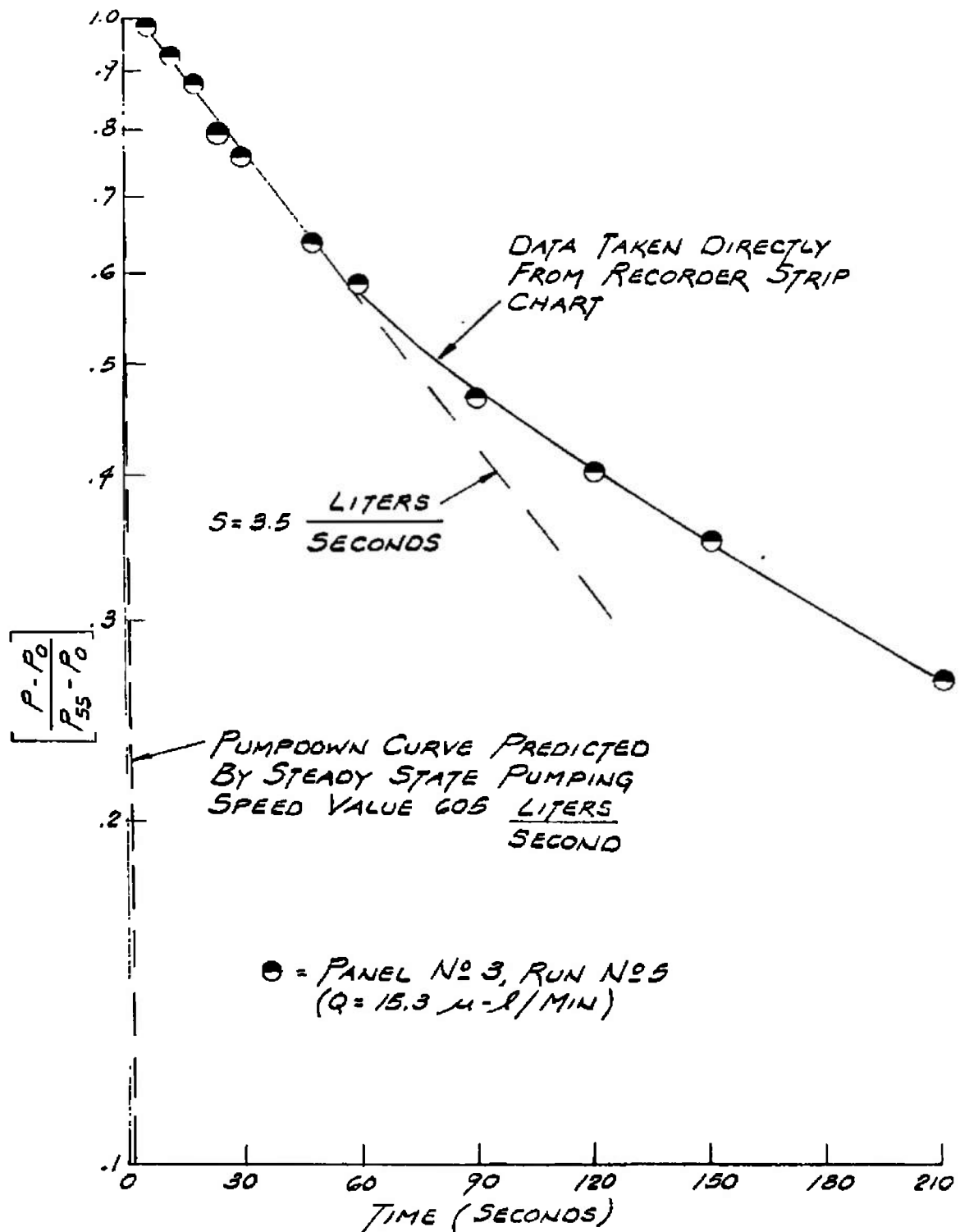


Fig. 26 Evaluation of Pumping Speed by the Pumpdown Technique Analysis

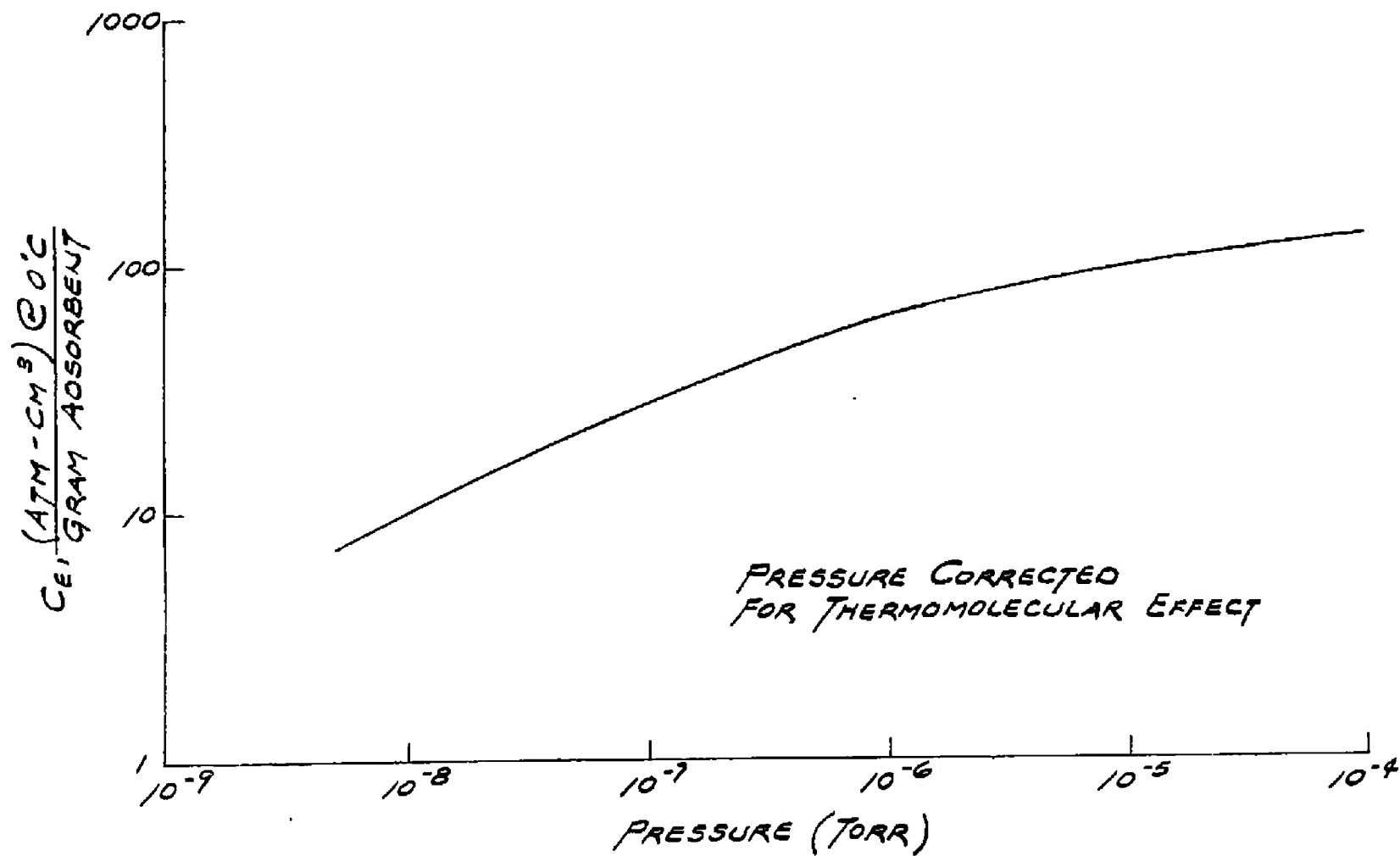


Fig. 27 Adsorption of Hydrogen on Molecular Sieve 5A at 20°C

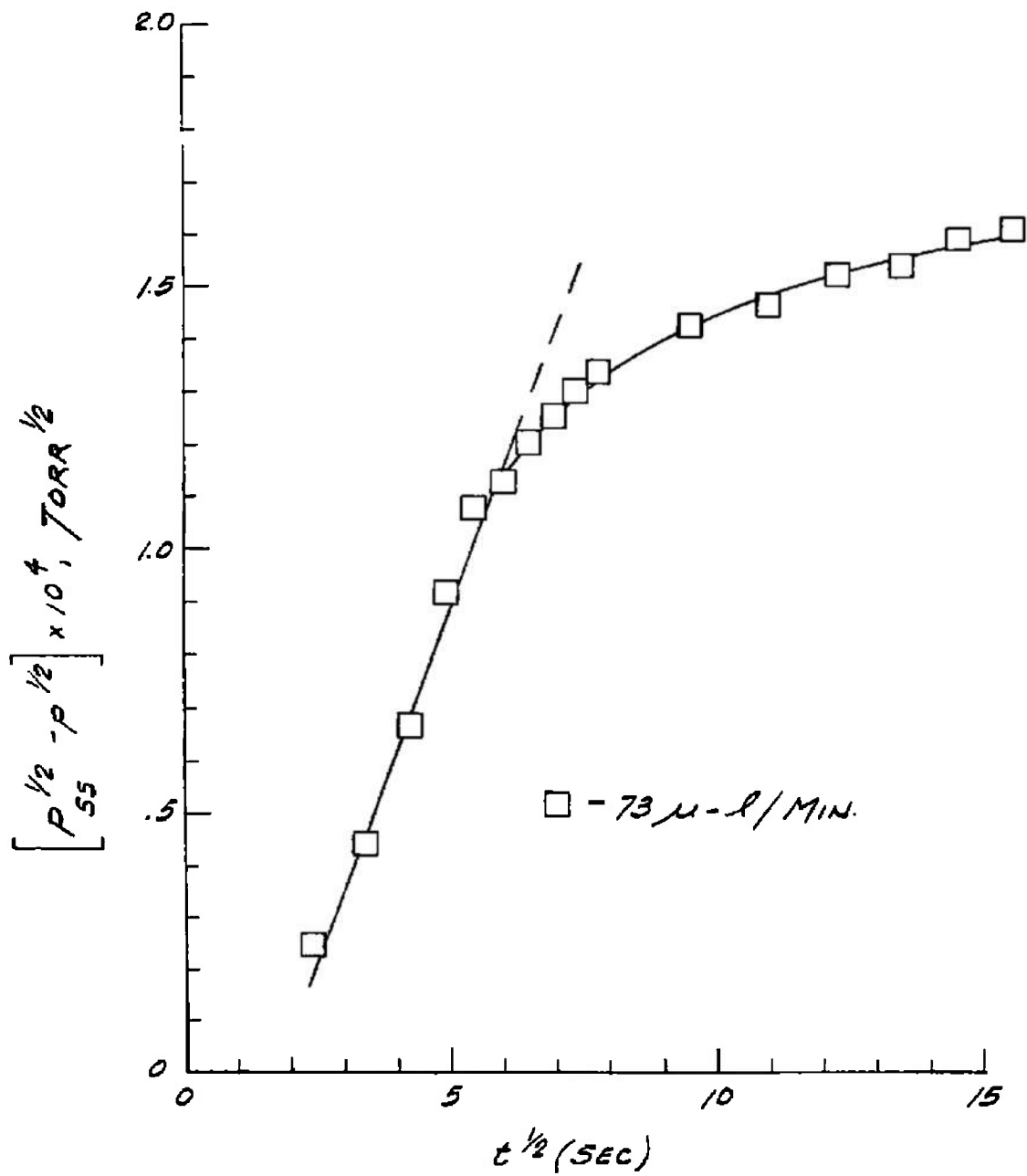


Fig. 28 Pumpdown Characteristics Panel No. 3 (Run No. 3)

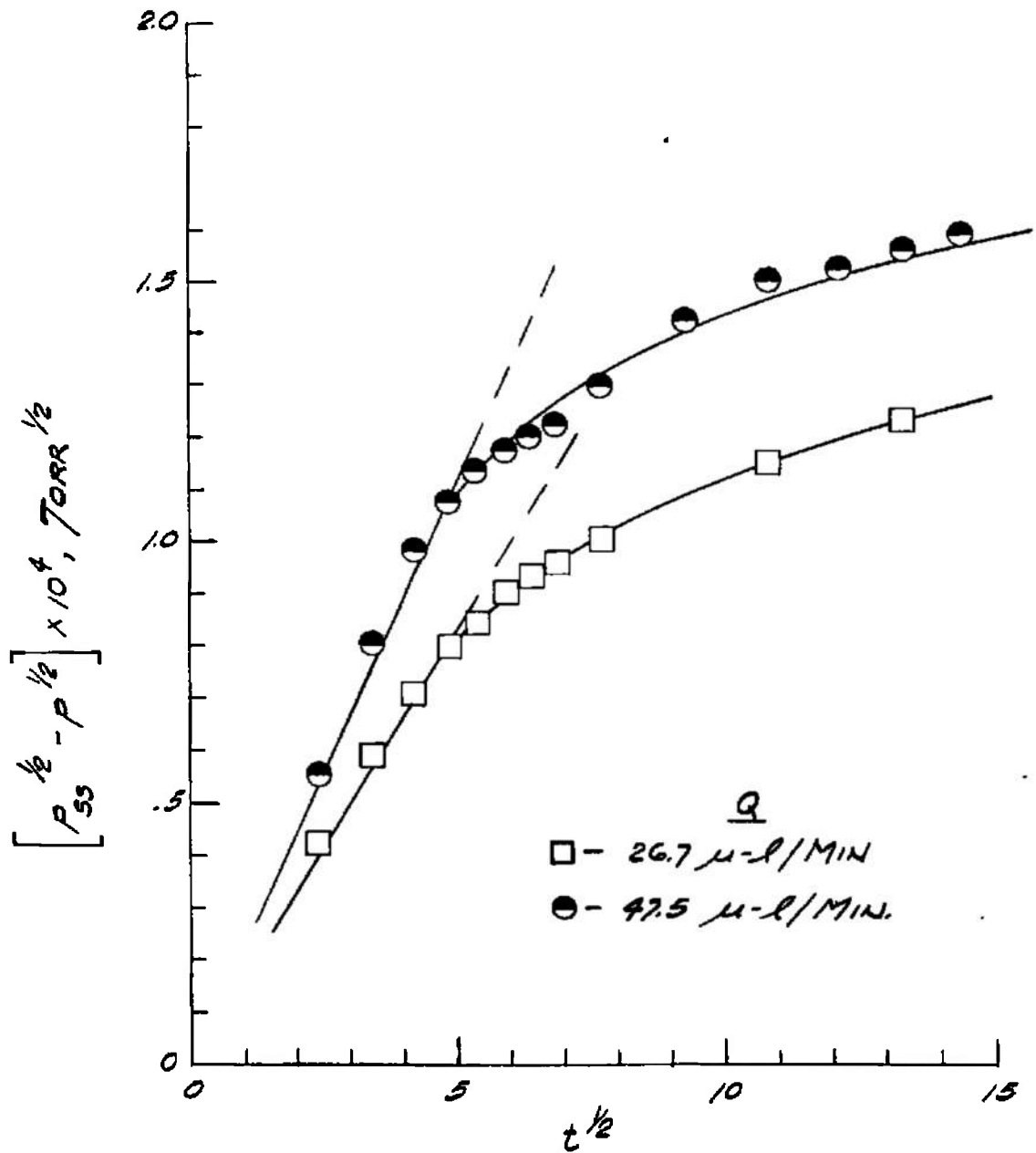


Fig. 29 Pumpdown Characteristics Panel No. 3 (Run No. 4)

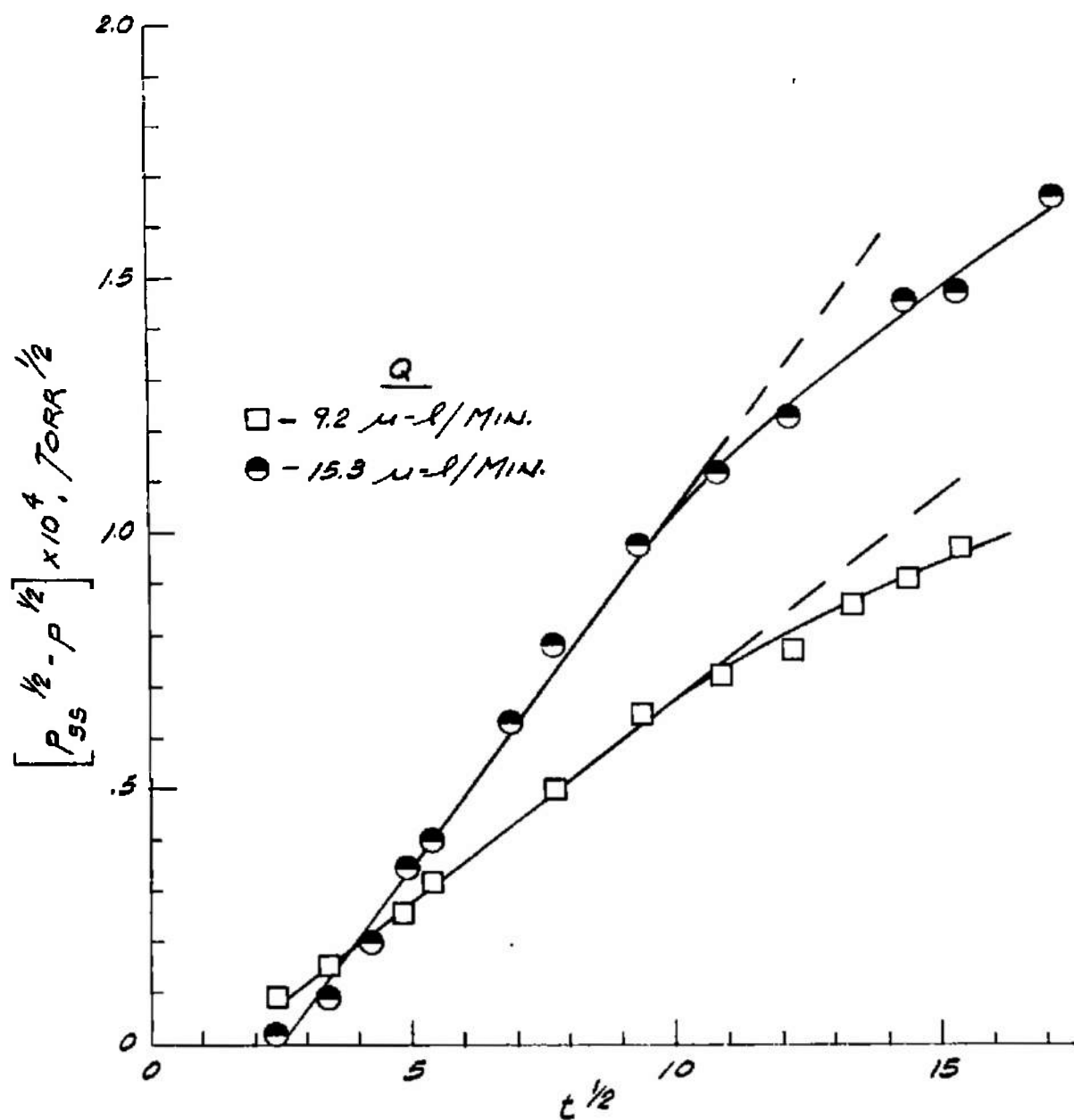


Fig. 30 Pumpdown Characteristics Panel No. 3 (Run No. 5)

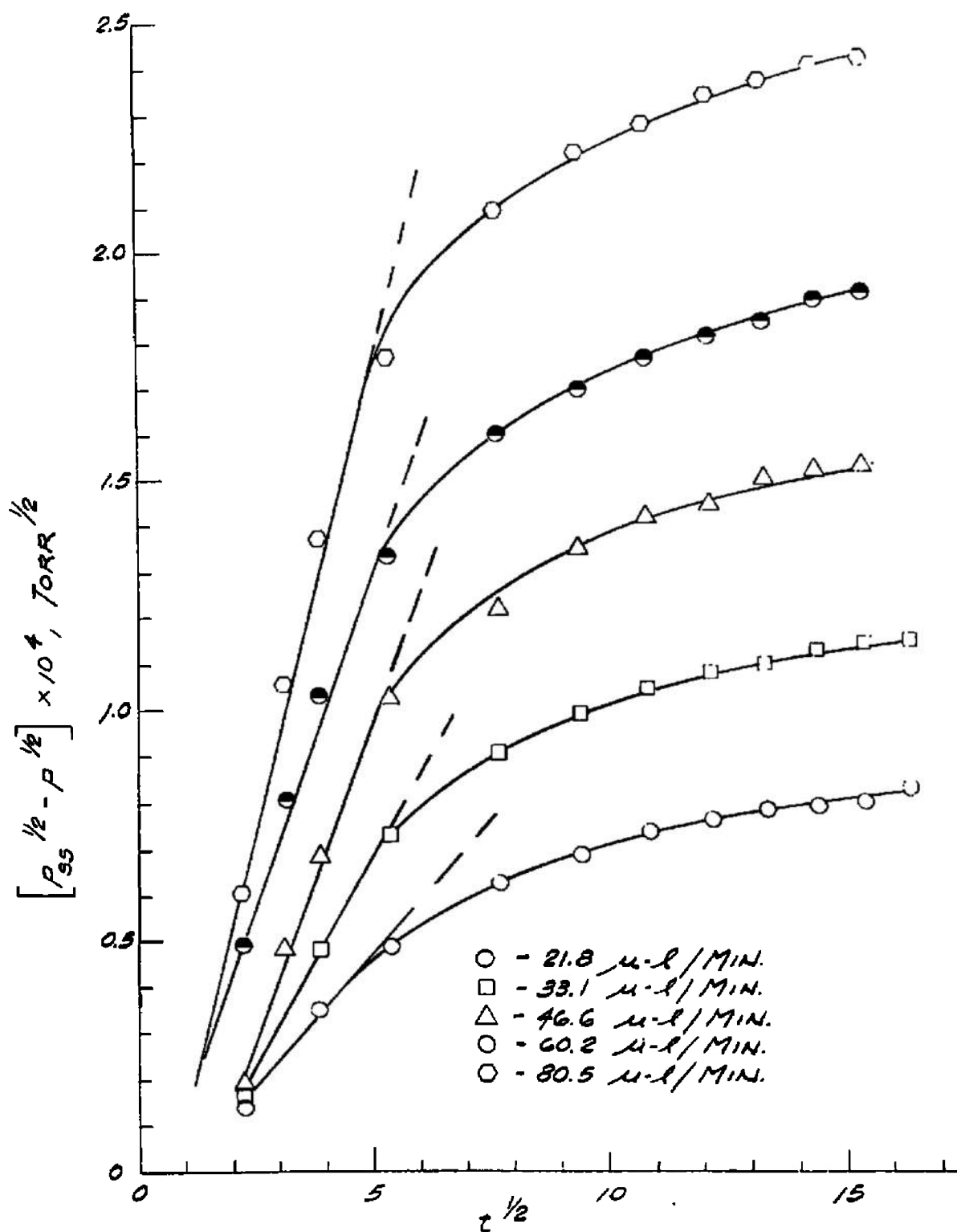


Fig. 31 Pumpdown Characteristics Panel No. 2 (Run No. 2)

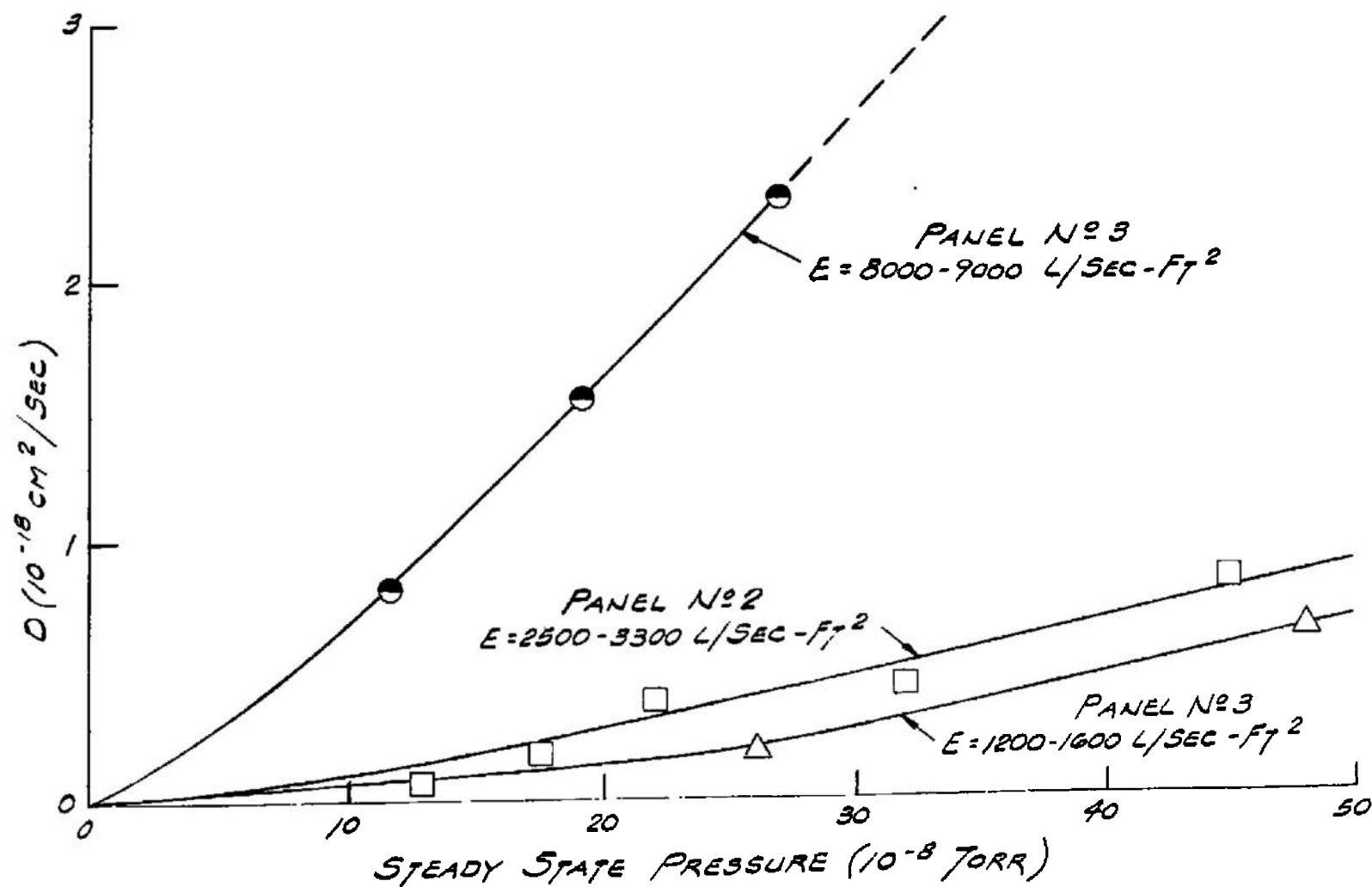


Fig. 32 Diffusion Constant as a Function of Surface Layer Concentration

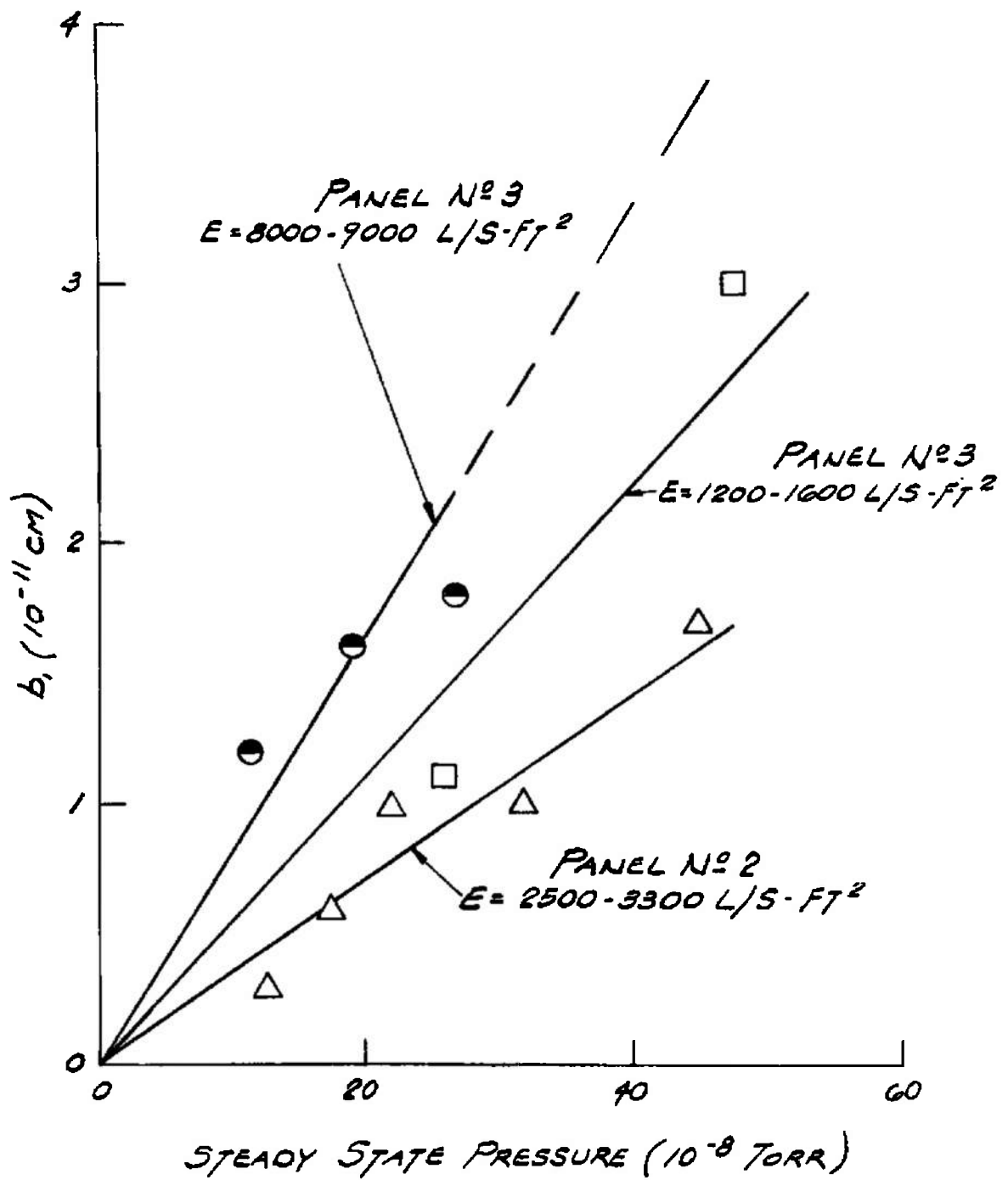


Fig. 33 Concentration Gradient Front as a Function of Surface Layer Concentration

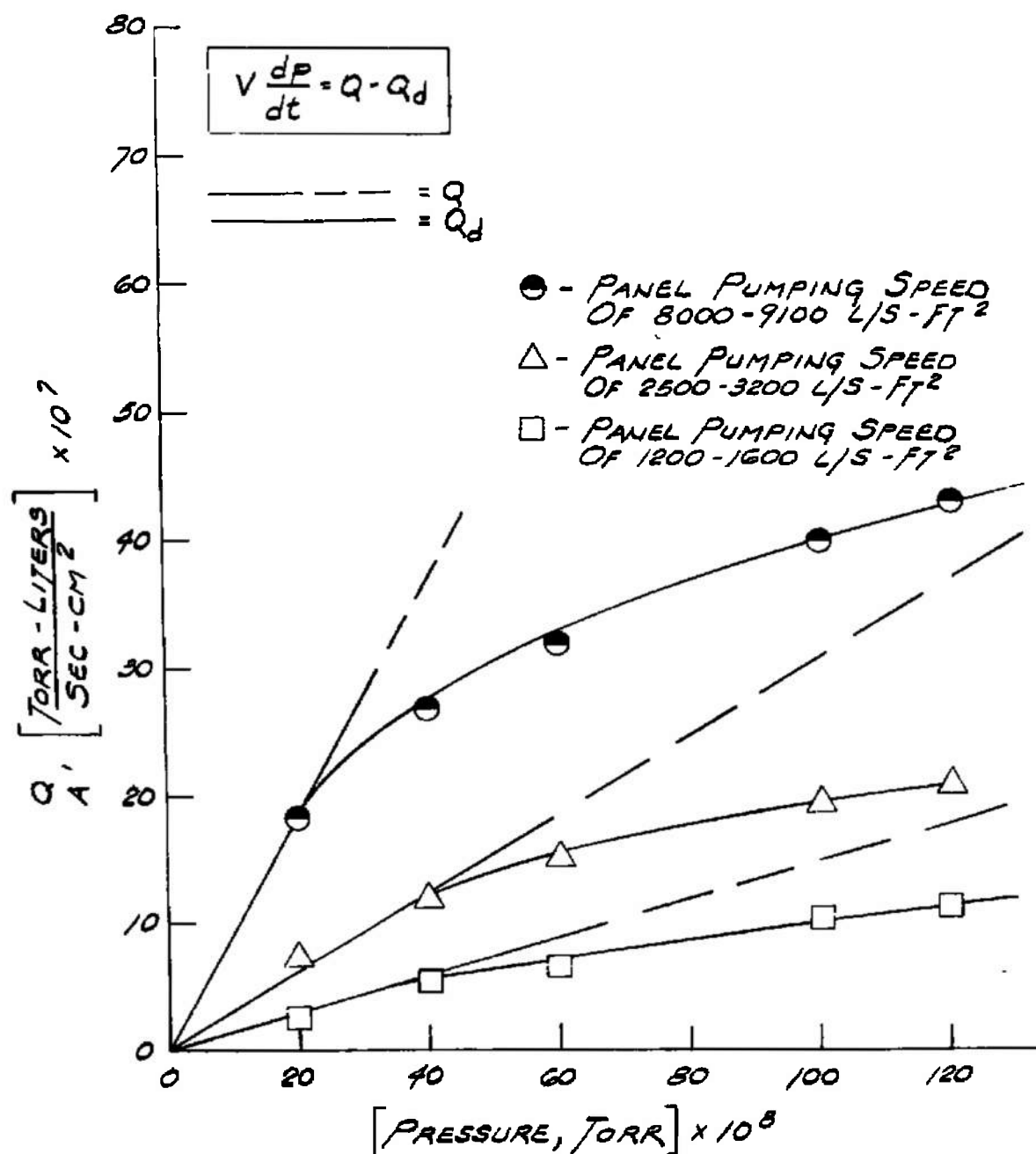


Fig. 34 Cryosorption Pumping Behavior as a Function of Pressure

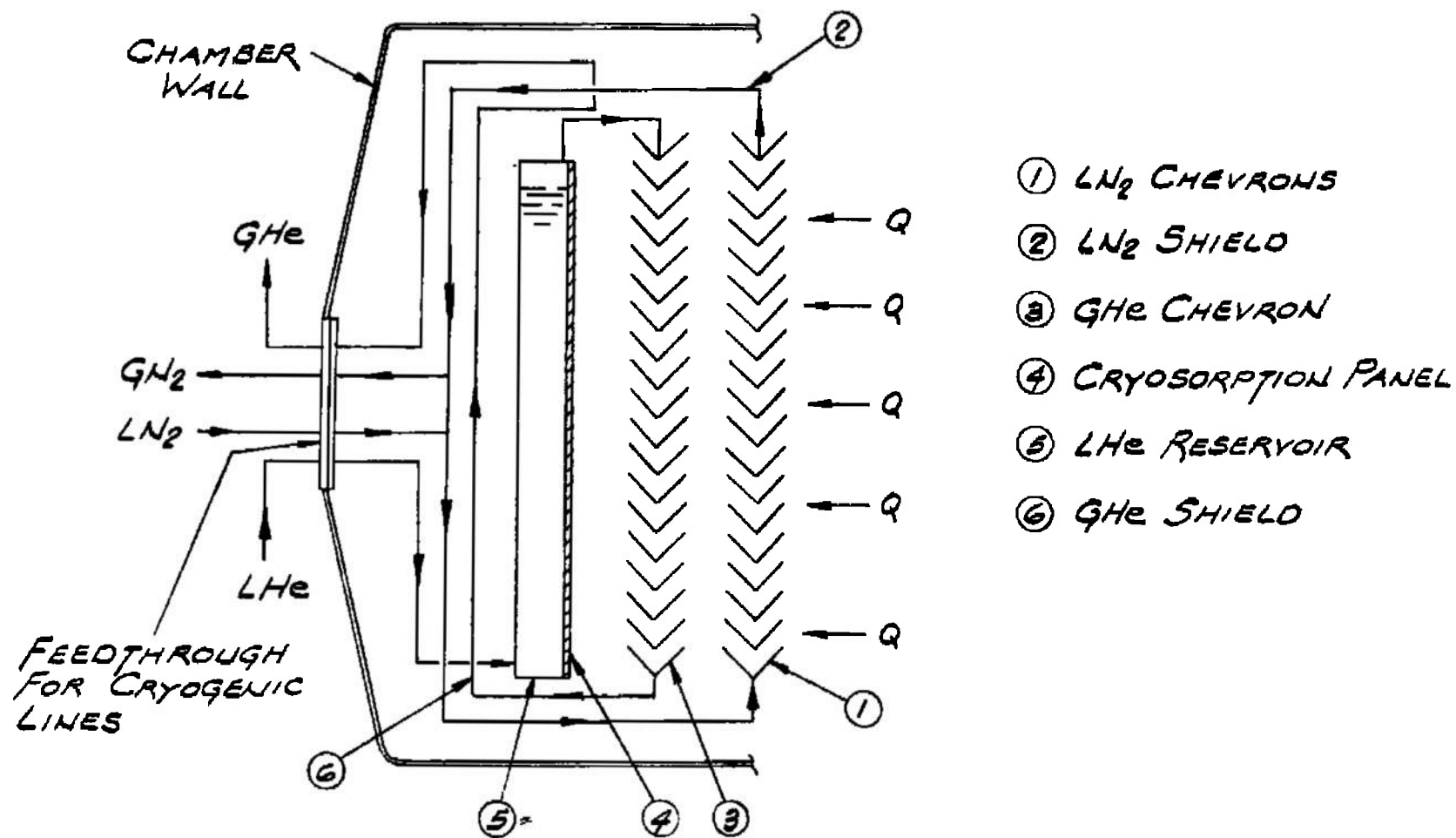


Fig. 35 Schematic Representation of a Cryogenic Array

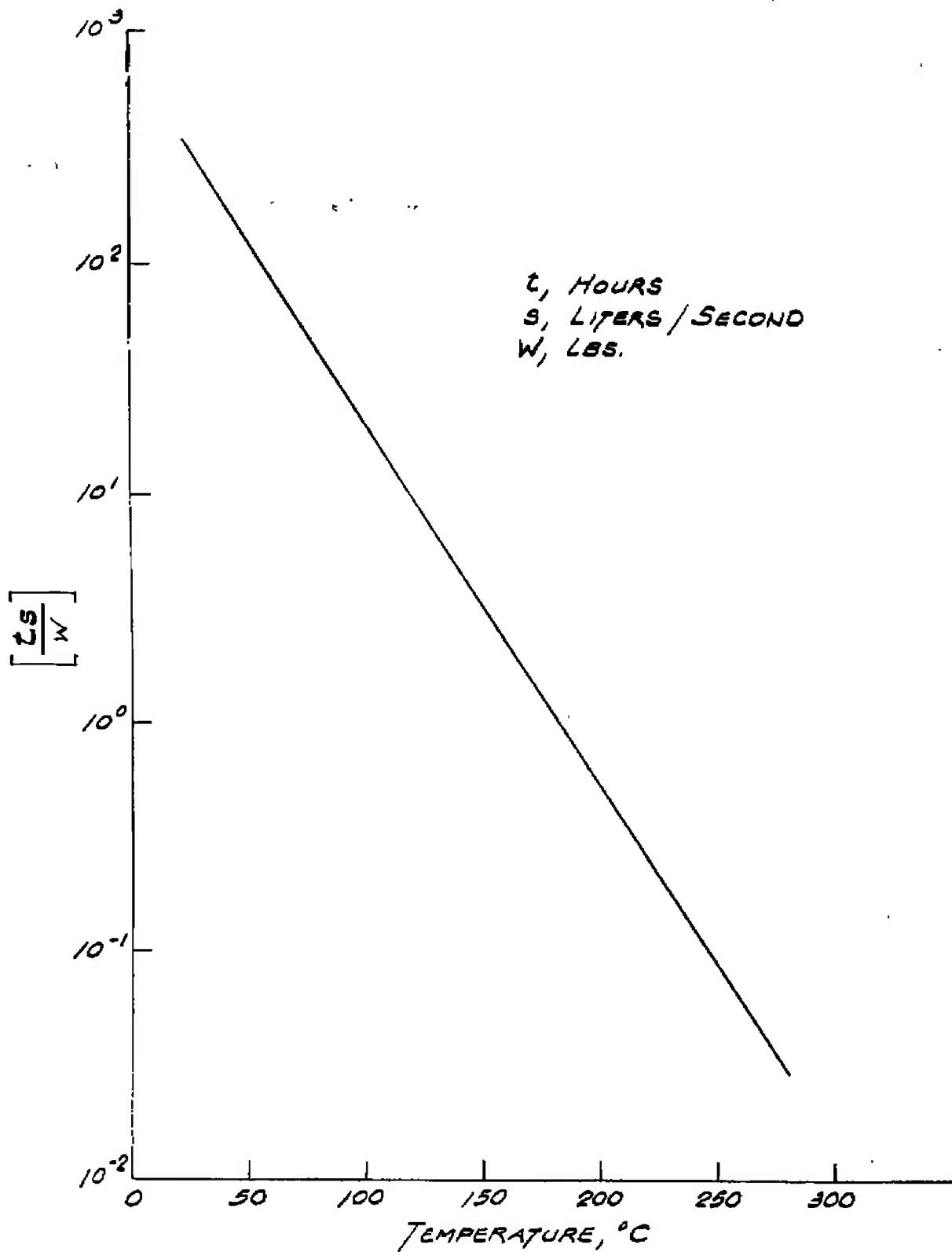


Fig. 36 Activation Time Required to Reduce Water Loading to Two Weight Per Cent

UNCLASSIFIED

Security Classification

## DOCUMENT CONTROL DATA - R&amp;D

(Security classification of title, body of abstract and indexing annotation must be entered when the overall report is classified)

1. ORIGINATING ACTIVITY (Corporate author) Engineering Department, Linde Division, Union Carbide Corporation		2a. REPORT SECURITY CLASSIFICATION Unclassified	
		2b. GROUP NONE	
3. REPORT TITLE DEVELOPMENT AND APPLICATION OF CRYOSORPTION PUMPING OF HYDROGEN AT 20°K BY MOLECULAR SIEVE ADSORBENT PANELS This document has been approved for public release			
4. DESCRIPTIVE NOTES (Type of report and inclusive dates) NONE its distribution is unlimited. <i>Re: DDC 10-75 AD 701 700 BTD July 1978</i>			
5. AUTHOR(S) (Last name, first name, initial) Gareis, P. J. and Pitlor, J. R.			
6. REPORT DATE January 1965	7a. TOTAL NO. OF PAGES 98	7b. NO. OF REFS 19	
8a. CONTRACT OR GRANT NO. AF40(600)-944	9a. ORIGINATOR'S REPORT NUMBER(S) AEDC-TR-65-18		
b. PROJECT NO. 7778			
c. Program Area 850E	9b. OTHER REPORT NO(S) (Any other numbers that may be assigned this report)		
d. Task 777801	NONE		
10. AVAILABILITY/LIMITATION NOTICES NONE			
11. SUPPLEMENTARY NOTES NONE		12. SPONSORING MILITARY ACTIVITY Arnold Engineering Development Center, Arnold Air Force Station, Tennessee	
13. ABSTRACT An experimental and theoretical investigation of the vacuum pumping of hydrogen by refrigerated panels consisting of Molecular Sieve 5A bonded to metallic substrates was performed in the pressure range of $10^{-9}$ to $10^{-6}$ Torr. Initial sticking coefficients approxi- mating unity were obtained with an array utilizing a shield and panel configuration, both refrigerated to 20°K. An effective, practical, initial activation procedure was developed for utilization with the shielded array wherein desorbed water vapor was cryopumped by the liquid nitrogen cooled elements surrounding the 20°K surfaces. Suc- cessive tests with a particular panel produced a progressive reduction in pumping speed. Methods were developed which resulted in partial recovery of prior pumping speed values; however, further effort is required to define precise conditions of efficient, successive acti- vation procedures capable of maintaining the initial high sticking coefficient values. A theoretical model is presented which relates observed pumping speed results to diffusion parameters of the cryo- sorption pumping mechanism. Criteria are discussed for application of cryogenic arrays, utilizing cryopumping and cryosorption, as practical untrahigh vacuum pumping units.			

DD FORM 1473  
1 JAN 64

UNCLASSIFIED

Security Classification

14	KEY WORDS	LINK A		LINK B		LINK C	
		ROLE	WT	ROLE	WT	ROLE	WT

## INSTRUCTIONS

1. **ORIGINATING ACTIVITY:** Enter the name and address of the contractor, subcontractor, grantee, Department of Defense activity or other organization (*corporate author*) issuing the report.

2a. **REPORT SECURITY CLASSIFICATION:** Enter the overall security classification of the report. Indicate whether "Restricted Data" is included. Marking is to be in accordance with appropriate security regulations.

2b. **GROUP:** Automatic downgrading is specified in DoD Directive 5200.10 and Armed Forces Industrial Manual. Enter the group number. Also, when applicable, show that optional markings have been used for Group 3 and Group 4 as authorized.

3. **REPORT TITLE:** Enter the complete report title in all capital letters. Titles in all cases should be unclassified. If a meaningful title cannot be selected without classification, show title classification in all capitals in parenthesis immediately following the title.

4. **DESCRIPTIVE NOTES:** If appropriate, enter the type of report, e.g., interim, progress, summary, annual, or final. Give the inclusive dates when a specific reporting period is covered.

5. **AUTHOR(S):** Enter the name(s) of author(s) as shown on or in the report. Enter last name, first name, middle initial. If military, show rank and branch of service. The name of the principal author is an absolute minimum requirement.

6. **REPORT DATE:** Enter the date of the report as day, month, year; or month, year. If more than one date appears on the report, use date of publication.

7a. **TOTAL NUMBER OF PAGES:** The total page count should follow normal pagination procedures, i.e., enter the number of pages containing information.

7b. **NUMBER OF REFERENCES:** Enter the total number of references cited in the report.

8a. **CONTRACT OR GRANT NUMBER:** If appropriate, enter the applicable number of the contract or grant under which the report was written.

8b, 8c, & 8d. **PROJECT NUMBER:** Enter the appropriate military department identification, such as project number, subproject number, system numbers, task number, etc.

9a. **ORIGINATOR'S REPORT NUMBER(S):** Enter the official report number by which the document will be identified and controlled by the originating activity. This number must be unique to this report.

9b. **OTHER REPORT NUMBER(S):** If the report has been assigned any other report numbers (*either by the originator or by the sponsor*), also enter this number(s).

10. **AVAILABILITY/LIMITATION NOTICES:** Enter any limitations on further dissemination of the report, other than those

imposed by security classification, using standard statements such as:

- (1) "Qualified requesters may obtain copies of this report from DDC."
- (2) "Foreign announcement and dissemination of this report by DDC is not authorized."
- (3) "U. S. Government agencies may obtain copies of this report directly from DDC. Other qualified DDC users shall request through \_\_\_\_\_."
- (4) "U. S. military agencies may obtain copies of this report directly from DDC. Other qualified users shall request through \_\_\_\_\_."
- (5) "All distribution of this report is controlled. Qualified DDC users shall request through \_\_\_\_\_."

If the report has been furnished to the Office of Technical Services, Department of Commerce, for sale to the public, indicate this fact and enter the price, if known.

11. **SUPPLEMENTARY NOTES:** Use for additional explanatory notes.

12. **SPONSORING MILITARY ACTIVITY:** Enter the name of the departmental project office or laboratory sponsoring (*paying for*) the research and development. Include address.

13. **ABSTRACT:** Enter an abstract giving a brief and factual summary of the document indicative of the report, even though it may also appear elsewhere in the body of the technical report. If additional space is required, a continuation sheet shall be attached.

It is highly desirable that the abstract of classified reports be unclassified. Each paragraph of the abstract shall end with an indication of the military security classification of the information in the paragraph, represented as (TS), (S), (C), or (U).

There is no limitation on the length of the abstract. However, the suggested length is from 150 to 225 words.

14. **KEY WORDS:** Key words are technically meaningful terms or short phrases that characterize a report and may be used as index entries for cataloging the report. Key words must be selected so that no security classification is required. Identifiers, such as equipment model designation, trade name, military project code name, geographic location, may be used as key words but will be followed by an indication of technical context. The assignment of links, rules, and weights is optional.